146410
HQ

FINAL REPORT

CONTRACT NO. NASW-3782

William K. Hartmann

Planetary Science Institute

(a) PRINCIPAL INVESTIGATOR: William K. Hartmann, Planetary Science Institute, 2030 E. Speedway Suite 201, Tucson, AZ 85719

Co-Investigator: None

Contract No.: NASW-3782

Award Amount: $53,513

Award Period: May 15, 1983 - November 14, 1987

Project Title: Comparative Planetology of Early Intense Cratering and Other Cratering Effects

(b) SUMMARY: This project studies the period of intense early cratering in the first few hundred million years of the solar system, its decline to the present rate, and the consequent effects on the evolution of planetary surfaces. It is a continuation of a small project on which I have been P.I. for several years. A notable early result from which some of the present work flows was my 1984 Icarus paper concluding that saturation equilibrium cratering may exist on many bodies of the solar system.

In 1987-88, progress was made in three areas. With Jack Lissauer and Steve Squyres, I completed and submitted for publication a paper on cratering of the Saturn satellites. It concluded that some previously reported crater density variations are correlated with solar lighting, and that saturation may exist among smaller diameter craters, but not larger ones. Second, I published an abstract showing that 4-100 m lunar craters have densities close to my 1984 proposed saturation equilibrium level. This supports the hypothesis of saturation equilibrium, because these small lunar craters must be saturated to create the lunar regolith. Third, I published an abstract and gave a talk on effects of early intense cratering on the formation of Earth's crust, at an international conference on crustal evolution.

(c) Results of these studies are reported in detail in the attached Appendices. These documents include scientific papers published in refereed journals and books, abstracts which were accepted for presentation at scientific conferences, and preprints of papers reporting on recent work under this contract which have not yet been published in final form. These papers include tables, graphs, diagrams, curves, sketches, photographs, drawings, and text in sufficient detail to explain comprehensively the results achieved under this contract. Recommendations for future work on the specific problems studied are included in these publications. The published papers attached have undergone peer review, both internally in our organization and externally as part of the scientific journal refereeing process.

If there are further questions regarding this final report, please contact the Principal Investigator at (602) 881-0332.

APPENDICES

Appendix A:
Technical Description of Completed Work.

Appendix B:
Bombardment History of the Saturn System. Paper by J. Lissauer, S. Squyres, and W.K. Hartmann, submitted to JGR.

Appendix C:
Crater Saturation Equilibrium in the Solar System. LPSC abstract by W.K. Hartmann.

Appendix D:
Early Intense Cratering: Effect on Early Growth of Earth's Crust. Abstract for conference on Growth of Earth's Crust, by W.K. Hartmann.

TECHNICAL DESCRIPTION OF COMPLETED WORK

In 1987- 88, I completed my contribution to a paper jointly authored by Jack Lissauer and Steve Squyres. The MS is included as an Appendix to this final report. A working meeting of the authors was held at the October 1987 DPS meeting, where Hartmann and Squyres made a detailed comparison of their independent crater counts on Rhea. As a result, Hartmann drafted an Appendix to the paper, detailing statistical uncertainties in the crater counting technique, and criticizing over-reliance on 1/ /n error bars used by some authors to claim significant differences in crater populations. The paper has been submitted to JGR and has received two positive reviews, including one which praised the Appendix in particular as a long overdue assessment of the uncertainties in crater counts. The paper was revised and publication in JGR is expected.

Meanwhile, Plescia has published crater counts for Miranda where he finds that the crater densities in the most heavily cratered regions exactly coincide with Hartmann's proposed saturation equilibrium curve, derived earlier from surfaces on moons and planets inward from Uranus. Plescia concludes that my hypothesis is correct and that the Miranda crater density marks an empirical saturation equilibrium level.

These results are important to pursue, because they profoundly affect the interpretation of surfaces in the Jupiter, Saturn, Uranus, and (we hope) Neptune systems, photographed by Voyager. The current Voyager team interpretations of all systems have assumed that there is no saturation. Only if that assumption is correct can their interpretations of impactor populations and satellite histories be correct.

In a related area, an abstract was published showing that the density crowded craters on the lunar regolith, with diameters around 4 to 100 m, also follow the hypothetical saturation equilibrium line proposed in my 1984 paper. Because the regolith itself must be a product of saturation, in order to pulverize the soil, this supports the hypothesis that saturation equilibrium does fall along the crater density I described. The abstract is included in an appendix to this final report.

Finally, I have applied the work on early intense cratering to the geology of the earth. In particular, I have fitted the early cratering rate time dependence derived from the moon back to 4.0 b.y. ago to the rate required to accrete Earth is roughly 50 m.y. The rate of decline fits with that derived by Wetherill from his studies of sweep up of families of planetesimals on various Earth-crossing orbits.

In June, 1987, I gave a talk on the heavy cratering effects on Earth's early crust at the LPI-sponsored Topical Conference on Early Crustal History, in Oxford. The good response to this talk suggested that these external effects have not been adequately considered by the traditional geological community in their modelling of Earth's early development. The talk led to an invitation to give a longer seminar on the same subject at an international conference on Evolution of Plate Tectonics in France in November, 1988. Another indication of growing interest in this topic is the recent paper by Stevenson (1988, Nature) on the "frustration" of the origin of life due to effects of intense bombardment in the earliest eras of Earth's development.

References:

Lissauer, J.J., Squyres, S.W., and Hartmann, W.K. (1988). The Bombardment History of the Saturn System. In press, JGR.

Plescia, J.B. (1988). Cratering History of Miranda: Implications for Geologic Processes. Icarus 73, 442-461.

Stevenson, D. (1988). Impact Frustration of the Origin of Life. Nature.

Wetherill, G.W. (1977). Evolution of the Earth's Planetesimal Swarm Subsequent to the Formation of the Earth and Moon. Proc. Lun. Sci. Conf. 8:1.

Appendix B

BOMBARDMENT HISTORY OF THE SATURN SYSTEM

Jack J. Lissauer*
Astronomy Program†
Dept. of Earth and Space Sciences
State University of New York
Stony Brook, NY 11794
and
Department of Physics
University of California
Santa Barbara, CA 93106

Steven W. Squyres
Center for Radiophysics and Space Research
Cornell University
Ithaca, NY 14853

and

William K. Hartmann
Planetary Science Institute
2030 E. Speedway
Tucson, AZ 85719

*Alfred P. Sloan Research Fellow

†Present address

Abstract

We analyze crater distributions on Voyager images of Saturn's satellites and develop models of relative cratering rates on these bodies based on orbital dynamics. Our goal is to construct a history of satellite bombardment, disruption, and resurfacing in the Saturn system. Our observations concentrate on Rhea, the largest and best-imaged of Saturn's airless moons. We divide the portion of Rhea imaged at high resolution into 44 latitude-longitude quadrats for counting purposes. Detailed analysis of the spatial distribution of craters shows no statistically significant evidence for local endogenic resurfacing on Rhea. The apparent spatial variability in the distribution of small craters is strongly correlated with lighting geometry and hence unlikely to have resulted from geologic processes. Also, we find that the spatial distribution of craters on Rhea with diameters $D \geq 32$ km is in fact more uniform than a majority of random distribution produced by Monte Carlo simulations. We interpret this observation as possible evidence that the surface has approached (but not necessarily reached) saturation equilibrium for craters with diameters up to 32 km. (Impacts on a heavily cratered surface will tend to preferentially obliterate craters in areas of randomly produced crater clustering, leading to an increase in spatial uniformity.) Craters with $D \geq 64$ km on Rhea have densitites significantly below any proposed saturation equilibrium density; therefore they probably represent a production function. The size-frequency relationship of these large craters on Rhea is well fit by the curve $\log_{10} N_L = -2.73 \log_{10} D - 0.064$, where N_L is the number of craters larger than D km per km^2. The analogous relationship for Iapetus is $\log_{10} N_L = -2.70 \log_{10} D + 0.109$. Iapetus is also clearly not saturated at large crater diameters. On Mimas, as on Rhea, the spatial distribution of craters shows no statistically significant evidence for spatial variability, and large craters appear to be present at densities below those expected for saturation equilibrium.

We compute relative cratering rates and collision energies for heliocentric projectiles impacting Saturn's moons, taking into account gravitational focussing by the planet. Using crater scaling laws, we project the large crater distributions seen on Rhea and Iapetus to expected integrated impact fluxes on other moons. Disruption probabilities of Saturn's inner moons estimated by this method vary by a factor of $\sim$2 depending on what crater scaling law we use and whether the impactors are predominantly Saturn-family comets or

long period comets. Computed disruption probabilities are 3–8 times higher when scaled to Iapetus' cratering record than to Rhea's. This could be due to Iapetus' surface being older than Rhea's, in which case the Iapetus scaling is correct; alternatively, Iapetus may have been cratered by a long-lived population of Saturn-orbiting debris which did not penetrate inside the orbit of Titan, in which case Rhea's record should be used. These uncertainties not withstanding, we calculate disruption probabilities significantly smaller than those of Smith *et al.* [*Science* **215**, 504 (1982)]. Our results are consistent with Mimas and larger moons being original aggregates and the smaller irregularly-shaped bodies being collisional fragments. Our results also constrain theories advocating recent formation of Saturn's rings from satellite disruption.

We conclude that *(a)* there is no evidence for local geologic resurfacing on Rhea or Mimas; *(b)* either the surface of Iapetus is older than that of Rhea, or Iapetus was bombarded by a population of Saturn-orbiting debris which did not extend inwards to Rhea; *(c)* if the heavily-cratered surfaces in the Saturn system have indeed reached stauration at small diameters, the cratering record on Saturn's moons may be due to a single population of impactors dominated by small bodies; *(d)* Rhea, Mimas, and Iapetus are not saturated with craters at large crater diameters, so that observed densities of large craters may be used to evaluate satellite disruption probabilities; *(e)* Saturn's classical satellites are probably original aggregates dating from about the period of Saturn's formation, as opposed to products of repeated disruption and reaccretion during more recent history; and *(f)* it is very unlikely that Saturn's rings were formed within the last 10^9 years by the disruption of a single moon.

I. Introduction

The Voyager spacecraft flybys of the Saturn system provided the first detailed look at the surfaces of the saturnian satellites [*Smith et al.*, 1981, 1982]. The images of these satellites revealed a surprising diversity of surface morphology and age. The key to determining the relative ages of the satellites' surfaces is the record of meteoritic bombardment that is preserved by impact craters. Because the satellites are generally small and have been heavily cratered, the possiblity exists that some of them have been disrupted by large impacts and then reaccreted, perhaps several times [*Smith et al.*, 1982]. Saturn's rings may even be the shattered remnants of a small moon that was disrupted by an impact [*Pollack et al.*, 1973; *Smith et al.*, 1982]. An understanding of the bombardment history of Saturn's satellites is therefore of central importance to interpreting many of the most basic characteristics of the system and its evolution.

The purpose of this paper is to present a detailed analysis of the bombardment history of the Saturn system. We briefly review previous studies of the cratering record on Saturn's moons and other work related to our analysis in Section II. We examine the cratering record preserved on the saturnian satellites, concentrating on Rhea (Section III) and Mimas (Section IV). These two satellites provide the best combination of high resolution imaging coverage and heavily cratered surfaces. We first examine the influence of image lighting geometry on apparent local crater density. We then present a detailed statistical analysis of the spatial distribution of craters on the satellites in order to evaluate the hypothesis that there has been local geologic resurfacing on Rhea and Mimas. This is an important issue, because if there has been significant resurfacing, these satellites may preserve a very incomplete record of their bombardment history. Finally, we present conventional crater size-frequency analyses. A size-frequency analysis of craters on Iapetus' bright hemisphere is presented in Section V. The cratering record on Saturn's other moons is dicussed briefly in Section VI.

In Sections VII and VIII, we present scaling methods and dynamical calculations that allow the cratering records observed on Rhea and Iapetus to be interpolated and extrapolated to the other satellites in the saturnian system. We use our observations and calculations to evaluate the hypotheses that the inner satellites have undergone multiple dis-

ruption and reaccretion events, and that Saturn's rings resulted from collisional disruption of a satellite (Section IX). We summarize our principal conclusions and their cosmogonic implications in Section X. In the Appendix we discuss the difficulties introduced by the subjectivity inherent in the crater counting process.

II. Previous work

The first analysis of the cratering history of the saturnian satellites was the work of *Smith et al.* [1981, 1982]. They provided a thorough morphologic description of each of the satellites as seen in Voyager spacecraft images, and presented some preliminary crater counts. They noted that Mimas is very heavily cratered, but suggested that there may be inhomogeneities in the distribution of large craters, perhaps indicating a period of local resurfacing early in the satellite's history. Enceladus was found to have a highly variable crater density, with some areas heavily cratered, but large areas that were crater-free at the best Voyager resolution. It has clearly undergone massive resurfacing, probably as a result of tidal dissipation of orbital energy [*Yoder*, 1979; *Squyres et al.*, 1983; *Lissauer et al.*, 1984]. Tethys and Dione both show significant spatial variability in crater density, although the variations are much less pronounced than those on Enceladus. *Smith et al.* noted that the lightly cratered regions on Tethys and Dione appear to exhibit a paucity of large craters relative to the number of small craters present. Regardless of the details of the cratering statistics, however, it is clear that Tethys and Dione underwent significant local geologic resurfacing early in their histories. Rhea was observed by Voyager 1 at high resolution, and was found to have a very heavily cratered surface. As on Mimas, however, regions were identified that seemed to have reduced concentrations of large craters. Again, this was attributed to an early episode of local geologic resurfacing.

A major conclusion of *Smith et al.'s* analysis of the cratering record in the saturnian system is that the system was bombarded by two distinct populations of impactors, termed population I and population II. Population I, present on only the oldest surfaces, was stated to be characterized by a relatively high abundance of craters larger than $\sim$ 20 km, with the more recent population II characterized by craters smaller than $\sim$ 20 km and a general absence of large craters.

A more detailed description of the crater densities on some of the saturnian satellites was presented by *Plescia and Boyce* [1982, 1983]. They presented crater size-frequency distributions for Mimas, Enceladus, Tethys, Dione, Rhea, and Iapetus, subdividing each of the satellites into a number of individual counting regions. Their major conclusion was that all but Iapetus have undergone local geologic resurfacing to various degrees. In agreement with *Smith et al.* [1981, 1982], they found that the evidence for local geologic resurfacing on Enceladus and Dione is unambiguous; variations in crater density of more than a factor of five are observed on Dione, and some areas on Enceladus are crater-free to the limit of Voyager resolution, $\sim$ 1 km pixel^{-1}. Tethys unfortunately was not imaged at high enough resolution for detailed crater counting to yield much information beyond what was presented by *Smith et al.* However, *Plescia and Boyce's* results seem to show that local resurfacing also has taken place there.

The evidence presented by *Plescia and Boyce* [1982] for local resurfacing on Mimas and Rhea is somewhat more subtle. Both satellites are very heavily cratered everywhere. On Mimas, they found that the leading hemisphere of the satellite has a number of craters larger than $\sim$ 40 km, while the south polar region is lacking in such craters. This observation was interpreted as evidence for resurfacing of the south polar region. On Rhea, two indicators of resurfacing were presented. First, they found that the density of small ($\sim$ 10 km) craters shows substantial variability across the satellite. Second, they noted that in the north polar region the area west of longitude 0° has a number of large (40 – 130 km) craters, while such craters are generally absent in the polar region east of longitude 0°. We will consider the implications of these observations in detail below. *Plescia and Boyce* [1983] found that Iapetus was very heavily cratered, and found no evidence for local resurfacing in the areas they studied.

In a subsequent paper, *Plescia and Boyce* [1985] summarized crater densities for all the saturnian satellites and attempted to derive absolute ages from the crater observations. A detailed critique of this work has been presented by *Chapman and McKinnon* [1986]. Other crater counts for some of the saturnian satellites have been presented in various forms by *Strom* [1981], *Plescia* [1983], and *Hartmann* [1984].

A number of authors have considered the sources of the impactors responsible for cratering in the Saturn system. The two general classes of impactors are those in helio-

centric orbits and those in saturnocentric orbits. *Smith et al.* [1981, 1982] reached no conclusions regarding the source of the large population I craters, but suggested that the smaller population II craters were produced by secondary saturnocentric debris that was generated by population I impacts. *Plescia and Boyce* [1985] suggested that both population I and population II impactors were in heliocentric orbits, since they argue that population I bombardment ended before population II bombardment began, so the two cannot have been linked. This view was sharply criticized by *Chapman and McKinnon*, on the grounds that *(a)* it is not clear that *Plescia and Boyce's* timing arguments are correct, and *(b)* there is no equivalent to population II in the Jupiter system. *Strom and Woronow* [1982], have argued that both populations resulted from planetocentric impactors. The key to their argument is the belief that heliocentric impacts should be concentrated at a satellite's apex of orbital motion, and that no such concentration is observed. *Horedt and Neukum* [1984] have done detailed calculations of expected lifetimes for particles in saturnocentric orbits. For particles in moon-crossing orbits from Rhea inward, they compute lifetimes of just 10^3 to 10^4 years. Based on these short timescales, they argue that heliocentric impactors have been important in the system, but suggest that cratering has also taken place due to bodies captured into temporary saturnocentric orbits.

Smith et al. [1982] estimated cratering rates and disruption probabilities for Saturn's inner moons. Assuming the cratering record on Iapetus was produced by projectiles in heliocentric orbits, they included gravitational focussing by the planet [*Shoemaker and Wolfe*, 1982] to compute expected impact densities on other moons. The increased energy and flux of impactors near Saturn suggested to them that Mimas was broken up and reaccreted ~ 5 times since the last global resurfacing of Iapetus, and that the inner "ringmoons" were disrupted even more frequently. A problem with extrapolating from the cratering record on Iapetus, however, is that Iapetus is sufficiently distant from Saturn and from other moons that sweepup of accretionary debris could have taken $\sim 10^6 - 10^7$ yrs [*Horedt and Neukum*, 1984]. Therefore, many of the craters now observed on Iapetus could be due to this long-lived planetocentric debris which would not have bombarded moons inwards of Titan, rather than to heliocentric debris.

Any investigation of the cratering history of the Saturn system must be placed in the context of the crater distributions observed on other outer solar system bodies. *Chapman*

and McKinnon [1986] give a good recent review. The most heavily cratered body in the Jupiter system is Callisto. The most striking thing about the crater size-frequency distribution there is the paucity of craters larger than about 50 km. While it has been suggested that the pronounced steepening of the crater distribution at about 50 km could be the result of removal of larger craters by viscous relaxation, this suggestion is not borne out by more detailed study [*Woronow and Strom*, 1982]. Instead, it appears that the production population in the jovian system had a distinctly steeper size-frequency distribution, at least at diameters greater than about 50 km, than the major production population in the inner solar system.

Results for the uranian satellites have been presented recently by *Strom* [1987], *Plescia* [1988*a*, 1988*b*], and *Croft* [1988]. In general, the most heavily cratered surfaces (the surfaces of Umbriel, Oberon, and heavily cratered regions on Miranda) have crater densities comparable to those of the most heavily cratered areas on the terrestrial planets (*e.g.*, the lunar highlands). *Plescia* [1988] has reported a steepening of the curves (*i.e.*, a paucity of larger craters) at diameters larger than about 8 km in heavily cratered terrain on Miranda; this steepening is not reported by *Strom* [1987] or *Croft* [1988]. On Titania, Ariel, and resurfaced regions on Miranda, the crater density is lower, and the curves steeper at all diameters. *Strom* interprets the differing slopes as evidence for two distinct impactor populations, analogous to the two populations hypothesized for the Saturn system. *Plescia* instead attributes the differing slopes to saturation effects. He suggests that the steep slopes (found at low densities) are production populations, but that the flatter slopes (found at the highest densities) have had their small crater abundances limited by attainment of saturation equilibrium. We will return to this rather contentious issue below.

One other set of literature is relevant to our effort here. Because our goals include determining the extent to which the saturnian satellites have undergone local geologic resurfacing, we are faced with the problem of testing the spatial distribution of craters on Saturn's moons for randomness. We know of no previous attempts to do this in a statistically rigorous fashion. Such tests are, however, commonly performed in geography and biostatistics [*e.g., Getis and Boots*, 1978 and reference therein]. The spatial distribution of lunar craters was analyzed extensively in the 1960's [*Marcus*, 1967 and reference therein]. This literature has largely been "lost" to the planetary community for a number of years, and

the reasons for its disappearance deserve comment. The major question that was being addressed during the 1960's was whether most lunar craters were formed by impacts or by endogenic (*i.e.*, volcanic) processes. This controversy has since been firmly resolved in favor of impacts. However, most of the statisticians arrived at the opposite conclusion, *i.e.*, that a significant fraction of lunar craters are endogenic in origin. Their erroneous result was largely due to a lack of understanding of certain physical processes such as the formation of secondary crater chains [*Fielder and Marcus*, 1967], and because they rejected as being random processes that χ^2 tests ruled out with probabilities as low as 90%. We hope our judgements will better withstand the test of time; however, as with all statistical analyses, especially those dealing with small numbers and uncertain externalities, *caveat emptor*.

III. Rhea

We begin our investigation with an analysis of the cratering record preserved on Rhea. The imaging data for Rhea are the best in the Saturn system, in terms of both resolution and total area covered. We performed crater counts using the highest resolution Voyager images of the satellite. Nine images were used, ranging in resolution from $\sim$ 0.75 to 1.1 km pixel^{-1}. Additional low resolution images were used to locate large craters in regions not imaged at the highest resolution. The portion of the surface of the satellite that was imaged at high resolution was subdivided into 44 quadrats, each bounded by latitude and longitude limits (Table 1). Quadrats were 15° $\times$ 15° in size at low latitudes, and were of the same latitudinal but greater longitudinal extent at high latitudes. They ranged in surface area from a minimum of 2.43×10^4 km^2 to a maximum of 3.96×10^4 km^2. Arbitrary subdivision by latitude and longitude was used to eliminate sampling bias that might be introduced by other types of selection. Counts were conducted independently by two of us (Squyres and Hartmann), and compared after they were completed. The size-frequency distributions obtained by the two crater counters agreed very well in all cases, but the details of the spatial distributions of highly degraded large craters showed some interesting differences. The spatial statisitics presented in the main body of the paper (Figs. 7 and 8 and discussion concerning them) are the result of a crater-by-crater "consensus" obtained by the two crater counters working together. In the Appendix we discuss the two original sets of independent

counts, their similarities and differences, and their implications for the role of subjective judgement in the crater counting process.

Spatial Distribution of Craters

We first address the question of local resurfacing on Rhea. Table 1 summarizes the observed variability in small crater density across the surface of the satellite. We tabulate the observed values of N_{8km}, the number of craters with diameters $D \geq 8$ km per km^2. A similar tabulation has been presented by *Plescia and Boyce* [1982]. They used a minimum diameter of 10 km rather than 8 km, and subdivided the surface differently. Allowing for these differences, however, our results are generally in very good agreement with theirs. The results of both studies show similar values of overall crater density, and grossly similar variations in crater density from one part of the satellite to another.

As noted by *Plescia and Boyce* [1982], substantial variability appears in the observed crater density from one area on Rhea to another. The variability is displayed clearly in Table 1, and in fact is evident from cursory visual inspection of some images. As an example, Figure 1 shows an area of heavily cratered terrain near the north pole, and Figure 2 shows another area near the equator. Cumulative and relative crater size-frequency distribution plots for the areas outlined on each image are shown in Figure 3. There are substantial differences between the two curves. The density of craters smaller than ~20 km in Figure 2 is markedly lower than that of Figure 1. This is the paucity of small craters pointed out by *Plescia and Boyce* [1982]. They suggested that it might be due to mantling of the surface with some sort of geologic deposit thick enough to bury the smaller craters but thin enough to leave the larger craters visible. However, they also noted that the proximity of the area to the subsolar point made the recognition of craters there difficult.

The spatial variability of N_{8km}, if due to geological causes, would be a clear indicator of some type of resurfacing or mantling process. Most of the area shown in Figure 2 has a value of N_{8km} that is sharply reduced relative to the rest of the satellite. However, we agree with *Plescia and Boyce* [1982] that lighting geometry could significantly affect the number of craters counted. In fact, we have concluded that the lower crater density observed in this area is simply due to the unfavorable lighting geometry, rather than to any geologic

resurfacing. An unfortunate characteristic of the Voyager data is that for most areas on most satellites, high resolution coverage is only available under a single illumination geometry. This is the case for the Rhea images. The recognition of topographic forms is of course influenced by both the solar illumination angle and the orientation of the surface with respect to the spacecraft. In general, viewing is best where the incidence angle i is large (that is, where shadows are well-developed), and where the emission angle ϵ is small (that is, where the surface is normal to the direction of viewing). The only major exception is when i is so large that shadows begin to dominate the surface, obscuring a significant fraction of it. As a crude quantitative measure of the "quality" of the viewing geometry, then, one may adopt the parameter $\tan i \cos \epsilon$. The basis for the use of this parameter is simply that projected shadow area, as viewed from the spacecraft, will in general be proportional to $\tan i$ and to $\cos \epsilon$.

Figure 4 shows a plot of N_{8km} *vs.* $\tan i \cos \epsilon$ for the eight quadrats we counted in the image shown in Figure 2 (see Table 1 for the location of the areas). The value of $\tan i \cos \epsilon$ is calculated at the center point of each quadrat. There is a strong positive correlation between crater density observed and the quality of the lighting geometry (correlation coefficient = 0.73). In fact, the correlation is not limited to this region, but holds for the entire satellite. Figure 5 shows N_{8km} *vs.* $\tan i \cos \epsilon$ for all 44 quadrats on the satellite that we examined. A positive correlation is still quite evident (correlation coefficient = 0.45). We believe that the reduced crater density observed in Figure 2 is attributable to the poor lighting geometry in the area, and that it is unnecessary to invoke geologic resurfacing as a means of reducing crater density. In fact, the global correlation between observed crater density and lighting geometry suggests that the spatial variability of N_{8km} holds no compelling evidence for significant geologic resurfacing anywhere on Rhea.

The other possible indicator of geologic activity on Rhea is the apparently inhomogeneous distribution of large craters. The spatial distribution of large craters is shown in Figures 6 through 8. These figures show the 44 quadrats we counted displayed on an equal-area projection, with the number of craters with $D \geq 16$, $D \geq 32$, and $D \geq 64$ km indicated in each. Visual inspection of the distribution of large craters does indeed show some clumping. The most obvious case, pointed out previously by *Smith et al.* [1981] and *Plescia and Boyce* [1982] is that, poleward of 60° N, there are substantially more large

craters west of 0° longitude than east of 0°. What is not immediately clear, however, is whether this apparent clumping of large craters is statistically significant, or whether it is simply due to the random distribution of what is a fairly small number of craters.

(It should be pointed out that there is considerable disagreement over the number of large craters in the eastern part of the polar region. *Plescia and Boyce* [1982] state that there are no craters in this region with $D > 30$ km. *Smith et al.* [1981] mapped this area and found nine craters with $D \geq 32$ km, of which two were described as "fresh" and seven as "apparent mantled craters, faintly visible." Four (1 "fresh", 3 "mantled") lay in the region bounded by 60° latitude, 0° longitude, and 300° longitude. We also found four craters with $D \geq 32$ within the same latitude and longitude limits, three of which were among the four identified by *Smith et al.* There is clearly an undesirable amount of subjectivity involved in counting highly degraded craters, an issue we discuss in greater detail in the Appendix.)

Deviations from a spatially random distribution of large craters could result from a variety of causes. Local endogenic resurfacing by some sort of volcanic process could result in areas of low crater density. Spatially inhomogeneous viscous relaxation due to local concentrations of heat flow could have the same effect. Departures from randomness could also result from crater production that was not spatially random; *e.g.*, due to excess impacts on the leading hemisphere of a synchronously rotating satellite [*Shoemaker and Wolfe* 1982].

Deviations from randomness could, of course, also result from the photometric effects that limit the usefulness of the 8 km crater data. Correlation coefficients between crater density, N_{8km}, and $\tan i \cos \epsilon$ are 0.27 for 16 km craters, and -0.12 for 32 km craters. In order to test the statistical significance of these results, we randomly "cratered" a surface divided into regions of the same relative sizes as the 44 quadrats used with the identical total numbers of 16 km and 32 km craters observed (see below for details). We then computed correlations between the actual lighting geometry on Rhea and the crater density in the random simulations. In only one of our twelve simulations was the magnitude of the correlation coefficient for the 16 km craters greater than that observed. Therefore, the correlation between N_{16km} and $\tan i \cos \epsilon$ is statistically significant, although marginally so. The correlation coefficent between N_{32km} and $\tan i \cos \epsilon$ is negative and smaller in magnitude; it is not statistically significant. The detrimental effects of uneven lighting

clearly become less important for larger craters. There is an indication that the 16 km data have also been degraded by photometric effects, although the degradation is less pronounced than for the 8 km craters. For craters 32 km in size and larger, photometric effects appear negligible, presumably because structural crater wall features can be picked out at Voyager resolution even under unfavorable viewing geometries.

Another factor that could influence the degree of randomness of the spatial distribution of larger craters is removal of craters by subsequent cratering events. This process could have several possible effects. Craters much larger than the minimum size of the population under consideration could wipe out craters over large areas, both by direct superposition and by blanketing them with ejecta. These effects would produce sparsely cratered regions similar to those created by endogenic resurfacing. On the other hand, if the major remover of craters in a given size range is the production of new craters in approximately the same size range, then very heavily cratered regions approaching (but not necessarily at) saturation equilibrium may exhibit a crater distribution *more uniform than random*. This is a key point. It is very important to recognize that "random" and "uniform" are very different concepts. A truly random spatial distribution has regions of clustering and of sparseness. Once a surface becomes sufficiently cratered that an impact event has a high probability of wiping out pre-existing craters, areas of random clustering of impacts will lose craters at a significantly more rapid rate than will crater-poor regions.

The data used in our statistical analysis were the maps of crater frequencies shown in Figures 6 through 8. These data all suffer from small number statistics, especially for the larger crater sizes. In order to study the degree of randomness of these distributions, we performed twelve numerical experiments in which we produced a spatially random distribution of "craters" in a grid of quadrats of the same sizes and configuration as those used in our Rhea counts. The total number of "craters" produced in each size range was the same as the number of craters in the size range of interest actually observed on Rhea. We then compared the statistical properties of the resulting spatial "crater distributions" to those of the actual craters observed on Rhea. We calculated the standard deviation of the number of craters per quadrat,

$$\sigma = \left[\frac{\Sigma_{j=1}^{n}(M_j - \lambda)^2}{n}\right]^{\frac{1}{2}} \qquad (1)$$

where n is the number of quadrats, M_j the number of craters (larger than a given size) in the j^{th} quadrat, and λ is the mean number of craters per quadrat. We also calculated the fourth root of the fourth moment about the mean (which is similar to the standard deviation, but places more statistical weight on the most extreme values) of the same distribution,

$$\sigma_4 = \left[\frac{\Sigma_{j=1}^{n}(M_j - \lambda)^4}{n}\right]^{\frac{1}{4}}. \qquad (2)$$

We performed two χ^2 tests. The first, χ_u^2, compared the observed and calculated spatial distributions to a homogeneous Poisson distribution, which would be expected for random crater production on a grid of uniform quadrat size. The second, χ_v^2, assumed an inhomogeneous Poisson distribution of crater centers with means proportional to quadrat sizes [see, *e.g.*, *Larson*, 1969; *Getis and Boots*, 1978]. We then computed correlation coefficients between locations of craters in different size ranges. In order to examine spatial variability on a scale larger than individual quadrat sizes a number of adjacent quadrats were combined into larger "super-quadrats". The layout of the super-quadrats boundaries is shown by thicker lines in Figures 6 and 7. The small number of super-quadrats preclude a χ^2 analysis; however we did compute σ and σ_4 for the 16 km and 32 km craters as well as the correlation coefficient between $(M_j(16) - M_j(32))$ and $M_j(32)$. Finally, we computed theoretical average values (for the more mathematically tractable case of constant quadrat sizes) for the same statistical parameters.

The results of these simulations and calculations are summarized and compared to the observations in Table 2. The 16 km crater distribution is statistically indistinguishable from random for every parameter tested (except for a possible correlation of observed density with lighting geometry; see above). This does not imply that we are viewing a production function, although it is consistent with one. However, if any major resurfacing mechanisms have operated, they must roughly cancel in their effects on the uniformity of the crater distribution.

When we look at craters with $D \geq 32$ km (which are not complicated by lighting geometry effects), however, we find that the spatial distribution may not be random. The standard deviation and the fourth root of the fourth moment about the mean of the 32 km data are both smaller than the values for the random data and theoretical expectations. If this result is indeed statistically significant, it appears that the observed craters on Rhea

may be more, not less, uniformly distributed than would be expected from randomness. We performed two χ^2 goodness-of-fit tests with three degrees of freedom of the 32 km data to the Poisson distribution expected for spatially random cratering. Comparing the resulting statistics, $X_u^2 = 6.5$, $X_v^2 = 6.8$, to the χ^2 distribution with 3 degrees of freedom allows randomness to be ruled out with a certainty of 91% and 92% respectively (*e.g.*, the chance that $X^2 \geq 6.8$ for random runs is 8%). Although there is only one empty quadrat in the observed data, the minimum number of empty quadrats among the twelve random runs was three; only one of the random runs lacked any quadrats with greater than five craters. In order to test this idea more thoroughly, we ran 200 additional random simulations for the 32 km craters, which are represented in Table 2 by the Grand Mean and Grand Median rows. Note that the mean values for 200 runs are similar to those of our first twelve simulations. Note also that the median values for the χ^2 tests are virtually identical to the theoretical value, which is the 50% confidence level for the χ^2 distribution with 3 degrees of freedom. Only two of the random simulations had just one quadrat totally devoid of 32 km craters (as did the observations). Only 13 runs had $\sigma \leq \sigma$(observed); only 14 had $\sigma_4 \leq \sigma_4$(observed). These statistical results imply that the major cause of destruction of craters $\geq$ 32 km in the area counted at high resolution ($\sim$ 20% of Rhea's surface) has been obliteration by other craters. Stated differently, the crater distribution may be well on its way to reaching saturation equilibrium. There is certainly no evidence of spatial inhomogeneity due to local endogenic resurfacing. Our ability to draw further or more definitive conclusions regarding the spatial distribution of craters on Rhea is limited by both statistical uncertainties and the subjectivity inherent in crater counting. In the Appendix, we apply the same statistical tests used above to the preliminary 32-km crater counts performed separately by SWS and WKH. Whereas the χ^2 results are very sensitive to minor changes in the distribution produced by such subjectivity, the values of σ and σ_4 are much more robust (see Table A1 in Appendix).

When grouped together into the larger super-quadrats, the 32 km data remain more uniform than the average random distribution. However, the difference is so small as to be statistically insignificant. We find, then, that the apparent shortage of large craters in the eastern part of the north polar region is explicable simply in terms of statistical fluctuations. Indeed, when one considers that the area in question comprises only about 6% of the surface area of Rhea imaged at high resolution, the random appearance of an area

of this size with a sparse density of 32 km crater does not seem surprising. The correlation coefficient between $(M_j(16) - M_j(32))$ and $M_j(32)$ is slightly negative, which indicates saturation effects dominate over other resurfacing and lighting geometry effects, but not by a statistically significant amount. The positive correlation for the larger quadrats would suggest the opposite interpretation, but at a completely statistically insignificant level. The correlation coefficient between the location $(M_j(32) - M_j(64))$ and $M_j(64)$ is -0.21, consistent with saturation effects being important. Note that the variable quadrat sizes used induce a slight positive bias in all of these correlation coefficients.

Due to the small number of craters larger than 64 km, fewer statistical tests are meaningful for them than for the smaller craters. However, it is clear that the distribution of craters on Rhea with $D \geq 64$ km is consistent with randomness. The observed standard deviation of craters per quadrat is 0.60; the mean value for the numerical experiments is 0.57. Values for the fourth root of the fourth moment are 0.87 and 0.81, respectively.

Size-Frequency Distribution of Craters

Our examination of the cratering record on Rhea has shown no evidence for significant endogenic resurfacing. We can therefore sum all areas in which we have counted craters to produce a cumulative curve for the entire satellite. In doing so, we can also use areas that lie outside our 44 quadrats, but that were imaged at sufficient resolution to observe very large craters. Figure 9 is a map showing all of the craters identified on Rhea with diameters larger than 90.5 km. (90.5 km is the next bin size larger than 64 km for the crater binning convention in which successive bin diameters differ by a factor of $\sqrt{2}$.) On this map, craters are indicated everywhere they were observed in Voyager images, including low resolution images that are not suitable for counting smaller craters. The cross-hatched areas on this map are those for which there is no coverage adequate to reveal craters of any size. It should be noted that the base for this map is the U.S. Geological Survey preliminary pictorial map of Rhea [*U.S. Geological Survey*, 1982], which has some positional errors in excess of 10°.

The cumulative crater curve for all areas counted on Rhea is shown in Figure 10. Points shown as circles on this plot are obtained from a summation of all counts in our 44 latitude-longitude quadrats. Points shown as triangles are obtained for large ($\geq$ 90.5

km) craters counted over the entire region of the satellite that was imaged at high enough resolution to distinguish craters of that size (*i.e.*, the area shown in Fig. 9, adjusted for the fact that large craters which are centered outside the imaged region can still have part of their rim visible).

The crater density on the surface of Rhea is close to the highest observed in the solar system. *Hartmann* [1984] has reviewed the cratering data for bodies throughout the solar system, and has shown that the most heavily cratered regions on a number of bodies show a cumulative crater distribution that can be fit crudely by:

$$\log N_{HC} = -1.83 \log D - 1.00 \tag{3}$$

where N_{HC} is the number of craters per km^2 larger than some diameter D in km. (The last term is modified from -1.33 cited by *Hartmann* to -1.00 to convert from his log incremental counts to the cumulative counts used here.) Because the crater densities in the most heavily cratered terrains of a number of bodies are fit approximately by Eq. (3), *Hartmann* has suggested that this equation is an approximate statement of crater "saturation equilibrium"; that is, that it represents the highest crater density attainable in nature. The essential point of his argument is that if this were not a state of saturation equilibrium, it would require an unlikely coincidence for the highest densities to agree so well (within a factor of 2 or 3) from one body to the next. The argument is a controversial one, as computer models of planetary surfaces subjected to impacts have suggested that crater densities can actually can actually rise to levels several times higher than the density given by Eq. (3) [*Woronow*, 1977, 1978]. This is an important point, because if a surface is unsaturated it provides a useful record of the impact flux to which it has been subjected, while if it is saturated, it yields only a lower limit for the number of impacts it has suffered. In Figure 10 we include the curve for N_{HC} given by Eq. (3). The Rhea crater curve, when compared to N_{HC}, has three distinct segments:

(1) For craters of about 8 km in diameter and smaller, the observed crater density is substantially less than N_{HC}. This apparent turndown is almost certainly not a feature of the crater production population. At the smallest diameters, many craters clearly are not being counted due to resolution effects (see Appendix). Also, since this curve incorporates areas with both favorable and unfavorable lighting geometry, we believe that a substantial

number craters are being lost due to poor illumination conditions. This segment of the curve therefore does not carry much useful information.

(2) For diameters ranging from about 8 km to about 32 km, the curve for Rhea lies close to *Hartmann's* [1984] expression for N_{HC}. If *Hartmann's* assertions are correct, then the surface of Rhea may have reached saturation equilibrium in this size range. If they are not, then all this segment shows us is that the crater density in this size range is similar to the density on the most heavily cratered surfaces of a number of other bodies. Recall, however, that the spatial distribution of 32 km craters may be more uniform than random, suggesting at least an approach to saturation.

(3) For diameters larger than about 32 km, the crater size distribution lies below the curve for N_{HC}. This "shortage" of craters of course cannot be attributed to resolution effects. On Ganymede and Callisto, it has been suggested that large craters have been selectively removed by viscous relaxation [*Passey and Shoemaker*, 1982; *Hartmann*, 1984], although as mentioned already this suggestion is not supported by quantitative studies of the process [*Woronow and Strom*, 1981]. On Rhea there is no evidence for significant viscous relaxation in the images, nor is viscous relaxation of craters smaller than several hundred km to be expected on such a small, cold satellite. There are at least two ways that a turndown in the observed crater distribution could take place. If the N_{HC} curve represents true saturation equilibrium, a shortage of large craters could result from a crater production curve with a steeper slope in this range. As a surface became more and more heavily cratered, the break in slope (*i.e.*, the transition from saturation to undersaturation) would gradually shift to larger and larger diameters. If N_{HC} does not represent saturation equilibrium, then the turndown at large diameters is inherent in the shape of the production population, as suggested by *Smith et al.* [1981, 1982].

Regardless of one's interpretation of the significance of the N_{HC} curve, it is clear that the surface of Rhea is not saturated for craters with diameters larger than 64 km. The shortage of large craters cannot be attributed to geologic resurfacing or viscous relaxation. This undersaturation is important, because it means that the surface of Rhea preserves a useful record of the large impacts it has suffered.

A linear least squares fit to the size-frequency distribution of craters with $D \geq 64$

km yields the expression

$$\log_{10} N_L = -2.73 \log_{10} D - 0.064 \quad (4)$$

where N_L is the crater density in craters per km^2. We shall use Eq. (4) together with scaling estimates derived in Sections VII and VIII in order to estimate probabilities that other saturnian satellites have been catastrophically disrupted since the last global resurfacing of Rhea.

IV. Mimas

For Mimas, we performed crater counts using the five best Voyager images. The resolution is highly variable, from 1.1 to 6.2 km pixel^{-1}. We divided the part of the surface that was well imaged by Voyager into 22 latitude-longitude quadrats, generally 30° × 30° in size. Unlike the situation on Rhea, we cannot make a meaningful tabulation of the spatial variability of N_{8km} on Mimas. The resolution is too variable, and over much of the satellite it is insufficient to allow recognition of 8 km craters. However, craters larger than 16 km can be recognized with a fair degree of certainty in all of the quadrats. In Figures 11 and 12 we show the spatial distribution of craters with $D \geq 16$ km and $D \geq 32$ km, respectively. There is only one crater observed with $D \geq 64$ km on Mimas, the 140 km crater Herschel.

Plescia and Boyce [1982] noted that the south polar region of Mimas is lacking in large craters, and suggested that this observation might be an indicator of resurfacing there. Our counts also show this lack of craters. The plot of craters with $D \geq 32$ km (Fig. 12) shows that there are no craters in this size range in the region south of −30°, west of 270°, and east of 30°.

We have performed a statistical analysis for the Mimas results like the one done for Rhea. The 16 km craters on Mimas give a χ^2 with 3 degrees of freedom value of $X^2 = 1.5$, which is lower than that expected for two-thirds of an ensemble of randomly generated crater distributions using the same number of total craters and equal-sized quadrats. Therefore, the pattern of $D \geq 16$ km craters is consistent with a surface of uniform age with little or no endogenic resurfacing. When we look at craters with $D \geq 32$, their overall paucity on Mimas renders any conclusions about local resurfacing statistically meaningless. An area

the size of the south polar region without craters of $D \geq 32$ km would occur in more than half of an ensemble of random distributions with the same total number of craters.

Figure 13 presents size-frequency curves for all of the craters counted on Mimas. The points shown as circles are for the 22 latitude-longitude quadrats counted, while the points shown as triangles are for the entire area of the satellite on which craters with $D \geq 64$ would be visible if present. Figure 13 also shows the curve for N_{HC}.

As on Rhea, there are three segments to the Mimas crater curve if one compares it to N_{HC}. At diameters smaller than about 10 km the curve lies below N_{HC}; this dropoff is due to the poor resolution of some of the images. From 10 km to perhaps 25–30 km, the curve lies close to N_{HC}. At diameters larger than 25–30 km, the curve drops well below N_{HC}, although it approaches it again at the largest sizes due to the one large crater Herschel (which has a diameter more than 70% the radius of Mimas). Like Rhea, then, Mimas shows no convincing evidence for local geologic resurfacing and is not saturated with large craters.

V. Iapetus

The Voyager data for Iapetus are substantially poorer than for Rhea or Mimas. Figure 14a shows the highest resolution image of Iapetus. The resolution is 8.8 km pixel^{-1}. The image was high-pass filtered and then contrast enhanced to maximize the visibility of topographic features. Most of the area observed lies in Iapetus' bright north polar region and trailing hemisphere; dark material on the leading hemisphere is visible along the limb. Due to the poor resolution of the data, it is not possible to achieve statistically significant results for crater counts subdivided by latitude-longitude quadrats. Accordingly, we have counted craters in a single large region, shown in Figure 14b. The boundary delineates the region in which we feel photometric factors allow recognition of craters with $D \geq 32$ km. The surface area of the region was determined by transformation to an equal-area projection and numerical integration, and is 9.0×10^6 km^2. Figure 14b also shows the locations and diameters of all the craters identified with $D \geq 32$ km.

The cumulative crater curve for Iapetus is shown in Figure 15. Our data are in agreement with those of *Plescia and Boyce* [1983] at large diameters. At smaller diameters,

their counts are significantly higher than ours. They examined a total area of 8.11×10^5 km^2 (90% of the area we counted), and reported a density of craters with $D \geq 30$ km of 205 ± 16 per 10^6 km^2. Their results would imply 157 ± 13 craters with $D \geq 32$ km in our counting area. We found only 55. In order to investigate possible image processing effects on image interpretability, we examined and processed the original digital data, applying a variety of filters and contrast stretches. This procedure produced no significant improvement over the image in Figure 14a, and yielded no more craters. We are therefore unable to resolve the discrepancy between their results and ours at small diameters.

At large diameters ($D \geq 64$ km) we find that the crater density on Iapetus is higher than on Rhea or Mimas, though still significantly less than N_{HC}. A linear least squares fit to the size-frequency distribution of craters with $D \geq 64$ km yields the expression

$$\log_{10} N_L = -2.70 \log_{10} D + 0.109 \qquad (5)$$

The slope of the curve is therefore very similar to that for Rhea, but is shifted upward to slightly higher crater densitities.

VI. 'ther Satellites

Because we are most interested here in heavily cratered terrains, we have restricted our crater counts to Mimas, Rhea, and Iapetus. However, counts on several other satellites are also of some relevance to our goals, and we discuss them briefly here. Unless noted otherwise, the results summarized in this section are from *Plescia and Boyce* [1982, 1983].

As mentioned in Section II, Tethys and Dione both show evidence for local geologic resurfacing. The densities of large craters show significant variability across the surfaces of these satellites. Both satellites have areas of very heavily cratered terrain. The crater curves for the heavily cratered areas, though based on relatively poor images and hence poor statistics, are similar in both shape and overall crater density to the Rhea data. Evidence for local resurfacing is provided by the regions of reduced crater density. On Dione, this evidence is unequivocal, as there are broad regions in which the crater density is substantially reduced relative to other surfaces in the Saturn system. By anyone's reckoning, these surfaces are not close to crater saturation equilibrium. Moreover, the curves for these

regions are much steeper than the curve for Rhea at diameters less than 32 km. Their slopes are similar, however, to that of the Rhea curve at larger diameters. The impactors responsible for the cratering of the resurfaced regions on Dione were regarded by *Smith et al.* [1982] as a separate population: population II, which is characterized by a relative shortage of large impactors. On Tethys, while there is also clear evidence for resurfacing, it is less striking. The density on the most lightly cratered terrains is less than on the most heavily cratered terrains, but well above that on Dione's least cratered regions.

Enceladus has substantial regions that are completely free of craters at Voyager resolution. Other regions are as heavily cratered as any other surfaces in the Saturn system. The slope of the curve for the heavily cratered regions on Enceladus is statistically indistinguishable from the slope for heavily cratered regions on Rhea. Curiously, *Plescia and Boyce* [1983] attribute this cratering to population II, apparently because there are no craters larger than 30 km. However, the area observed in the Voyager images is so small ($\sim 1.3 \times 10^4$ km^2, much smaller than our smallest quadrat on Rhea) that no craters larger than 30 km need be expected, even for a population I (*i.e.*, Rhea-like) distribution.

The only other satellites on which crater counts even can be attempted are the small, irregular satellites Hyperion, Janus (1980S1), and Epimethius (1980S3). For all three, image resolution and crater statistics are very poor. It appears that all three are very heavily cratered. Crater densities quoted for Hyperion by *Plescia and Boyce* [1983] are comparable to those that we find for Rhea. The densities they quote for Janus and Epimethius are more than a factor of three higher. *Thomas et al.* [1986] have also presented crater counts for these three satellites. Their results for all three are substantially lower than those of *Plescia and Boyce* at small diameters, by factors ranging from 2 (for Hyperion) to 6 (for Janus). More than anything else, these counts illustrate the uncertainty in counts of craters near the limit of resolution. However, the high crater densities are clearly consistent with the impression given by the satellites' shapes: that they are collisional fragments.

VII. Crater Scaling and Disruptive Impacts

In order to extrapolate the cratering record observed on a given satellite to other satellites in the Saturn system, a crater scaling law is needed. However, the physics of cratering

and catastrophic disruption is extremely complex, and it is not yet possible to predict crater diameters from first principles even when all of the properties of the projectile and target are well understood. *Holsapple and Schmidt* [1982] have placed theoretical bounds on how crater diameter scales with the energy and momentum of the impactor and with the surface gravity and strength of the target; *Holsapple and Housen* [1986] have placed similar limits for scaling of disruptive impacts. However, these general bounds are sufficiently broad that a wide range of scaling laws is possible, and they do not provide any direct connection between crater-producing impacts and disruptive impacts. Also, the scaling depends on many variables that are poorly known (*e.g.*, strengths of satellite surfaces) or are interconnected (*e.g.*, energy and momenta of the impactors), making the problem even more complex.

The diameters of craters produced by explosives in the Nevada desert are well-fitted by a $D \propto E^{1/3.4}$ scaling law, where E denotes energy [*Chabai*, 1959]. *Shoemaker and Wolfe* [1982] have generalized this result to allow for scaling from one celestial body to another. Their formula can be written in c.g.s. units as:

$$D = 0.06\left(\frac{R_m^2}{GM_m}\right)^{1/6}\left(\frac{E}{\rho_c}\right)^{1/3.4} \tag{6}$$

where E is the kinetic energy of the impactor, M_m and R_m are the mass and radius of the moon in question, and ρ_c is the density of the moon's crust, which for simplicity we shall assume to be the same for all of the moons in question. Equation (6) and very similar scaling formulae have been used by *Smith et al.* [1982, 1986] and in most other planetary impact studies. However, the explosion-produced craters on which Eq. (6) is based are far from ideal analogs for the large planetary impact craters that concern us. *Holsapple and Schmidt* [1979, 1982] have attributed the 1/3.4 energy scaling to a transition between the strength scaling regime in which $D \propto E^{1/3}$ and the gravity regime where the exponent is bounded between 1/3.5 and 1/4; using only data for the largest desert explosions, they find a 1/3.6 power-law slope. Moreover, impact crater size depends on the momentum of the projectile as well as its energy [*Holsapple and Schmidt*, 1982].

Laboratory impact experiments differ greatly in size from the craters with which we are concerned, so extrapolation is very difficult. However, hypervelocity impact craters in water probably provide the best available analog, as Saturn's moons are likely to be

less porous than laboratory sand. Using the laboratory results of *Gault and Sonett* [1982], *Schmidt and Holsapple* [1982] deduce the scaling relationship

$$D \propto v_c^{0.45} d^{0.78} \tag{7}$$

where v_c is the collision velocity and d is the projectile's diameter. We have omitted the constant of proportionality in Eq. (7) because the extrapolation required is too great to be justified by either the data or by our understanding of the physics [*K. Holsapple, private communication*]. Equation (7) implies that crater diameter scales with impact energy to the 0.26 power as impactor size varies (constant v_c) and energy to the 0.225 power as collision velocity varies (constant d). Since we are interested in scaling a fixed population of impactors that vary in impact velocity through the Saturn system, it is the latter exponent that concerns us here. Therefore, an alternate scaling relation to that given by Eq. (6) has the form

$$D \propto \left(\frac{R_m^2}{M_m} \right)^{1/6} E^{1/4.44} \tag{8}$$

We will use Eq. (6) and Eq. (8) alternatively, together with the intermoon mean velocity scaling (Section VIII), in order to scale crater diameters among the saturnian moons.

Scaling crater-forming impacts to disruptive impacts is even more uncertain than scaling crater sizes with impact energy and target properties. *Smith et al.* [1982, 1986] make the simple but reasonable assumption that catastrophic disruption requires an impact that would produce a crater greater in diameter than the satellite. Let us say more generally that disruption occurs for a crater of critical diameter $D_c = 2kR_m$, where k is expected to be of order unity. Equation (6) can be inverted to determine the energy necessary for an impact to produce a crater of diameter D_c:

$$E_{D_c} = 2.9 M_m^{47/30} (kR_m)^{-11/15} \tag{9}$$

where we have assumed that the satellite's bulk density equals its surface density and c.g.s. units have again been used. (The proportionality relationship (8) cannot be used here because it contains an unspecified constant.)

In order to cause catastrophic disruption, an impact must supply enough energy to both fracture the moon and disperse the fragments. The energy required for fracture is

$$E_F = S M_m \tag{10}$$

where the impact strength $S \approx 3 \times 10^5$ erg g^{-1} for ice [*Hartmann*, 1978]. The gravitational binding energy of a homogeneous spherical body is:

$$E_G = \frac{3}{5}\frac{GM^2}{R} = 4.1 \times 10^{-8} M_m^2 R_m^{-1}. \quad (11)$$

Therefore, the total impact energy required to fragment and disperse an icy moon is approximately

$$E_I = E_F + E_G = 3{\times}10^5 M_m + 4.1{\times}10^{-8} M_m^2 R_m^{-1}. \quad (12)$$

The two terms on the right hand side of Eq. (12) are comparable for an icy moon ~12 km in radius; the strength term dominates for smaller moons and the gravitational term for larger moons.

Note that the functional dependancies of Eqs. (9) and (12) differ. This difference is due to the fact that crater diameter depends on many factors, some of which are not accounted for in Eq. (12). Equations (9) and (12) should both be acceptable estimates of the energy required to disrupt Saturn's icy moons. Equation (12) may underestimate the energy necessary for catastrophic disruption especially for small moons because "losses" occur due to impact heating, which increases at higher velocities, and to the kinetic energy "at infinity" of the fastest moving ejecta. On the other hand, not all of the gravitational binding energy must be supplied if by "catastrophic fragmentation" we only require sufficient fragmentation and ejection that the moon is completely resurfaced, and that all evidence of cratering (including the catastrophic event itself) is erased. Nonetheless it is (deceptively) reassuring that Eqs. (9) and (12) agree to within a factor of 10% for Mimas. The ratio of energies required by the two expressions varies as $R_m^{14/15}$ for large (gravitationally dominated) moons of identical density.

VIII. Relative Cratering Rates on Saturn's Moons

We now wish to use the crater scaling laws discussed in the previous section to extrapolate the cratering records on Rhea and Iapetus to other parts of the Saturn system. Both heliocentric and planetocentric impactors can and do produce craters on these satellites. However, circumplanetary debris from fragmented satellites or other sources could be distributed extremely nonuniformly in radial position. Therefore, it is impossible to compute

relative crater production rates on moons due to impacts of projectiles in planetocentric orbits. Fortunately, impacts from planetocentric debris are unlikely to be responsible for a significant fraction of the larger craters that are the major concern of this work.

Debris orbiting Saturn on satellite-crossing orbits inwards of Rhea typically collides with a moon within $10^3 - 10^4$ years [*Horedt and Neukum*, 1984]. These lifetimes assume debris on orbits with eccentricities of 0.6 and inclinations of 15°. Lifetimes are approximately proportional to $(\sin i)$ [*Öpik*, 1951], so debris in near-polar orbits would have lifetimes ~ 4 times as long; however, such trajectories would not be expected if Saturn's moons accreted from a dissipative equatorial disk. Highly eccentric trajectories could increase survival times by allowing debris with larger semi-major axes, and thus longer orbital periods, to be in orbits intersecting the paths of the inner moons. However, in addition to cosmogonic difficulties in populating such orbits, Titan would rapidly sweep up debris crossing its orbit, and particles with orbital periods greater than a few years would be removed from saturnocentric orbit by solar perturbations. Long-term storage of debris in the inner Saturn system could only be accomplished in resonant orbits that prevent close approaches (such as libration about the L_4 and L_5 triangular Lagrange points of a moon's orbit) or in relatively circular orbits between the moons. Such material would impact at very low velocities, similar to the velocity of debris ejected from the moons by hypervelocity impacts. Therefore, unless the cratering record is a remnant of the early stages of the moons' formation, the preponderance of large craters in the inner Saturn system must be due to heliocentric projectiles. Sweepup times for Iapetus-crossing debris are three orders of magnitude longer [*Horedt and Neukum*, 1984], so moderately high velocity saturnocentric debris cannot be ruled out as a major source of cratering on Iapetus.

Bodies in heliocentric orbits, such as comets, present a much more predictable distribution of potential impactors. This regularity allows the relative crater production rates from heliocentric debris to be computed, provided several simplifying assumptions are made [*Shoemaker and Wolfe*, 1982; *Horedt and Neukum* 1984]. Our treatment presented below is somewhat more detailed than that of *Shoemaker and Wolfe* [1982, applied to the Galilean satellites of Jupiter], which was used by *Smith et al.* [1982, 1986] to compute relative cratering rates on the moons of Saturn and Uranus respectively, and reduces the number of assumptions required.

We assume that impactors are in heliocentric orbits which are uniformly distributed with respect to Saturn prior to feeling the gravitational focussing effects of the planet. We consider two classes of cometary orbits. "Saturn family" comets and remnant planetesimals have semi-major axes comparable to that of Saturn, are predominately in low-inclination prograde orbits, and approach Saturn from all directions with roughly equal probability. "New" comets from the Oort cloud move in nearly parabolic orbits with velocities scattered about a mean value of zero in the Sun's rest frame. New comets thus suffer a systematic aberration in Saturn's rest frame. However, since the effect of variations in radiant directions due to this abberation is comparable for all of the moons being considered, we shall not include it in our computations of relative cratering rates.

The major differences in cratering rates from one moon to another are due to gravitational focussing by Saturn, which increases both impactor fluxes and impact energies close to the planet [*Shoemaker and Wolfe*, 1982]. Gravitational focussing by the moons themselves has a $\sim 1\%$ effect on cratering rates on the satellites with which we are concerned; nevertheless, we include it so that our formulae will also be applicable to larger moons such as the Galilean satellites and Titan. We also include two effects omitted by *Shoemaker and Wolfe* [1982]: aberration due to the moon's orbital motion about Saturn, which increases both impact velocities and rates, and interception of comets by the planet, which decreases impact fluxes especially for moons close to Saturn.

Let v_∞ be an impactor's velocity relative to Saturn "at infinity," *i.e.*, at the point where Saturn's gravity becomes more important than the Sun's tidal force in determining the trajectory of the impactor relative to Saturn. At a distance r from Saturn's center, the flux of projectiles measured in Saturn's rest frame is

$$n(r, v_\infty) = 1 + \frac{2GM_p}{rv_\infty^2} \tag{13}$$

where M_p denotes the planet's mass and n has been normalized to a value of unity in the absence of gravitational perturbations and collisions with the planet.

The primary effect of aberration due to the satellite's orbital motion about the planet is to increase cratering on the leading hemisphere and decrease it on the trailing hemisphere [*Cook and Franklin*, 1971]. (In order to fully account for the effects of aberration, the location as well as the size of each large crater on the reference satellite would have to be

measured and used in order to derive the mass distribution of impacting debris. This projectile flux would then have to be projected to determine expected cratering rates and disruption frequencies on other moons, again taking into account variations with position relative to the apex. Calculations of apex/antapex cratering asymmetries are quite tedious [*Cook and Franklin*, 1971; *Cuzzi and Durisen*, 1988]. Moreover, these cratering asymmetries are highly dependent on the distribution of v_∞ among the impactors. The uncertainties in projecting satellite-averaged impact rates and velocities due to our incomplete knowledge of v_∞ (see Table 4) is probably greater than that due to our neglect of hemispheric asymmetries. Note, however, that omitting apex/antapex asymmetries from our calculations results in a slight but systematic underestimate of disruption probabilities due to near-apex impacts on moons orbiting interior to the reference moons.)

In addition to creating apex/antapex asymmetries, aberration increases the RMS velocity of the comets relative to the satellite, causing an increase in the number of impacts by a factor of

$$\frac{(v_i{}^2 + v_m^2)^{1/2}}{v_i} = \frac{\left(v_\infty^2 + \frac{3GM_p}{r_m}\right)^{1/2}}{\left(v_\infty^2 + \frac{2GM_p}{r_m}\right)^{1/2}} \tag{14}$$

where v_i and v_m are the velocities of the comet and the moon (assumed to be on a circular orbit of radius r_m) with respect to Saturn. Impact energy is increased by the square of this quantity. Note the maximum possible effect of this aberration on impact flux is $\sqrt{3/2}$.

The gravitational attraction of the moon itself increases the impact rate by a factor of

$$A_m = 1 + \frac{2GM_m}{R_m\left(v_\infty^2 + \frac{3GM_p}{r_m}\right)} \tag{15}$$

where M_m, and R_m are the mass and radius of the moon.

For a moon orbiting near Saturn, a significant fraction of potential outbound (post-periapse) impactors will never arrive due to collisions with the planet. The simplest estimation of the reduction in outbound impactor flux due to planetary collisions would be to subtract the fraction of comets passing within the moon's orbit that actually collide with Saturn. However, such a correction would overestimate the effect of planetary collisions because the low angular momentum bodies that hit the planet have more nearly radial velocities (with respect to the planet) at the moon's orbit, and thus have less chance of

encountering the moon. A better approximation is to compute this ratio after weighting each impactor by the amount of time it spends crossing the moon's orbit, $1/v_r(r_m)$, where $v_r(r_m)$ is the radial component of the projectile's velocity (with respect to the planet) at the moon's orbital radius. Conservation of angular momentum gives

$$b_0 v_\infty = r\left[v^2(r) - v_r^2(r)\right]^{1/2} = b_f\left(v_\infty^2 + \frac{2GM_p}{b_f}\right)^{1/2} \tag{16}$$

where b_0 is the unperturbed planetary impact parameter and b_f is the actual closest approach distance to the planet. The radial velocity of the projectile can be derived from Eq. (16) and conservation of energy:

$$v_r^2 = \left[1 - \left(\frac{b_0}{r}\right)^2\right] v_\infty^2 + \frac{2GM_p}{r} \tag{17}$$

Therefore, the fraction of potential impactors crossing the moon's orbits that are lost due to collisions with a spherical planet of radius R_p is

$$f_o = \frac{\int_0^{b_f=R_p} \frac{b_0 db_0}{v_r(r_m)}}{\int_0^{b_f=r_m} \frac{b_0 db_0}{v_r(r_m)}} \tag{18}$$

The overall fraction of impacts lost is 1/2 the value given by Eq. (18), as inbound projectiles can hit a moon even if $b_f < R_p$. The fraction of impacts *not* lost to planetary collisions is found from Eq. (18) to be:

$$f_i = \frac{1}{2} + \frac{1}{2}\left[1 - \left(\frac{R_p}{r_m}\right)^2 \left(\frac{v_\infty^2 + \frac{2GM_p}{R_p}}{v_\infty^2 + \frac{2GM_p}{r_m}}\right)\right]^{1/2} \tag{19}$$

The fraction of potential impacts lost to planetary collisions, $1 - f_i$, is 11% for v_∞ = 10 km s^{-1} at the orbit of the satellite Prometheus and smaller for moons farther from Saturn and projectiles moving at faster v_∞. The overall impact rate can be computed from Eqs. (13), (14), (15), and (19):

$$\begin{aligned} n_c(M_p, R_p, M_m, R_m, r_m, v_\infty) &= \left(1 + \frac{3GM_p}{r_m v_\infty^2}\right)^{1/2} \left(1 + \frac{2GM_p}{r_m v_\infty^2}\right)^{1/2} \\ &\times \left(\frac{1}{2} + \frac{1}{2}\left[1 - \left(\frac{R_p}{r_m}\right)^2 \frac{v_\infty^2 + \frac{2GM_p}{R_p}}{v_\infty^2 + \frac{2GM_p}{r_m}}\right]^{1/2}\right) \\ &\times \left(1 + \frac{2GM_m}{R_m\left(v_\infty^2 + \frac{3GM_p}{r_m}\right)}\right) \end{aligned} \tag{20}$$

where the terms on the left hand side of Eq. (20) are listed in decreasing order of importance for all of the moons under consideration.

The mean impact velocity varies from moon to moon due to gravitational accelerations by the planet and the moon and also due to the moon's orbital motion. Collisions with the planet preferentially remove bodies with predominantly radial saturnocentric velocities at the moons' orbits. Projectiles with saturnocentric velocities parallel and antiparallel to the moons which they impact are unaffected. Therefore, although collisional removal increases the variance in impact velocities, the mean velocity of impact on any given moon remains the same to first order. The mean impact velocity is

$$\bar{v}(v_\infty, r_m, M_p, M_m, R_m) = \left(v_\infty^2 + \frac{3GM_p}{r_m} + \frac{2GM_m}{R_m}\right) . \tag{21}$$

Equations (20) and (21) must be viewed as approximations due to all of the assumptions made in deriving them. In addition to the assumptions stated above, we have assumed that v_∞ is large enough that the Sun has neglible influence on the encounter of the comet with the Saturn system. This requires

$$v_\infty^2 \gg \frac{GM_p^{2/3}M_\odot^{1/3}}{r_p} \tag{22}$$

where $M_\odot$ is the mass of the Sun and r_p is the distance between the Sun and the planet. For Saturn, v_∞ of a few km/sec, much less than that of most comets, satisfies this criterion. The planet is assumed to be spherical, both in its impact cross section and its dynamical effects (*i.e.*, orbital trajectories are assumed to be conic sections with one focus at the planet's center). Even for Saturn, the most oblate planet in the solar system, this approximation is very good. Averaging has been performed separately for several of the effects included, so possible correlations among these effects have been neglected. The largest "averaging" error is due to our neglect of the apex/antapex cratering asymmetry, which has already been discussed in some detail. Most of the other approximations induce errors at the few percent level. The major uncertainties in our analysis involve the distribution of v_∞, crater scaling laws, and, above all, the impact energy required for catastrophic disruption.

The results of our dynamical calculations are presented in Tables 3 and 4. In Table 3 we list relative impact rates per unit surface area (Eq. (20)), mean projectile velocities (Eq. (21)), and relative crater diameters for impactors of the same mass and v_∞ for several

saturnian moons. We include separate columns for Saturn family comets (v_∞ = 10km/sec) and Oort cloud comets (v_∞ = 16.6 km/sec), which are focussed less by Saturn due to their greater velocity. For computing relative crater diameters, we use both *Shoemaker and Wolfe's* [1982] crater scaling law (Eq. (6), denoted by "SW") and *Schmidt and Holsapple's* [1982] crater scaling law (Eq. (8), denoted by "SH").

In Table 4, we estimate disruption frequencies based on the cratering record observed on Rhea and Iapetus. Again, we tabulate our results for impactors with $v_\infty = 10$ km s^{-1} and with $v_\infty = 16.6$ km s^{-1} and the crater scaling laws given by Eqs. (6) and (8). For each combination of parameters used, we tabulate the size of the crater created on Rhea by an impactor energetic enough to disrupt the moon in question (using the criterion $D_c = 2R_m$). These results may be scaled to equivalent crater sizes on Iapetus using the formulae listed in Table 4's footnotes. We also list the estimated number of disruptive impacts since the last global resurfacing of Rhea or Iapetus for each combination of v_∞ and crater scaling law.

The "disruption frequency" listed in Table 4 is the mean of the Poisson distribution that specifies the probability of the number of disruptions of the moon in question since the last global resurfacing on Rhea or Iapetus. In the cases where the probabilities of disruption of Rhea and Iapetus are estimated from their own cratering records, the estimates are *a priori*, based on extrapolating the measured crater distribution to larger sizes capable of disrupting the moon. The *a posteriori* probabilities of disruption since the last global resurfacing are, of course, zero. Note that all of our disruption frequencies are significantly smaller than those of *Smith et al.* [1982].

IX. Discussion

Disruption Probabilities from Crater Scaling

The disruption frequencies listed in Table 4 have some important implications. Significantly larger disruption frequencies are calculated by scaling to Iapetus rather than Rhea. This fact implies that either Iapetus' surface is older than Rhea's, or that Iapetus' cratering record preserves large impacts by a population of planetocentric debris which did not cross

Rhea's orbit. In the latter case the scaling of the Iapetus record to other satellites would be invalid except for Hyperion and possibly Phoebe. A population of heliocentric impactors with smaller v_∞ is focussed more by the planet and therefore produces a larger gradient in cratering rate as a function of distance from the planet (Table 3). This accounts for the fact that larger disruption probabilities are calculated assuming $v_\infty = 10$ km s^{-1} than assuming $v_\infty = 16.6$ km s^{-1} (except in the cases where the moon in question is located farther from Saturn than the moon whose cratering record is used to establish the chronology). The higher disruption frequencies computed by *Smith et al.* [1982] may be due to their assuming $v_\infty < 10$ km/sec. Changing the crater scaling law from that of *Shoemaker and Wolfe* [1982] (Eq. (6)) to that of *Schmidt and Holsapple* [1982] (Eq. (8)) decreases the sensitivity of crater size to impact energy and results in changes similar to increasing v_∞, although the magnitude is smaller.

Our estimates for disruption frequency of a given moon vary by approximately an order of magnitude depending on the moon whose cratering record is being scaled to, the v_∞ assumed for the impactors and the crater scaling law used. This fact prevents a definitive interpretation of the quantities listed in Table 4. Nonetheless, we believe it noteworthy that our results are clearly consistant with Mimas and other spherical moons being original aggregates, and the smaller, irregular "ringmoons" being collisional fragments.

Saturn's rings may also be the remnants of a catastrophically disrupted moon (or several smaller moons, which would have been easier to fragment) ground down by repeated impacts, and unable to reaccrete because they are inside Saturn's Roche limit for tidal disruption. However, it is not known how a moon could be formed (or moved to) this close to Saturn. Additionally, if we assume that the heavy bombardment epoch in the Saturn system was contemporaneous with that on Earth's Moon, a disruptive impact is most likely to have occurred prior to 4×10^9 years ago. Such a non-primordial origin of the rings would not eliminate the "short timescale" problems of rapid ring/ringmoon evolution due to density wave torques [*Goldreich and Tremaine* 1982; *Lissauer et al.* 1984, 1985] and micrometeorite erosion [*Northrop and Connerney* 1987].

Hyperion's irregular figure implies that it has been shaped by one or more very large impacts [*Smith et al.,* 1982]. However, we compute smaller disruption probabilities for Hyperion than for Mimas, Enceladus, and in the case of slower, more focussed impactors,

Tethys. The disruption probabilities are large enough that a chance major impact is not that unlikely; nonetheless we would prefer a less *ad hoc* explanation. As mentioned above, the Iapetus scaling almost certainly applies to Hyperion, even if Iapetus' cratering record is due in large part to a population of circumsaturnian debris absent inside the orbit of Titan. Moreover, the dynamical environment near the 4:3 resonance with Titan can induce large non-circular motions in an initially quiescent disk of impactors. (Note Hyperion's large forced eccentricity at the present epoch.) The resulting rapid collision velocities could lead to a disruptive fragmentation, and Titan could sweepup the debris before reaccretion.

It is reassuring to note that Phoebe is unlikely to have been disrupted, as reaccretion of such a small body so far from Saturn is virtually impossible.

Large Impact Craters, Complete Crater Saturation, and Disruption

The "saturation density" of craters larger than a given size on the surface of a celestial body is determined by the physics of crater obliteration and the shape of the production function. For instance, moons that lack very large craters can support a larger density of small craters given sufficient time (*i.e.*, integrated flux of impactors) that crater production and obliteration have reached a (statistical) equilibrium. Assuming impacts are the only process for creating and destroying craters and that the shape (although not necessarily the magnitude) of the production function remains constant in time, then a surface is near crater saturation equilibrium if any crater which existed at or near the beginning of the bombardment has an *a priori* small chance of remaining identifiable. As larger craters are more difficult to wipe out than are smaller ones, the approach to saturation equilibrium will be fastest for craters of the smallest sizes, and gradually extend to larger craters.

The crater density at saturation equilibrium, especially for the larger size ranges, will be limited not only by the production of new craters but also by the possibility of disruptive impacts wiping out the entire previous cratering record. In the case of asteroids, a disruptive impact leaves permanent scars; either several asteroids are produced or, in a less catastrophic collision, a gravitationally bound rubble pile may result. However, in the case of Saturn's moons, a disruptive impact may not have such permanent consequences [*Smith et al.*, 1982; *Shoemaker*, 1984]. The dynamical environment of near-planet, circular

orbits makes reaccretion of most of the debris from fragmentation likely. Therefore, in the inner Saturn system, a true crater saturation equilibrium including disruptive impacts could, at least in theory, exist.

There is substantial evidence in the solar system for disruptive and near-disruptive impacts of the sort considered here. The best evidence for disruptive impacts comes from asteroid families. For example, pronounced spectral and orbital similarities indicate that the Themis, Eos, and Koronis asteroid families are each composed of collisional fragments of single parent bodies [*e.g., Gradie et al.*, 1979]. Increasingly strong evidence suggests that the Moon may have formed as a result of a near-disruptive impact on the Earth [*Hartmann and Davis*, 1975; *Cameron and Ward*, 1976; *Hartmann et al.*, 1986]. The high Fe content of Mercury may be due to partial collisional stripping of that planet's mantle [*Cameron and Benz*, 1987]. Very large impact basins provide the evidence for near-disruptive impacts. The largest confirmed impact basin in the inner solar system (relative to the size of the body on which it formed) is the South Pole-Aitken basin on the Moon, with a diameter 72% of the Moon's. The proposed lunar Procellarum basin [*Cadogan*, 1974; *Whitaker*, 1981; *Wilhelms*, 1982], if real, has a diameter 92% of the Moon's. On Mars, it has been suggested that the martian "hemispheric" dichotomy actually resulted from a very large impact in the northern hemisphere [*Wilhelms and Squyres*, 1984]. This "Borealis basin", if real, may have a diameter as large as 110% that of Mars. (Note that basin diameters are always measured along the arc of a planet or moon's surface.) Stickney, on Phobos, is 43% of Phobos' mean diameter. In the outer solar system, the largest impacts are Herschel on Mimas (36%), Odysseus on Tethys (41%), and a possible basin on Umbriel (43%) [*P. C. Thomas*, personal communication]. Using the energy-crater diameter relationship of Eq. (6) and the energy for disruption of Eq. (12), all of these confirmed and proposed basins are indeed below the size required for disruption.

If Saturn's inner moons have been disrupted and reaccreted many times during their history [*Smith et al.*, 1982], they should currently be in complete crater saturation equilibrium, unless some endogenic resurfacing mechanism operated (as it certainly must have in the case of Enceladus). Therefore, given an ensemble of moons, the extrapolation of their crater production curves to impacts energetic enough to catastrophically disrupt the moon (defined here as complete resurfacing, including obliteration of direct evidence of the

catastrophic impact itself) should give a probability of disruption of $\sim\frac{1}{2}$. Extrapolation of crater size-frequency curves on all of Saturn's nearly spherical moons (including Mimas) yields much smaller disruption probabilities, consistent with our conclusion derived from scaling the cratering flux at Rhea and Iapetus that these bodies are likely to be original aggregates.

Population I and Population II

As discussed previously, one of the major conclusions of the initial examination of the Saturn system by *Smith et al.* [1981, 1982] was that its moons have been bombarded by two impactor populations, termed population I and population II. Very ancient, heavily cratered moons (like Rhea) were interpreted as dominated by population I impacts. Younger surfaces (like resurfaced regions on Dione) were believed to have had their population I craters removed, and to have later undergone cratering by primarily population II impactors. Population II was interpreted to have a steeper size-frequency distribution (*i.e.*, fewer large craters) than population I. And indeed, it has been amply demonstrated by many sets of crater counts that locally resurfaced regions on the saturnian satellites have steeper crater curves than heavily cratered regions.

We cannot refute the hypothesis that the saturnian satellites were cratered by a second distinct population of impactors after local resurfacing took place on several of them. However, neither do we find compelling evidence to support it. The whole issue hinges on the saturation question. We are convinced that Mimas, Rhea, and Iapetus are not saturated at crater diameters larger than about 64 km, so that we are seeing something like a production population at those diameters. At smaller diameters, however, we have presented evidence from the spatial distribution of craters on Rhea that Rhea's surface may be near (but is not necessarily at) saturation. Additionally, the size-frequency distribution of craters in the 16-32 km diameter range is close to the magnitude of *Hartmann's* [1984] empirical saturation curve (see Figure 10) and of results obtained in experimental saturation studies [*Gault*, 1970]. Also, the slope of the size-frequency curve is near the theoretically expected saturation slope of $\sim$2 for steep crater production functions [*Marcus*, 1970]. The need to invoke another distinct population depends on whether the curve at smaller diameters significantly deviates from the shape of the production population. If it does not, then there

must have been two populations of impactors. However, if the surface is saturated, then a single population could suffice. This population would have a slope steeper than that presently observed for diameters smaller than $\sim$ 32 km on Rhea; the flattening of the curve in this size range would be attributed to saturation. In this context, it is worth noting that the slope of the curve observed at large diameters on Rhea is very similar to that found for population II-cratered regions on Dione and Tethys (although the craters on Dione lie at smaller diameters and there is no reason *a priori* to assume that the population would have a constant slope over all diameters).

How do these arguments fit in with the cratering record observed in the rest of the solar system? The situation on the satellites of Jupiter, Saturn, and Uranus can be generally summarized as follows: The oldest surfaces observed exhibit crater size-frequency distributions that, at small diameters, resemble *Hartmann's* [1984] empirical saturation curve. This observation is true for Callisto, Mimas, Rhea, Iapetus, Miranda's heavily cratered terrain, Umbriel, and Oberon. For some of these bodies (at least Callisto, Mimas, Rhea, and Iapetus), the size-frequency distribution drops below the N_{HC} line at large diameters. Younger surfaces, for example on Dione, Miranda's resurfaced terrain, and Ariel, show lower overall crater densities and steeper size-frequency distributions over the entire diameter range observed. So one fact that emerges for the entire outer solar system is that all of the production populations conclusively observed there have slopes at large diameters that are steeper than N_{HC}, and that are steeper than the major production population found in the inner solar system.

The question of whether or not a number of distinct production populations are required throughout the outer solar system, however, again hinges on the saturation issue. If there are no saturated surfaces, then two populations are required in the uranian system just as in the saturnian system, and the jovian production population must have a sharp inflection at about 50 km. However, if saturation does occur at small diameters, the picture is much simpler. We would then conclude that Callisto, Mimas, Rhea, Iapetus, Miranda's heavily cratered terrain, Umbriel, and Oberon are all saturated at small diameters. A single production population would suffice for each of the three satellite systems, with the observed inflections in size-frequency distributions on the most ancient surfaces all due to saturation effects. In fact, the production populations would be rather similar throughout

the outer solar system, though all markedly steeper than what is found in the inner solar system. Again, the issue cannot be resolved without better understanding of the saturation phenomenon.

The Age of Saturn's Rings

Our calculations of the flux of projectiles impinging on the Saturn system can be used to assess the hypothesis that Saturn's rings may have been created by catastrophic disruption of a small moon [*Pollack* et al., 1973]. The first line in Table 4 indicates that a moon located in the middle of Saturn's main rings that was large enough to account for the mass of the present ring system could well have been disrupted since the last global resurfacing on Rhea or Iapetus. The next few lines imply that disruption of several smaller moons located in the same region would have been even more probable; this result is also applicable to subsequent grind-down of the fragments of a catastrophic disruption of a larger moon. Thus, we conclude that the impact flux has been sufficient to produce the rings by disruption of one or many pre-existing inner saturnian moons.

If Saturn's rings were formed by impact disruption of a small moon, they are most likely to be ancient. While we know very little about the impact flux in the outer part of the solar system, it seems probable that most of the bombardment was, as in the inner solar system, concentrated in the first half billion years or so. Given this likelihood and the disruption probabilities we calculate, collisional formation of the rings is only very likely early in the history of the Saturn system. The rapid evolution of Saturn's rings predicted from angular momentum removal by density waves at resonances [*Goldreich and Tremaine*, 1982] and mass and angular momentum loss due to erosion [*Northrup and Connerney*, 1987] suggest that the saturnian rings may be young. However, if this is the case, origin by collision requires an unlikely event.

While we find that an early collisional origin for the rings is possible, we do not find compelling evidence for it. The principal argument against an impact origin for the rings is that it is difficult to form a moon that close to Saturn. Ring particles presumably do not accrete into moons at the present due to tidal forces caused by their proximity to the planet; the same forces would have prevented formation of a ring parent moon 4.5×10^9

years ago. Therefore, some *ad hoc* ring parent near Saturn must be assumed. Alternatively, it is possible that the rings are the inner remnant of a viscously-spreading accretion disk produced as a result of fragmentation of a moon just exterior to Saturn's Roche limit. However, this scenario would require fragmentation of a more massive moon, in order to account for the material in the disk that must have moved outward in order to conserve angular momentum. In summary, we have not solved the problem of the origin of Saturn's rings. An ancient collisional origin is quite possible if there was some way of placing a moon sufficiently close to Saturn; a recent collisional origin is much less likely.

X. Conclusions

We have examined the cratering record on Saturn's moons, concentrating on the oldest, most heavily cratered surfaces. We find no statistically significant evidence for local endogenic resurfacing of either Rhea (Section III) or Mimas (Section IV). Craters larger than 32 km in diameter on Rhea are in fact distributed more uniformly than a majority of randomly-produced spatial patterns. This observation suggests that the major destruction mechanism for craters larger than 32 km on Rhea is the production of craters of similar size, and that Rhea's surface is at least approaching saturation for craters in this size range.

The density of craters in diameter bins 64 km and larger on Iapetus is approximately 50% greater than that on Rhea (Section V). As gravitational focussing by Saturn should increase the cratering rate by heliocentric projectiles on Rhea relative to that on Iapetus, this result implies that either Iapetus' surface is older than Rhea's or that Iapetus was bombarded by a population of saturnocentric debris that did not cross Rhea's orbit (Section IX).

We have extrapolated the cratering records on Rhea and Iapetus to Saturn's inner moons assuming the impactors were in cometary orbits (Section VIII). Our results are consistent with Mimas and larger moons being original aggregates and the smaller irregular moons being collisional fragments (Table 4). The cratering records on Mimas and larger moons support this conclusion: satellites being repeatedly disrupted and reaccreted would have much greater crater density than that observed most of the time even if reaccretion

resulted in a pristine surface (Section IX). We find that Saturn's rings could have had a collisional origin; however, if this is the case they are probably ancient.

All of our results must be regarded as tentative to the extent that Voyager data are incomplete. A Saturn orbiter is needed to provide the data for a definitive analysis of the bombardment history and physical evolution of the Saturn system. Onward Cassini!

Appendix: Consistency of Crater Count Statistics

In this appendix we address the following question: To what degree of consistency and empirical uncertainty can different observers characterize the crater diameter distribution on a heavily cratered planetary surface? While those of us who use crater densities to investigate planetary surfaces do not like to admit it, the subjective judgement of the crater counter as to what is and what is not a crater plays a significant role in the crater counting process. This is particularly true for terrains where many craters are highly degraded. The counts of craters on Rhea and Mimas, because they were originally performed independently by two individuals (SWS and WKH), and because statistical tests showed no evidence for endogenically-caused non-randomness in the spatial distributions of craters, offer an opportunity to investigate the importance of subjectivity. We make two comparisons: (1) of size-frequency plots generated independently by SWS and WKH, and (2) of individual crater-by-crater diameter and position determinations of all the observed craters on Rhea with $D \geq 32$ km. In our analysis here, we also include counts for areas on Rhea and Mimas made by WKH in 1983, using the "nesting photo" technique described by *Hartmann* [1984]. For counts made for this paper during 1986-87, SWS and WKH both used the technique described in the text, although SWS counted to lower resolution limit than WKH in all quadrats. Thus, the small craters in SWS's data set are from the whole region, while the small craters in WKH's data sets come primarily from the 1983 nested photo technique with small craters counted only in certain regions.

Size-Frequency Curves

A useful format for comparison of counts independently in each diameter bin is that of Figure A1. This figure is not cumulative like those in the main body of the text. Rather, it plots the incremental diameter distribution; *i.e.*, the crater density in each logarithmic diameter bin of width D to $\sqrt{2}D$. We compare WKH's various data sets for Rhea with that generated by SWS. This comparison allows a test of consistency; the scatter among the different data points in each diameter bin is an empirical measure of the repeatability and precision of the crater density characterization at that diameter. Data points representing fewer than six craters in a diameter bin (usually representing the largest, scarcest craters)

are distinguished from the higher quality (in a statistical sense) data points with more than six craters. WKH's individual photos counted in 1983, 1986, and 1987 are plotted, along with a summary by SWS of all his counts for the total areas of all quadrants. Generally, we see a well defined curve with a characteristic scatter of plus or minus some tens of percent.

The scatter in Fig. A1 implies that different investigators making independent counts from different photo sets characterize the density with variations up to $\sim$ 50%. Among 85 data points in the well-resolved diameter range of 5.7 to 256 km on Rhea and 8 to 256 km on Mimas, 67% of the points were within $\pm$50% of a smooth curve drawn through the points to represent the diameter distribution. These results are roughly consistent with those found in the Basaltic Volcanism Study Project [*Hartmann et al.*, 1981] for an even wider variety of authors and geologic provinces. In that study, among 122 pairs of counts from 13 different authors, the median ratio of high value to low value among counts of the same region was 1.5. Our point here is that while strict $1/\sqrt{n}$ error bars are generally used to characterize the uncertainty in a given size-frequency plot, the empirical record of the field shows that different authors trying independently to define a geologic province on a planet and then to characterize the crater density in it generally may disagree by more than 50% roughly half the time for counts in a fixed diameter bin of $\sqrt{2}D$ width. A plot of the same data as in Fig. A1 but with standard $1/\sqrt{n}$ error bars is shown in Figure A2. For most diameter bins, Figure A2 shows overlapping error bars between the counts of SWS and WKH, which is gratifying. However, the figures also illustrate the magnitude of the problem. Clearly, $1/\sqrt{n}$ error bars do not adequately characterize the uncertainty in a crater size-frequency distribution.

It is in the nature of the data base that uncertainties, or at least issues of judgement, are largest at the largest and smallest diameters. At the largest, the number of craters decreases toward zero per bin, due to the nature of the size-frequency distribution, so the statistics get poorer. As we push toward higher resolution, and smaller diameter, problems of completeness also arise. If one attempts to count the smallest craters one can resolve in an image, and then recounts the area in a higher-resolution image, one consistently finds that the higher resolution image reveals more craters in that size bin than does the first image. Generally, this problem is revealed in a "rollover" of the crater curve, away from the prevailing slope of the distribution. This effect is seen in Figure A1b. For completeness,

SWS provided all his counts down to small diameters, and it can be seen that the counts in the last three bins roll away from a linear (power law) distribution. WKH generally cut off his counts at a size well above the resolution limit on the photos. However, in Figure A1b, WKH went back to the original counts and plotted in parentheses some counts beyond these cutoffs. The same rollover can be seen.

The $1/\sqrt{n}$ error bars decrease in size as the sample size increases. As seen in Figure A2, if the smallest craters are included, the n value may be so high as to produce extremely small error bars, but experience shows that these data points may fall many "standard deviations" below the true curve determined from higher resolution images. In Figure A2a, at the upper left, the error bars are tiny but the craters show the rollover almost certainly due to incompleteness. Errors of a few percent could be claimed for points that, in fact, may be a factor two or more below the positions found to be correct for higher resolution photos. Similarly, in the upper left of Figure A2b, SWS's counts illustrate incompleteness and show a rollover, and the error bars do not overlap with the WKH counts, which were made in smaller areas but with greater effort to attain completeness at the smallest sizes. Large sample size does not guarantee low uncertainty unless the observer's judgement has been correct in estimating at what diameters the counts are complete.

Comparison of Individual Craters

After making independent counts of the diameter distributions and positions of all the craters with $D \geq 32$ km for our data set, SWS and WKH performed a crater-by-crater analysis of these counts, and a study of the causes of discrepancies. As seen in Figure A1, the two diameter distributions were found to be quite consistent. Nonetheless, some 24% of the 93 craters in the final sample were ones for which SWS and WKH disagreed by more than one diameter bin as to the diameter recorded. This apparently high "disagreement rate" arises from the fact that these provinces are very heavily cratered. All of the disagreements concerned very degraded craters; about half were cases where both authors saw a feature but disagreed significantly on its outline. The other half were cases where only one author recorded a feature. In agreeing on the final sample, each author made about the same number of changes to his initial crater determinations. Some of the marginal craters were retained, others dropped, after arguments were presented and decisions were made. Again,

it should be stressed that judgements of this type are common only in counts of heavily cratered areas, where degraded craters are common; crater density uncertainties should be lower in less heavily cratered regions.

Two other sources of discrepancy were involved with spatial and diameter binning of the sample. Another 16% of the 93 craters were measured by the two authors as having diameters near the division between two diameter bins, and were placed by one author in one bin and by the other in the adjacent bin. Similarly, the area was divided in this study into small quadrats, and about 8.5% of the craters were placed in different, adjacent quadrats by the two authors. Division into larger quadrats clearly would have reduced this source of disagreement. Neither of these effects represents a serious problem with the crater counting procedure. The differences between the original SWS and WKH counts are summarized in Figure A3 (note that this figure includes *all* sources of discrepancy).

Because there was very good agreement among the several independent and one "consensus" size-frequency distributions, we feel confident that the conclusions we have drawn from the size-frequency distributions, including the extrapolation to other satellites and use to calculate disruption probabilities, are valid. Also, for both sets of original independent counts, the evidence against local endogenic resurfacing on Rhea and Mimas was clearly confirmatory.

The argument that the spatial distribution of craters on Rhea is more uniform than random, because it is so sensitive to the numbers of craters in each quadrat, is less secure. This point is illustrated by the summary of statistical parameters presented in Table A1. (The relevant experimental and theoretical properties of a random distribution are also repeated here from Table 2.) In the original counts by SWS, the values of $\sigma(32)$ and $\sigma_4(32)$ were both less than expected for a Poisson distribution, indicating a more-uniform-than-random spatial pattern. Moreover, the statistics $X_u^2 = 13.2 = X_v^2$ yielded by this distribution, when compared to the χ^2 distribution with 3 degrees of freedom, appeared to allow randomness to be ruled out with a certainty of 99.6%. Only one of the 200 random runs performed in our numerical experiments had $X_u^2 > 13.2$; two had $X_v^2 > 13.2$. Only 17 runs had $\sigma \leq \sigma(\text{obs})$; only 10 had $\sigma_4 \leq \sigma_4(\text{obs})$. However, the counts by WKH, while producing nearly identical values of $\sigma(32)$ and $\sigma_4(32)$, produced a much smaller χ^2 statistic, $X_u^2 = 2.08$, fully consistent with spatial randomness. This large drop

was primarily due to WKH finding three quadrats devoid of 32-km craters, while SWS found none. As noted in Figure 7 and Table 2, the consensus result obtained by SWS and WKH together had one quadrat with no 32-km craters, and yielded $X_u^2 = 6.5$, $X_v^2 = 6.8$, and a statistical confidence level for non-randomness of 91 to 92%. This consensus result represents our best estimate of the true spatial distribution of these craters on Rhea. However, the difference between the two original counts gives a measure of the importance of subjectivity in this determination. While spatial statistical techniques appear to hold some promise for investigation of the crater saturation phenomenon, it is clear that great care must be exercised in their application.

ACKN' WLEDGEMENTS

We thank our colleagues for many hours of productive discussions. Particularly helpful were Jeff Cuzzi, Janet Franklin, and Keith Holsapple. Ken Lin and Debbie Schwartz helped with counts of the smaller craters on Rhea. Lori Hamilton and Carol Polacek skillfully prepared the manuscript. This research was supported in part by the NASA Planetary Geology and Geophysics Program under the following grants and contracts: NAGW-1107 (SUNYSB), NGR05-010-062 (UCSB), NAGW-1023 (Cornell), NASW-3728 (PSI), and NASW-4295 (PSI). This is contribution number 245 from the Planetary Science Institute, which is a division of Science Applications International Corporation.

Table 1
Quadrat Locations, Areas, and 8 km Crater Densitites.

Voyager Picture Number	North Latitude Limit	South Latitude Limit	West Longitude Limit	East Longitude Limit	Area, km^2	N_{8km}
541S1+000	90	75	90	15	2.60×10^4	1.92×10^{-3}
	75	60	90	60	3.05×10^4	1.21×10^{-3}
	75	60	60	30	3.05×10^4	9.83×10^{-4}
	75	60	30	0	3.05×10^4	1.41×10^{-3}
	60	45	60	45	2.43×10^4	1.11×10^{-3}
	60	45	45	30	2.43×10^4	1.15×10^{-3}
	60	45	30	15	2.43×10^4	9.05×10^{-4}
	60	45	15	0	2.43×10^4	1.15×10^{-3}
393S1+000	45	30	30	15	3.16×10^4	6.33×10^{-4}
	45	30	15	0	3.16×10^4	9.49×10^{-4}
	45	30	0	345	3.16×10^4	1.04×10^{-3}
	30	15	30	15	3.69×10^4	4.07×10^{-4}
	30	15	15	0	3.69×10^4	1.11×10^{-3}
	30	15	0	345	3.69×10^4	1.27×10^{-3}
	15	0	30	15	3.96×10^4	4.29×10^{-4}
	15	0	15	0	3.96×10^4	5.05×10^{-4}
539S1+000	90	75	15	300	2.60×10^4	1.42×10^{-3}
	75	60	330	300	3.05×10^4	1.25×10^{-3}
405S1+000	45	30	315	300	3.16×10^4	9.49×10^{-4}
547S1+000	75	60	120	90	3.05×10^4	9.83×10^{-4}
	60	45	120	105	2.43×10^4	1.03×10^{-3}
	60	45	105	90	2.43×10^4	7.41×10^{-4}
401S1+000	45	30	345	330	3.16×10^4	4.43×10^{-4}
	45	30	330	315	3.16×10^4	6.33×10^{-4}
	30	15	345	330	3.69×10^4	6.78×10^{-4}
	30	15	330	315	3.69×10^4	5.69×10^{-4}
	15	0	0	345	3.96×10^4	1.09×10^{-3}
	15	0	345	330	3.96×10^4	5.55×10^{-4}
	15	0	330	315	3.96×10^4	5.55×10^{-4}
545S1+000	60	45	90	75	2.43×10^4	6.17×10^{-4}
	60	45	75	60	2.43×10^4	6.58×10^{-4}
	45	30	90	75	3.16×10^4	9.18×10^{-4}
	45	30	75	60	3.16×10^4	8.86×10^{-4}
	45	30	60	45	3.16×10^4	1.01×10^{-3}
	45	30	45	30	3.16×10^4	7.91×10^{-4}
	30	15	75	60	3.69×10^4	6.23×10^{-4}
551S1+000	45	30	105	90	3.16×10^4	8.86×10^{-4}
	30	15	105	90	3.69×10^4	5.69×10^{-4}
	30	15	90	75	3.69×10^4	3.25×10^{-4}
537S1+000	75	60	0	330	3.05×10^4	1.02×10^{-3}
	60	45	0	345	2.43×10^4	8.23×10^{-4}
	60	45	345	330	2.43×10^4	8.64×10^{-4}
	60	45	330	315	2.43×10^4	1.02×10^{-3}
	60	45	315	300	2.43×10^4	6.17×10^{-4}

Table 2

Craters on Rhea: Statistical Properties

Run No.	C.C. (16-32:32)	C.C. (16-32:32L)	$\sigma(16)$	$\sigma_4(16)$	$\sigma(16L)$	$\sigma_4(16L)$	$\chi^2_n(16)$ (5 d.o.f.)	$\chi^2_\sigma(16)$ (5 d.o.f.)	$\sigma(32)$	$\sigma_4(32)$	$\sigma(32L)$	$\sigma_4(32L)$	$\chi^2_n(32)$ (3 d.o.f.)	$\chi^2_\sigma(32)$ (3 d.o.f.)	$\sigma(64)$
Obs	−.03	−.29	2.98	3.80	7.35	8.14	3.4	2.8	1.23	1.55	3.24	3.60	6.5	6.8	.57
1	.16	.02	3.00	4.05	3.78	5.04	3.1	2.7	1.68	2.10	3.45	4.86	6.6	5.7	.61
2	.02	.36	2.63	3.36	6.14	7.38	4.4	5.9	1.37	1.93	3.84	4.69	2.3	2.8	.53
3	.06	−.07	2.94	3.67	7.80	8.67	2.3	1.9	1.56	2.02	4.43	5.25	7.9	7.4	.65
4	−.05	−.12	2.98	4.12	9.64	12.86	6.2	7.2	1.42	2.06	2.60	3.01	2.4	2.5	.61
5	.19	−.71	2.72	3.48	2.78	3.09	5.0	5.3	1.61	2.25	1.98	2.33	1.3	1.2	.65
6	.00	.49	3.00	3.77	7.65	9.64	2.8	2.0	1.28	1.67	4.23	4.67	3.2	3.6	.61
7	.26	.66	3.81	4.64	13.11	15.36	12.2	7.3	1.89	2.48	4.95	6.27	7.5	6.3	.71
8	−.11	−.20	2.40	2.92	5.98	7.20	3.4	4.6	1.34	1.87	3.01	4.20	3.6	4.4	.57
9	−.02	.09	3.12	4.08	8.04	9.53	3.6	2.4	1.48	2.00	3.73	4.79	0.01	0.1	.53
10	−.23	−.46	2.29	3.00	3.63	5.02	6.8	9.1	1.43	1.68	4.06	5.25	4.3	3.7	.61
11	−.15	−.05	3.16	3.97	6.99	8.49	2.4	1.3	1.63	2.11	3.28	4.18	3.4	3.0	.57
12	.19	.61	3.22	4.37	9.12	12.48	7.6	6.0	1.37	1.73	2.31	2.70	1.9	2.0	.53
Mean	.03	.05	2.94	3.79	7.05	8.73	5.0	4.7	1.50	1.99	3.49	4.35	3.7	3.6	.60
Median	.01	−.03	2.99	3.87	7.32	8.58	4.0	5.0	1.46	1.96	3.59	4.68	3.3	3.3	.61
Mean Abs. Val.	.12	.32				Grand Mean			1.47	1.94	3.43	4.15	3.17	3.15	
Median Abs. Val.	.13	.28				Grand Median							2.36	2.36	
Theory	0	0	2.72	3.58	6.60	8.68	4.35		1.45	1.90	3.51	4.62	2.37		.62

Table 3
Relative Cratering Rates on Saturn's Moons

	Saturn Family Comets v_∞=10 km s^{-1}				Oort Cloud Comets v_∞=16.6 km s^{-1}			
Moon[a]	$n_c^{(b)}$	$\bar{v}$(km s^{-1})	$D_{SW}^{(b,c,d)}$	$D_{SH}^{(b,c,e)}$	$n_c^{(b)}$	$\bar{v}$(km s^{-1})	$D_{SW}^{(b,c,d)}$	$D_{SI}^{(b,c,e)}$
Ring Parent[f]	2.82	32.7	1.89	1.74	2.09	35.3	1.73	1.63
Atlas[g]	2.53	30.4	2.66	2.47	1.92	33.2	2.46	2.33
Prometheus[g]	2.50	30.3	2.14	1.98	1.90	33.0	1.97	1.87
Pandora[g]	2.48	30.0	2.21	2.06	1.89	32.8	2.05	1.94
Janus[g]	2.36	29.2	1.94	1.81	1.82	32.0	1.80	1.71
Mimas	2.04	26.7	1.63	1.54	1.63	29.8	1.52	1.46
Enceladus	1.70	24.0	1.45	1.39	1.43	27.5	1.38	1.34
Telesto/ Calypso	1.46	22.0	2.29	2.22	1.28	25.7	2.20	2.16
Tethys	1.47	22.1	1.23	1.19	1.28	25.7	1.18	1.15
Dione	1.24	20.0	1.12	1.10	1.14	24.0	1.09	1.08
Rhea	1	17.8	1	1	1	22.2	1	1
Hyperion[g]	0.60	13.3	1.13	1.18	0.75	18.8	1.22	1.24
Iapetus	0.46	11.5	0.80	0.85	0.67	17.6	0.90	0.93
Phoebe[h]	0.39	10.4	1.06	1.14	0.63	16.9	1.23	1.28

(*a*) Satellite parameters from Lissauer and Cuzzi (1985).
(*b*) Relative to Rhea.
(*c*) Crustal densities of all moons assumed equal to that of Rhea.
(*d*) Shoemaker and Wolfe's crater scaling law, see Eq. (6).
(*e*) Schmidt and Holsapple's crater scaling law, see Eq. (8).
(*f*) Hypothetical ring parent body at outer edge of B ring, $M_m = 3 \times 10^{22}$g, $\rho = 1$ g cm^{-3}.
(*g*) Parent body with diameter equal to moon's longest axis and $\rho = 1$ g cm^{-3}.
(*h*) Assumed $\rho = 1$ g cm^{-3}.

Table 4
Catastrophic Disruption Probabilities

	Surface Area (10^6 km^2)	Equivalent Crater on Rhea (km)				Disruption Frequency Using Rhea's Cratering Record				Disruption Frequency Using Iapetus' Cratering Record			
v_∞(km/sec):		10	10	16.6	16.6	10	10	16.6	16.6	10	10	16.6	16.6
Scaling Law:		SW[a]	SH[b]	SW[c]	SH[d]	SW	SH	SW	SH	SW	SH	SW	SH
Moon													
Ring Parent[e]	0.468	204	222	223	237	0.56	0.44	0.33	0.27	3.86	2.62	1.14	0.88
Atlas[f]	0.0045	14	15	15	16	6.92	5.95	4.24	3.64	44.45	30.91	13.65	10.76
Prometheus[f]	0.062	66	71	71	75	1.45	1.19	0.89	0.77	9.75	6.80	3.01	2.37
Pandora[f]	0.038	50	53	54	57	1.89	1.55	1.16	1.00	12.57	8.78	3.89	3.08
Janus[f]	0.152	114	122	122	129	0.75	0.63	0.47	0.41	5.16	3.64	1.63	1.30
Mimas	0.488	242	256	259	269	0.26	0.23	0.18	0.16	1.85	1.35	0.62	0.51
Enceladus	0.792	346	361	365	376	0.13	0.12	0.10	0.09	0.95	0.72	0.35	0.29
Telesto/ Calypso[f]	0.0028	13	13	14	14	3.17	2.92	2.49	2.35	20.27	15.90	7.99	6.93
Tethys	3.53	865	891	900	918	0.04	0.04	0.03	0.03	0.31	0.24	0.12	0.11
Dione	3.94	1003	1020	1027	1038	0.03	0.03	0.02	0.02	0.20	0.16	0.08	0.08
Rhea	7.35	1530	1530	1530	1530	0.01	0.01	0.01	0.01	0.09	0.08	0.05	0.04
Hyperion[f]	0.385	310	298	288	281	0.03	0.03	0.05	0.05	0.22	0.21	0.17	0.16
Iapetus	6.70	1829	1722	1624	1572	0.003	0.004	0.007	0.007	0.02	0.02	0.02	0.02
Phoebe[g]	0.152	208	193	178	172	0.02	0.03	0.06	0.07	0.17	0.17	0.20	0.21

(a) To determine equivalent crater on Iapetus, multiply by 0.798.
(b) To determine equivalent crater on Iapetus, multiply by 0.848.
(c) To determine equivalent crater on Iapetus, multiply by 0.899.
(d) To determine equivalent crater on Iapetus, multiply by 0.928.
(e) Hypothetical moon equal in mass to Saturn's rings, density of 1 g cm^{-3} located at outer edge of B ring.
(f) Parent body with diameter equal to longest axis and density of 1 g cm^{-3}.
(g) Density of 1 g cm^{-3} assumed.

Table A1
Craters on Rhea: Statistical Properties of Different Counts

Determination	$\sigma(32)$	$\sigma_4(32)$	$\chi^2_u(32)$ (3 d.o.f.)	$\chi^2_v(32)$ (3 d.o.f.)
SWS	1.25	1.54	13.2	13.2
WKH	1.30	1.62	2.1	
Consensus	1.23	1.55	6.5	6.8
Experiment Grand Mean	1.47	1.94		
Experiment Grand Median			2.36	2.36
Theory	1.45	1.90	2.37	

References

Cadogan, P.H. Oldest and largest lunar basin? *Nature* **250**, 315-316, 1974.

Cameron, A.G.W., and W. Benz. Planetary collision calculations: Origin of Mercury. *Lunar and Planetary Science XVIII*, 151-152, 1987.

Cameron, A.G.W., and W.R. Ward. The origin of the Moon. *Lunar Science VII*, 120-122, 1976.

Chabai, A.J. Crater scaling laws for desert alluvium. *Rep. SC-4391*, Sandia Corp., Albuquerque, NM, 1959.

Chapman, C.R. and McKinnon, W.B. Cratering of planetary satellites, in *Satellites* (J. Burns and M. Mathews, eds.) University of Arizona Press, Tucson, 492-580, 1986.

Cook, A.F. and Franklin, F.A. An Explanation of the Light Curve of Iapetus. *Icarus* **13**, 282-291, 1970.

Croft, S.K. Crater populations on the uranian satellites. *Lunar Planet. Sci.* **19**, 223-223, 1988.

Cuzzi, J.N., and Durisen, R. In preparation, 1988.

Fielder, G. and Marcus, A. Further tests for randomness of lunar craters. *Mon. Not. R. Astr. Soc.* **136**, 1-10, 1967.

Gault, D.E. Saturation and equilibrium conditions for impact cratering on the lunar surface: Criteria and implications. *Radio Science* **5**, 273-291, 1970.

Gault, D.E., and Sonett, C.P. Laboratory simulations of pelagic asteroidal impact: Atmospheric injection, benthic topography, and the surface wave radiation field. *Geol. Soc. Amer. Spec. Paper* **190**, 69-92, 1982.

Getis, A. and Boots, B. *Models of Spatial Processes*, Cambridge University Press, England, 1978.

Goldreich, P. and Tremaine, S. The Dynamics of Planetary Rings, *Ann. Rev. Astron. Astrophys.* **20**, 249-283, 1982.

Gradie, J.C., Chapman, C.R., and Williams, J.G. Families of Minor Planets, in *Asteroids* (T. Gehrels, ed.), University of Arizona Press, 359-390, 1979.

Hartmann, W.K., *et al.* Chapter 8 in *Basaltic Volcanism on the Terrestrial Planets*. Pergamon Press, Inc., New York, 1286 pp., 1981.

Hartmann, W.K. Planet formation: Mechanism of early growth. *Icarus* **33**, 50-61, 1978.

Hartmann, W.K. Does crater "saturation equilibrium" occur in the Solar System? *Icarus* **60**, 56-74, 1984.

Hartmann, W.K., and Davis, D.R. Satellite-sized planetesimals and lunar origin. *Icarus* **24**, 504-519, 1975.

Hartmann, W.K., Phillips, R.J. and Taylor, G.J. (eds.) *Origin of the Moon*, Lunar and Planetary Institute, Houston, 1986.

Holsapple, K.A. and Housen, K.R. Scaling laws for the catastrophic collisions of asteroids. *Mem. Soc. Astron. Ital.* **57**, 65-85, 1986.

Holsapple, K.A. and Schmidt, R.M. A material-strength model for apparent crater volume. *Proc. Lunar Planet. Sci. Conf.* **10**, 2757-2777, 1979.

Holsapple, K.A. and Schmidt, R.M. On the Scaling of Crater Dimensions 2, Impact Processes. *J. Geophys. Res.* **87**, 1849-1870, 1982.

Horedt, G.P. and Neukum, G. Planetocentric venus heliocentric impacts in the Jovian and Saturnian satellite system. *J. Geophys. Res.* **89** 10,405-10,410, 1984.

Larson, H.J. *Introduction to Probability Theory and Statistical Inference.* John Wiley & Sons, Inc., USA, 1969.

Lissauer, J.J. and Cuzzi, J.N. Rings and Moons: Clues to understanding the Solar Nebula. *Protostars and Planets II*, D.C. Black and M.S. Matthews eds., Univ. Arizona Press, Tucson, 920-956. 1985.

Lissauer, J.J., Peale, S.J. and Cuzzi, J.N. Ring Torque on Janus and the Melting of Enceladus. *Icarus* **58**, 159-168, 1984.

Lissauer, J.J., Goldreich, P. and Tremaine, S. Evolution of the Janus-Epimetheus coorbital resonance due to torques from Saturn's rings. *Icarus* **64**, 425-434, 1985.

Marcus, A.H. A multivariate immigration with multiple death process and applications to lunar craters. *Biometrika* **54**, 251-261, 1967.

Marcus, A.H. Comparison of equilibrium size distributions for lunar craters. *J. Geophys. Res.* **75**, 4977-4984, 1970.

Northrop, T.G. and Connerney, J.E.P. A Micrometeorite Erosion Model and the Age of Saturn's Rings. *Icarus* **74**, 259-273, 1988.

Opik, E.J. Collision probabilities with the planets and the distribution of interplanetary matter. *Proc. Roy. Irish Acad.* **54**, 165-199, 1951.

Passey, Q.R. and Shoemaker, E.M. Craters and Basins on Ganymede and Callisto: Morphological indications of Crustal evolution. *Satellites of Jupiter*, D. Morrison, ed., Univ. of Arizona press, Tucson, 379-434, 1982.

Plescia, J.B. The Geology of Dione. *Icarus* **56**, 255-277, 1983.

Plescia, J.B. Cratering history of Miranda: Implications for geologic processes. *Icarus* **73**, 442-461, 1988*a*.

Plescia, J.B. Cratering history of the uranian satellites: Umbriel, Titania, and Oberon. *J. Geophys. Res.* 92, 14918-14932, 1988*b*.

Plescia, J.B. and Boyce, J.M. Crater densities and geological histories of Rhea, Dione, Mimas and Tethys. *Nature* **295**, 285-290, 1982.

Plescia, J.B. and Boyce, J.M. Crater numbers and geological histories of Iapetus, Enceladus, Tethys and Hyperion. *Nature* **301**, 666-670, 1983.

Plescia, J.B. and Boyce, J.M. Impact cratering history of the Saturnian satellites. *J. Geophys. Res.* **90**, 2029-2037, 1985.

Pollack, J.B., Summers, A. and Baldwin, B. Estimates of the Size of the Particle in the Rings of Saturn and their Cosmogenic Implications. *Icarus* **20**, 263-278, 1973.

Schmidt, R.M., and K.A. Holsapple. Estimates of crater size for large-body impact: Gravity scaling results. *Spec. Pap. Geol. Soc. Am.* **190**, 93-102, 1982.

Shoemaker, E.M. Kuiper Prize Lecture, Division of Planetary Sciences of the American Astronomical Society Annual Meeting, Kona, HI. 1984.

Shoemaker, E.M. and Wolfe, R. Cratering time scales for the Galilean Satellites. In *Satellites of Jupiter*, D. Morrison, ed., Univ. of Arizona Press, Tucson, 277-339. 1982.

Smith, B.A. *et al.* Encounter with Saturn: Voyager 1 Imaging Science Results. *Science* **212**, 163-191, 1981.

Smith, B.A. *et al.* A New Look at the Saturn System: The Voyager 2 Images. *Science* **215**, 504-537, 1982.

Smith, B.A. *et al.* Voyager 2 in the Uranian system: Imaging Science Results. *Science* **233**, 43-64, 1986.

Squyres, S.W., Reynolds, R.T., Cassen, P.M. and Peale, S.J. The Evolution of Enceladus. *Icarus* **53**, 319-331, 1983.

Strom, R.G. Crater populations on Mimas, Dione, and Rhea. *Lunar Planet. Sci.* **XII**, 7-9, 1981.

Strom, R.G. The solar system cratering record: Voyager 2 results at Uranus and implications for the origin of impacting objects. *Icarus* **70**, 517-535, 1987.

Strom, R.G., and A. Woronow. Solar system cratering populations. *Luanr Planet. Sci.* **XIII**, 782-783, 1982.

Thomas, P.C., Veverka, J., and Dermott, S.F. Small satellites. In *Satellites* (J. Burns and M.S. Matthews, eds.), Univ. of Arizona press, 802-835, 1986.

U.S. Geological survey, *Preliminary pictorial map of Rhea*, U.S. Geol. Surv. Sr 10M 2AN, scale 1:10,000,000, 1982.

Whitaker, E.A. The lunar Procellarum basin. *Geochim. Cosmochim. Acta Suppl.* **15**, 105-111, 1981.

Wilhelms, D.E. Effects of the Procellarum Basin on Lunar Geology, Petrology, and Tectonism. *Lunar Planet. Sci.* **14**, 845-846, 1982.

Wilhelms, D.E. and Squyres, S.W. The martian hemispheric dichotomy may be due to a giant impact. *Nature* **309**, 138-140, 1984.

Woronow, A. Crater saturation and equilibrium: A Monte Carlo simulation. *J. Geophys. Res.* **82**, 2447-2456, 1977.

Woronow, A. A general cratering-history model and its implications for the lunar highlands. *Icarus* **34**, 76-88, 1978.

Woronow, A., and Strom, R.G. Limits on larger-crater production and obliteration on Callisto. *Geophys. Res. Lett.* **8**, 891-894, 1982.

Yoder, C.F. How tidal heating in Io drives the Galilean orbital resonance locks. *Nature* **279**, 767-770, 1979.

Figure Captions

Figure 1 — Voyager image 541S1+000 (FDS 34952.57). The area counted to produce the crater curve in Figure 3 is indicated.

Figure 2 — Voyager image 393S1+000 (FDS 34950.29). The area counted to produce the crater curve in Figure 3 is indicated.

Figure 3 — *(a)* Cumulative and *(b)* relative crater size-frequency curves for the the two areas on Rhea outlined in Figures 1 (filled circles) and 2 (open squares). (The relative plot, or "R" plot, gives the ratio of the observed differential size frequency distribution to the function $dN = D^{-3}dD$.) Note the apparent shortage of smaller craters in Figure 2 relative to Figure 1. The dashed line gives N_{HC}, as defined by Eq. (3).

Figure 4 — Plot of N_{8km}, the number of craters with $D \geq 8$ km per km^{-2}, as a function of the lighting parameter $\tan i \cos \epsilon$ for the eight quadrats counted in image 393S1+000 (Figure 2); see Table 1 for locations. A strong positive correlation between crater density and lighting geometry is evident.

Figure 5 — Plot of N_{8km}, the number of craters with $D \geq 8$ km per km^{-2}, as a function of the lighting parameter $\tan i \cos \epsilon$ for all 44 quadrats counted on Rhea. A positive correlation between crater density and lighting geometry is evident.

Figure 6 — Map of the 44 latitude-longitude quadrats in which we counted craters on Rhea, in an equal-area projection. The numbers of craters with diameters ≥ 16 km in each quadrat are indicated. The heavy lines give the boundaries of the "super quadrats" discussed in the text. Quadrats marked with asterisks are characterized by particularly poor lighting geometry, which probably rendered some craters in this size range impossible to detect.

Figure 7 — Map of the 44 latitude-longitude quadrats in which we counted craters on Rhea, in an equal-area projection. The numbers of craters with diameters ≥ 32 km in each quadrat are indicated. The heavy lines give the boundaries of the "super quadrats" discussed in the text.

Figure 8 — Map of the 44 latitude-longitude quadrats in which we counted craters on Rhea, in an equal-area projection. The numbers of craters with diameters ≥ 64 km in each quadrat are indicated.

Figure 9 — Mercator projection map of all of the craters observed on Rhea with diameters larger than 90.5 km. The diameter of each crater is rounded to the nearest 5 km. Cross-hatched region shows areas for which there is no Voyager coverage adequate to reveal craters of any size. Dashed line gives a typical boundary of the counting region for large craters, taking into account the fact that craters with centers outside the imaged region can still have part of their rims visible.

Figure 10 — *(a)* Cumulative and *(b)* relative crater curves for Rhea. The points shown as circles are for counts in the 44 latitude-longitude quadrats; the points shown as triangles are for the entire area shown in Figure 9. The dashed line gives N_{HC}, as defined by Eq. (3).

Figure 11 — Map of the 22 latitude-longitude quadrats in which we counted craters on Mimas, in an equal-area projection. The numbers of craters with diameters $\geq$ 16 km in each quadrat are indicated.

Figure 12 — Map of the 22 latitude-longitude quadrats in which we counted craters on Mimas, in an equal-area projection. The numbers of craters with diameters $\geq$ 32 km in each quadrat are indicated.

Figure 13 — *(a)* Cumulative and *(b)* relative crater curves for Mimas. The points shown as circles are for counts in the 22 latitude-longitude quadrats; the points shown as triangles are for the entire of the satellite in which craters with $D \geq 64$ would be visible if present. The dashed line gives N_{HC}, as defined by Eq. (3).

Figure 14 — *(a)* The best Voyager image of Iapetus (1259S2–004, FDS 43906.36), with a resolution of 8.8 km pixel^{-1}. *(b)* The craters with $D \geq 32$ km observed in this image, with the boundaries of the counting area and the diameter of each crater (rounded to the nearest 5 km) indicated.

Figure 15 — *(a)* Cumulative and *(b)* relative crater curves for Iapetus. The curve shown is for the craters indicated in Figure 14.

Figure A1 — Comparison of crater counts from different sources for Rhea and Mimas. Among WKH data, each data set from a different photograph is plotted separately and the scatter is interpreted as a measure of consistency. Solid line gives the crater curve of Eq. (3). In (b), parentheses show data that had been rejected by WKH as showing incompleteness due to low resolution at the low-diameter end of the curve, but are plotted here to compare with roll-over in SWS data also attributed to incompleteness.

Figure A2 — Another method of comparing crater counts from different sources. Counts from each source are summed to give one diameter distribution, and error bars are based on $1/\sqrt{n}$, where n is the number of craters in each diameter bin of that data set. Rollover attributed to incompleteness due to low resolution is apparent in the SWS data set at small diameter. "Curve A" in (a) is an eyeball fit to the data, showing the steeper segment at large diameters.

Figure A3 — Comparison of number of craters with $D \geq 32$ km reported in each quadrat on Rhea in original independent counts by SWS and WKH. This figure includes *all* sources of discrepancy, including disagreement over the diameter bin or spatial quadrat in which a "borderline" crater belongs.

Fig. 1

ORIGINAL PAGE
BLACK AND WHITE PHOTOGRAPH

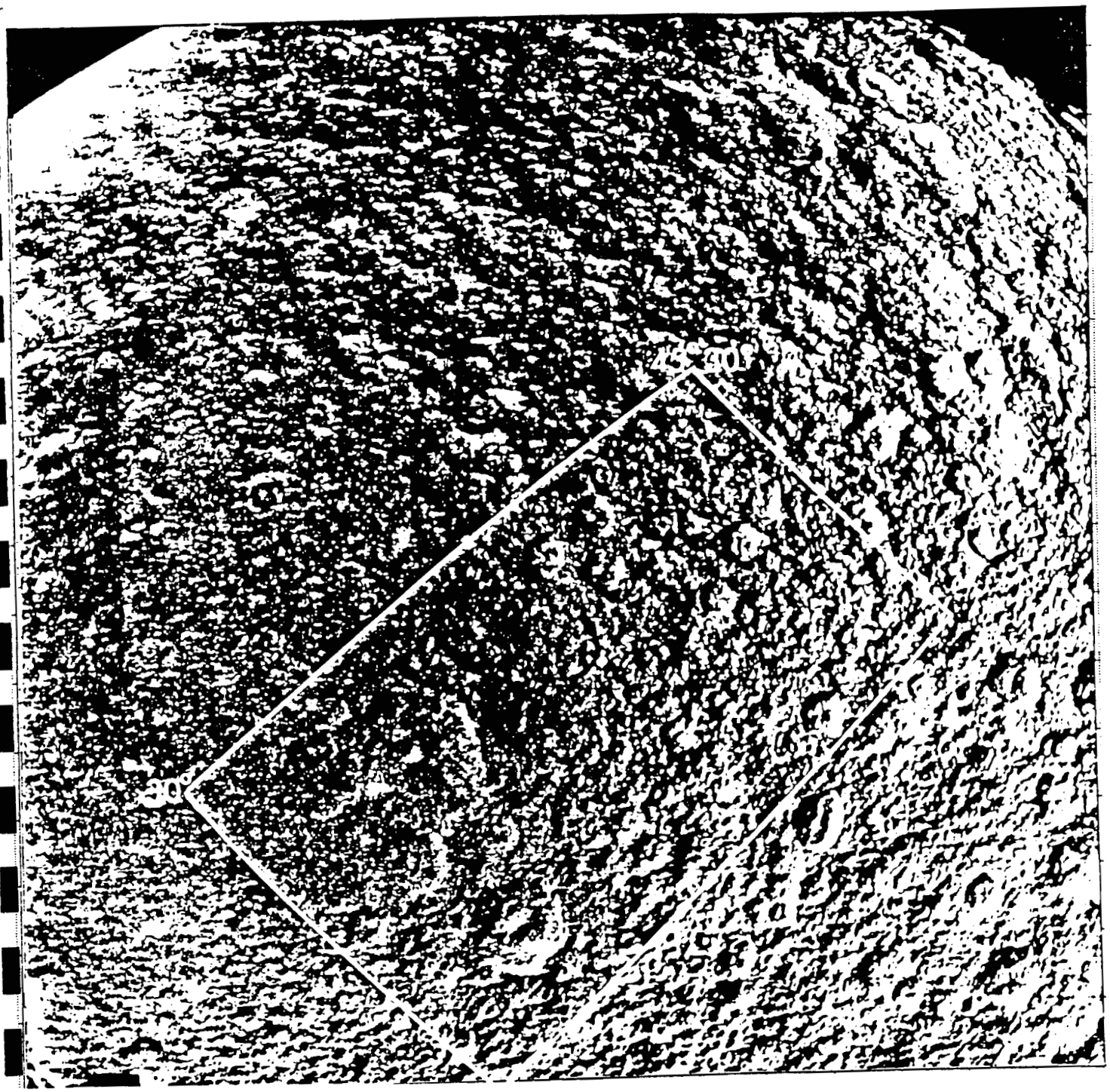

Fig. 2

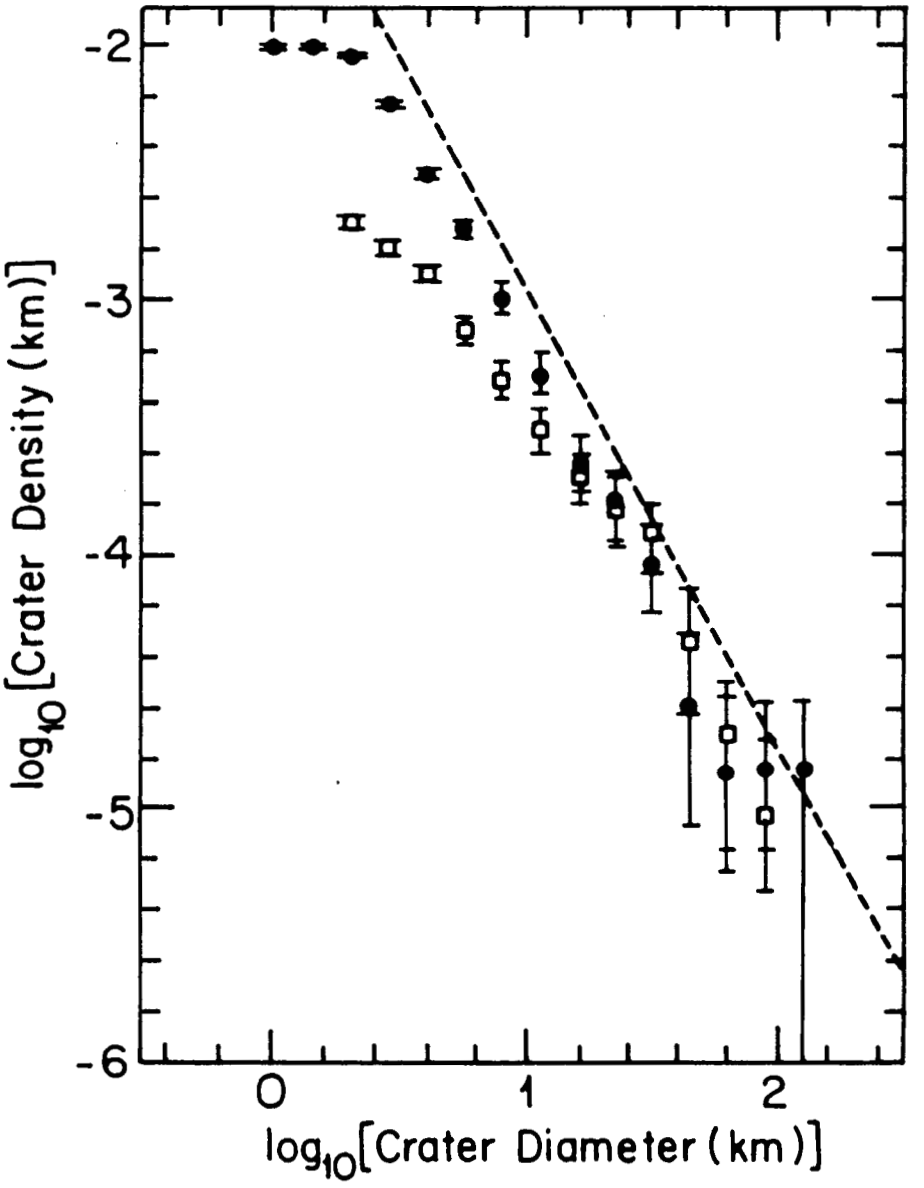
-2
-3
-4
-5
-6
0
1
2
log10[Crater Density (km)]
log10[Crater Diameter (km)]

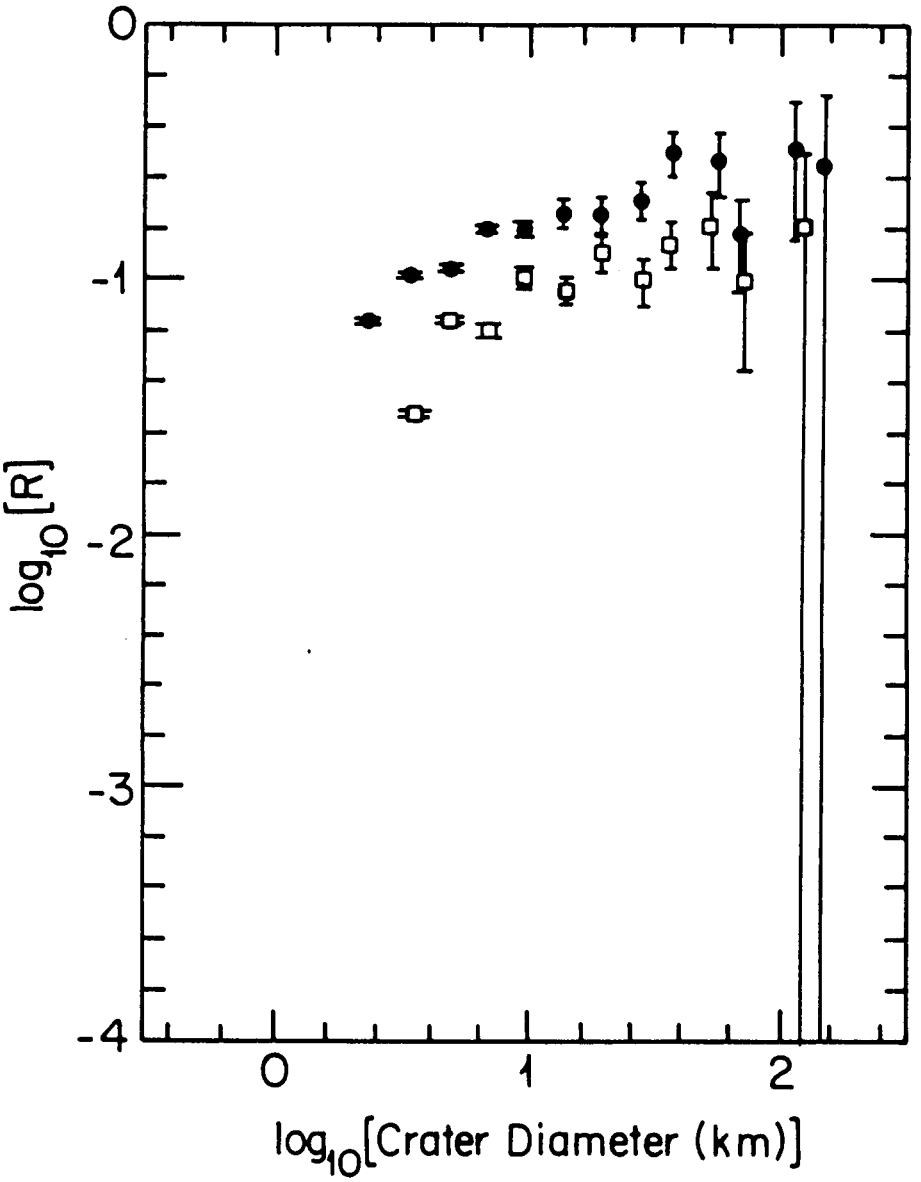
0
-1
-2
-3
-4
log10[R]
0
1
2
log10[Crater Diameter (km)]

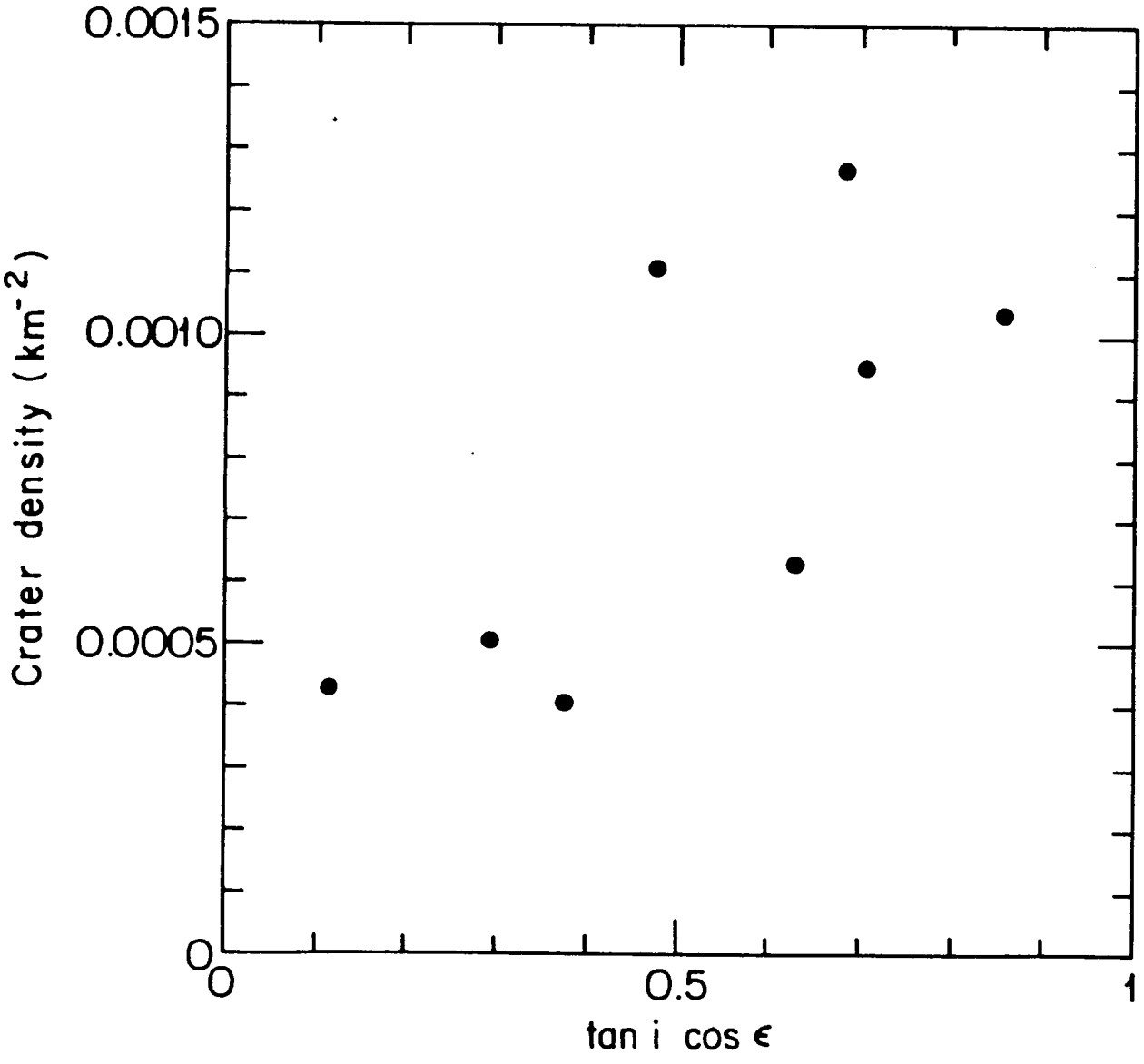
0.0015
0.0010
0.0005
0
Crater density (km^{-2})
0
0.5
1
tan i cos ϵ

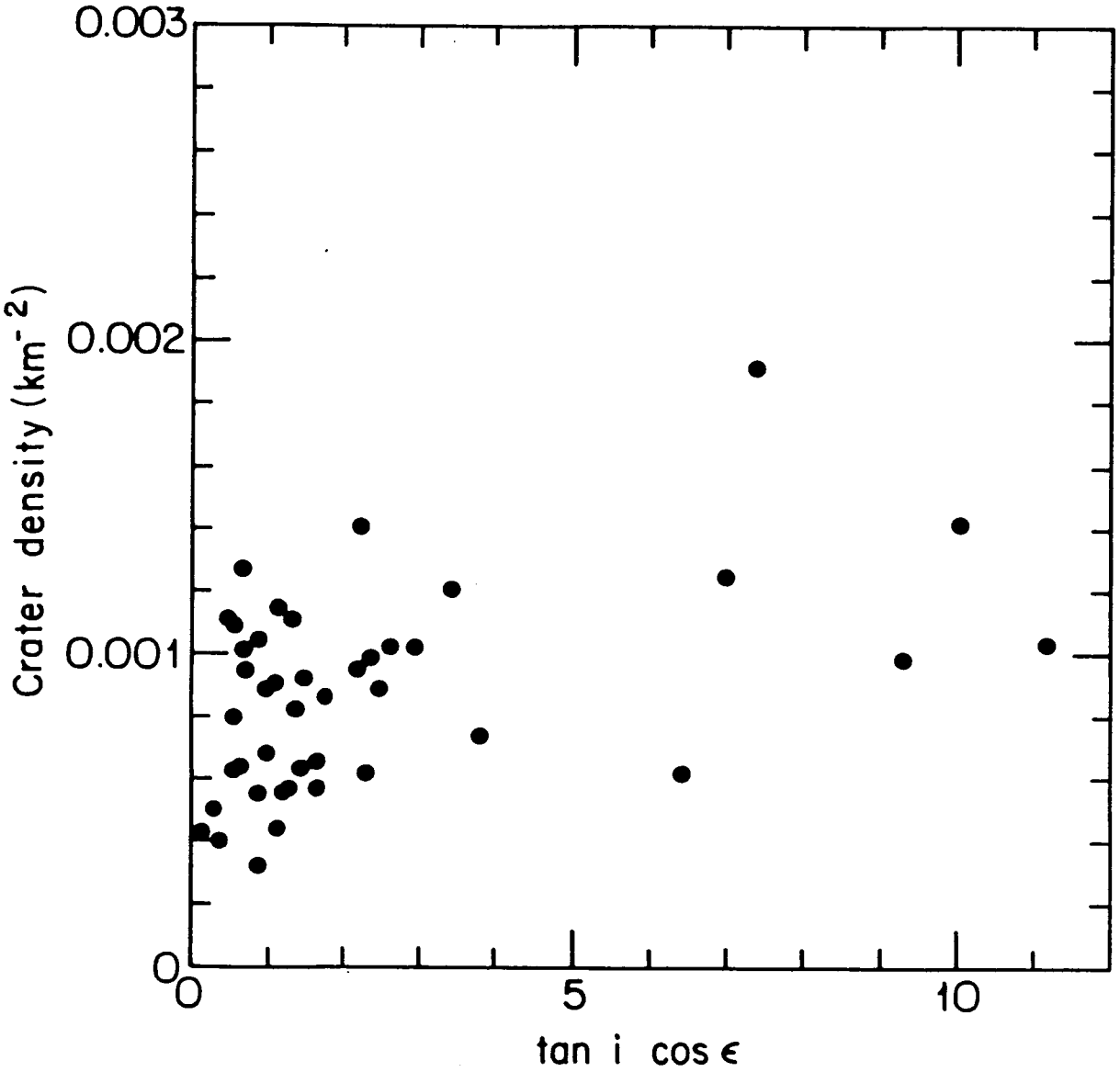
0.003
0.002
0.001
0
Crater density (km^{-2})
0
5
10
tan i cos ϵ

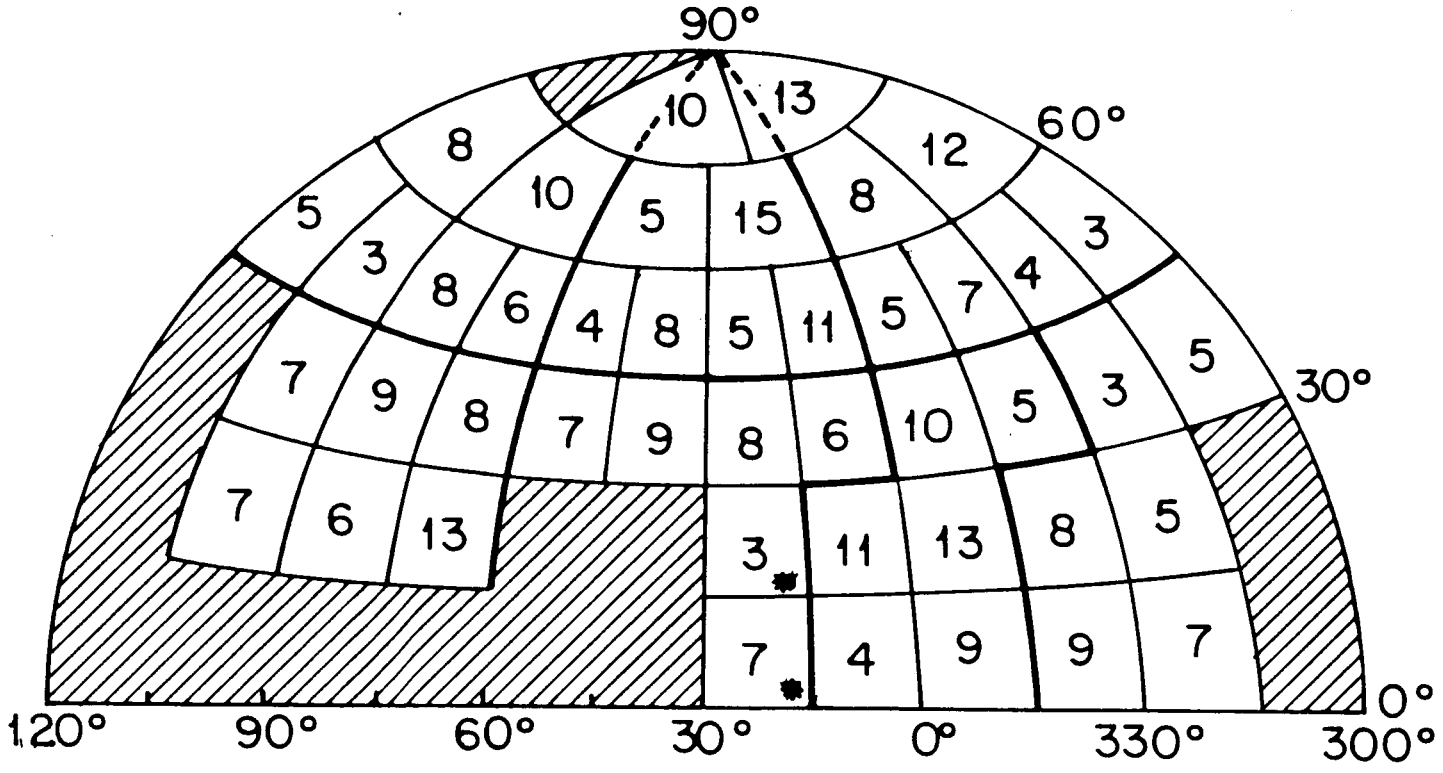
90°
60°
30°
0°
120°
90°
60°
30°
0°
330°
300°
10
13
8
12
5
10
5
15
8
3
3
8
6
4
8
5
11
5
7
4
7
9
8
7
9
8
6
10
5
3
5
7
6
13
3
11
13
8
5
7
4
9
9
7

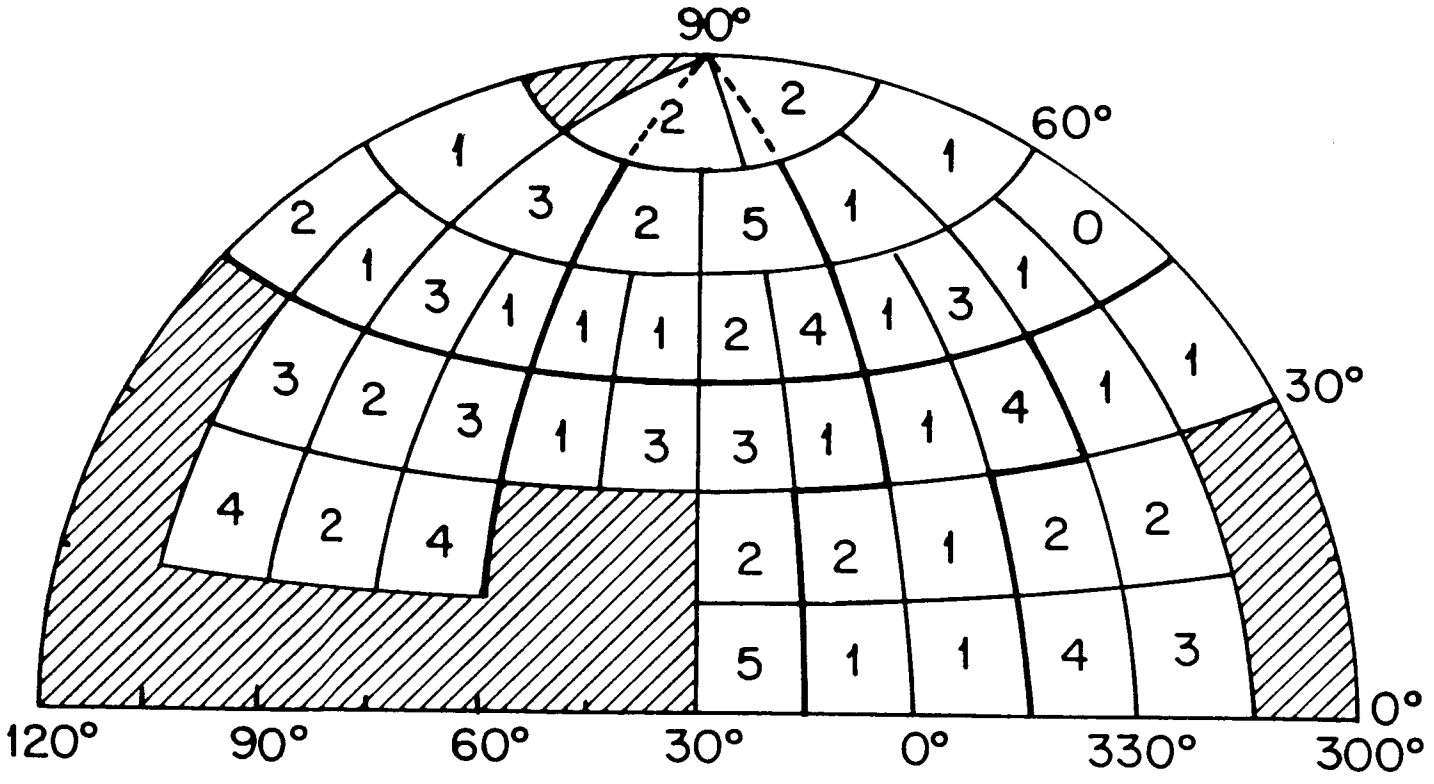
90°
60°
30°
0°
120°
90°
60°
30°
0°
330°
300°

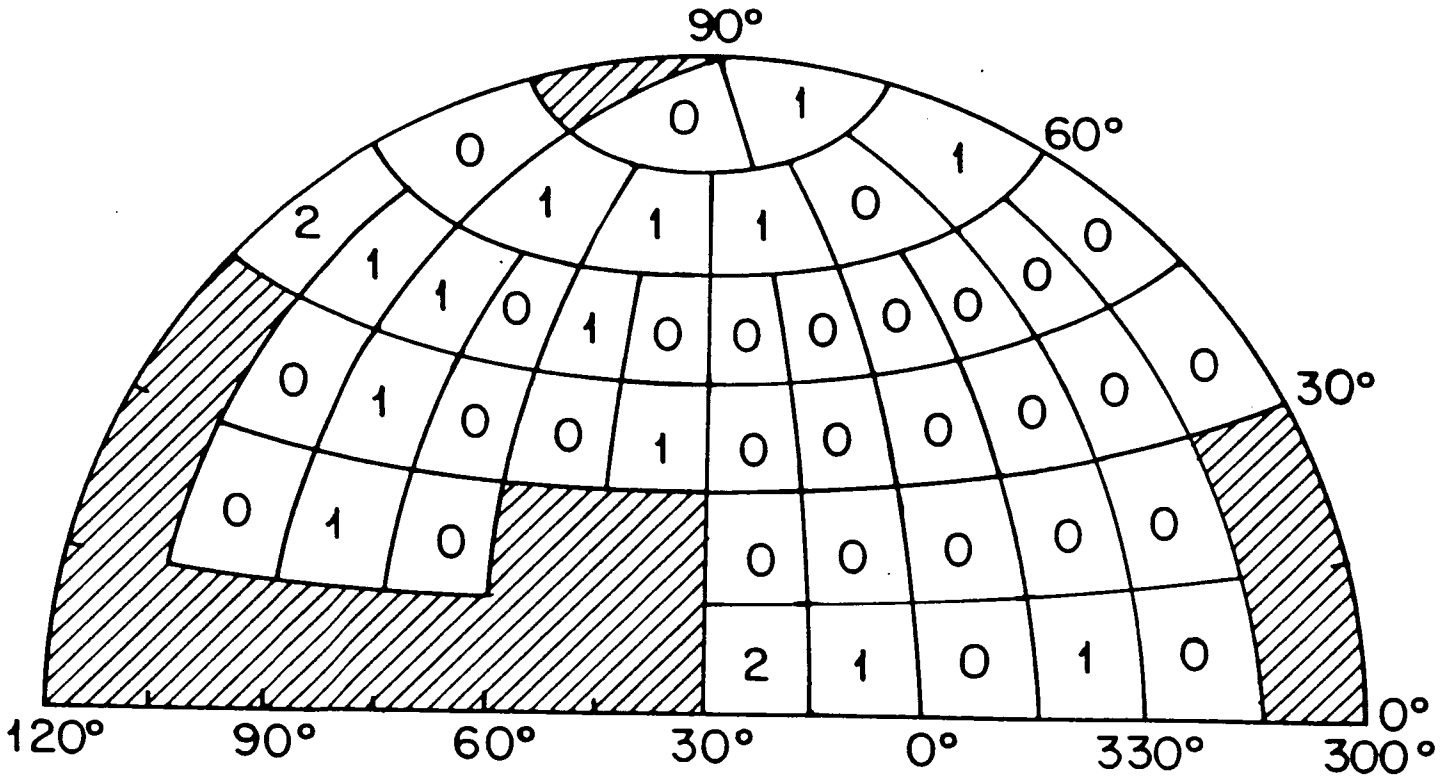
90°
60°
30°
0°
120°
90°
60°
30°
0°
330°
300°

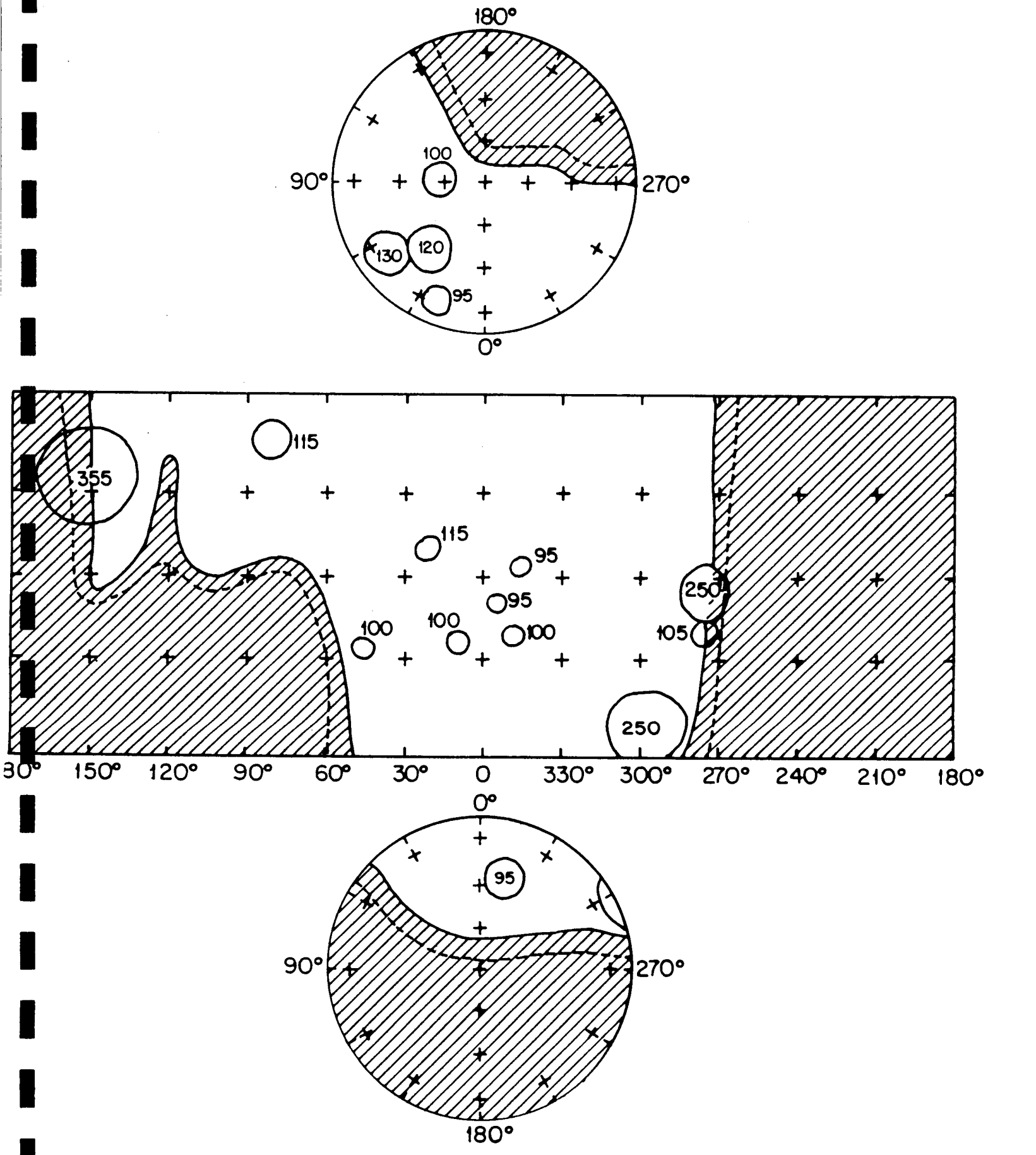
180°
90°
270°
0°
100
130
120
95
115
355
115
95
95
100
100
100
105
250
250
30°
150°
120°
90°
60°
30°
0
330°
300°
270°
240°
210°
180°
0°
95
90°
270°
180°

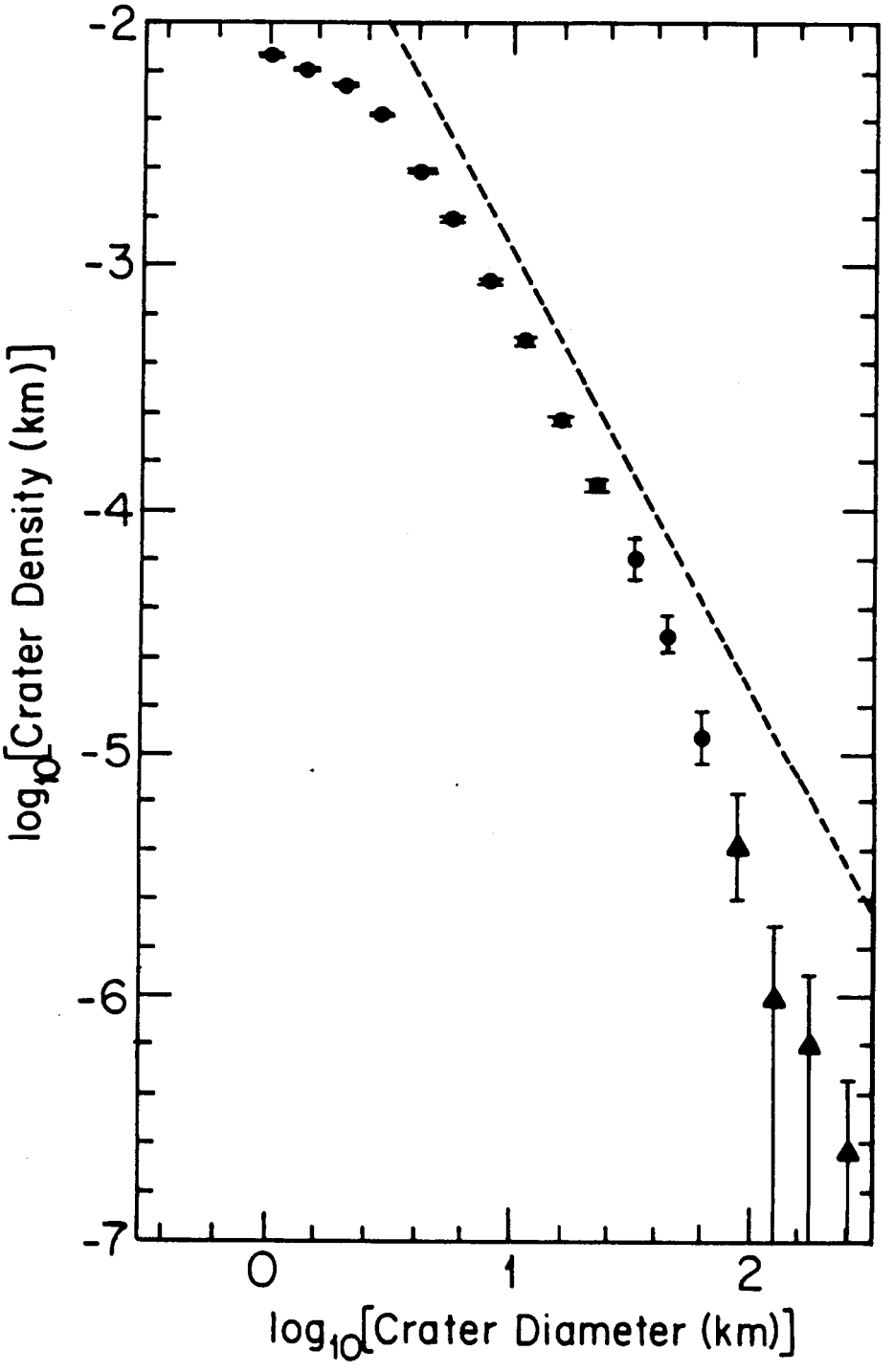
-2
-3
-4
-5
-6
-7
0
1
2
log10[Crater Density (km)]
log10[Crater Diameter (km)]

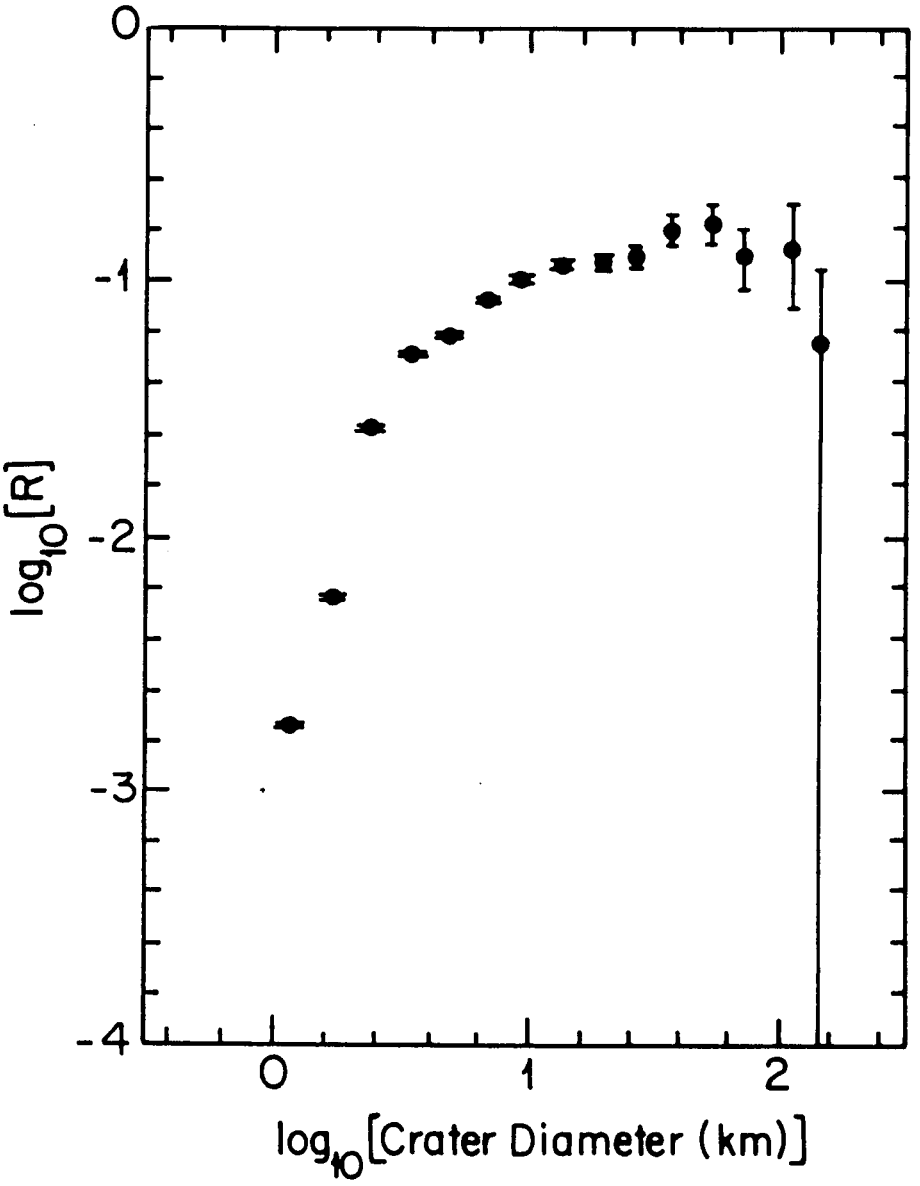
0
-1
-2
-3
-4
0
1
2
log10[R]
log10[Crater Diameter (km)]

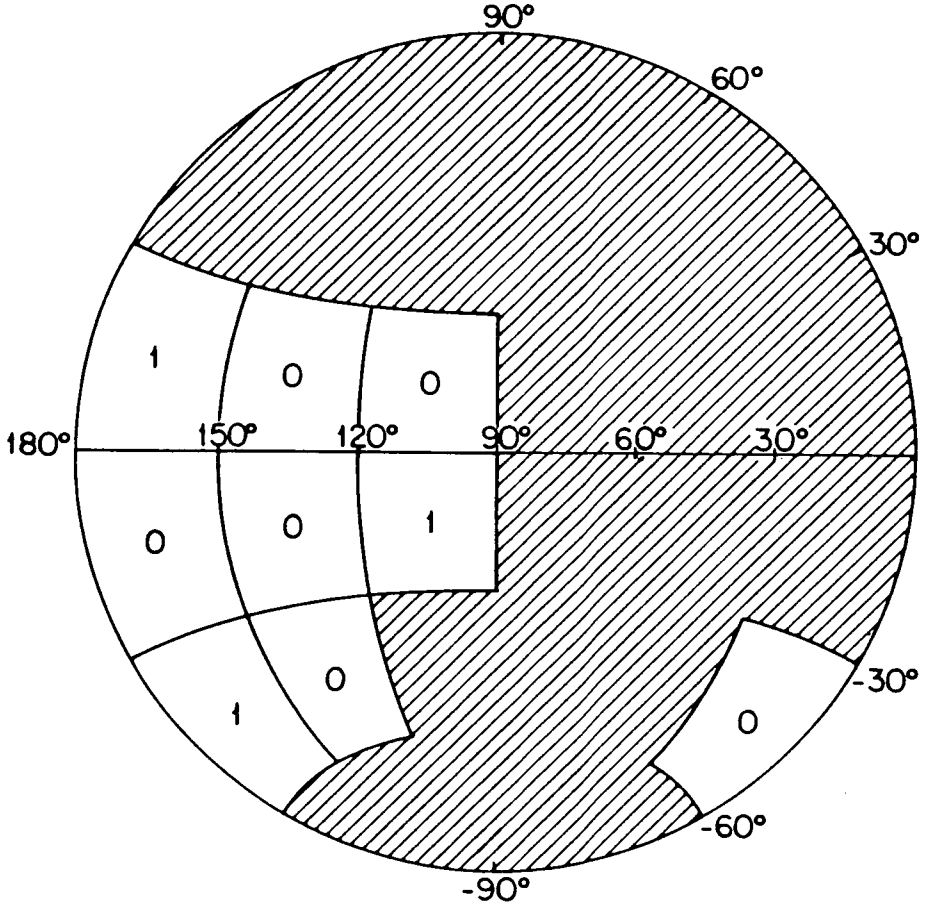
90°
60°
30°
180°
150°
120°
90°
60°
30°
-30°
-60°
-90°
1
0
0
0
0
1
1
0
0

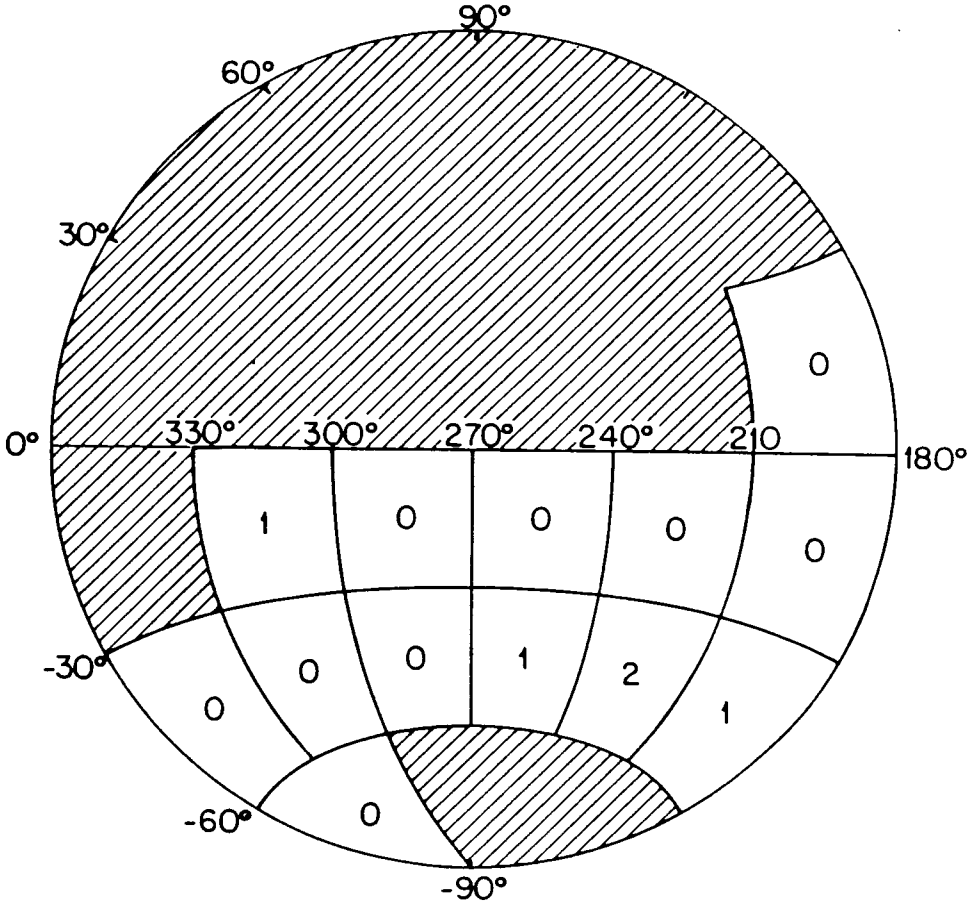
90°
60°
30°
0°
330°
300°
270°
240°
210
180°
-30°
-60°
-90°
0
1
0
0
0
0
0
0
0
1
2
1
0

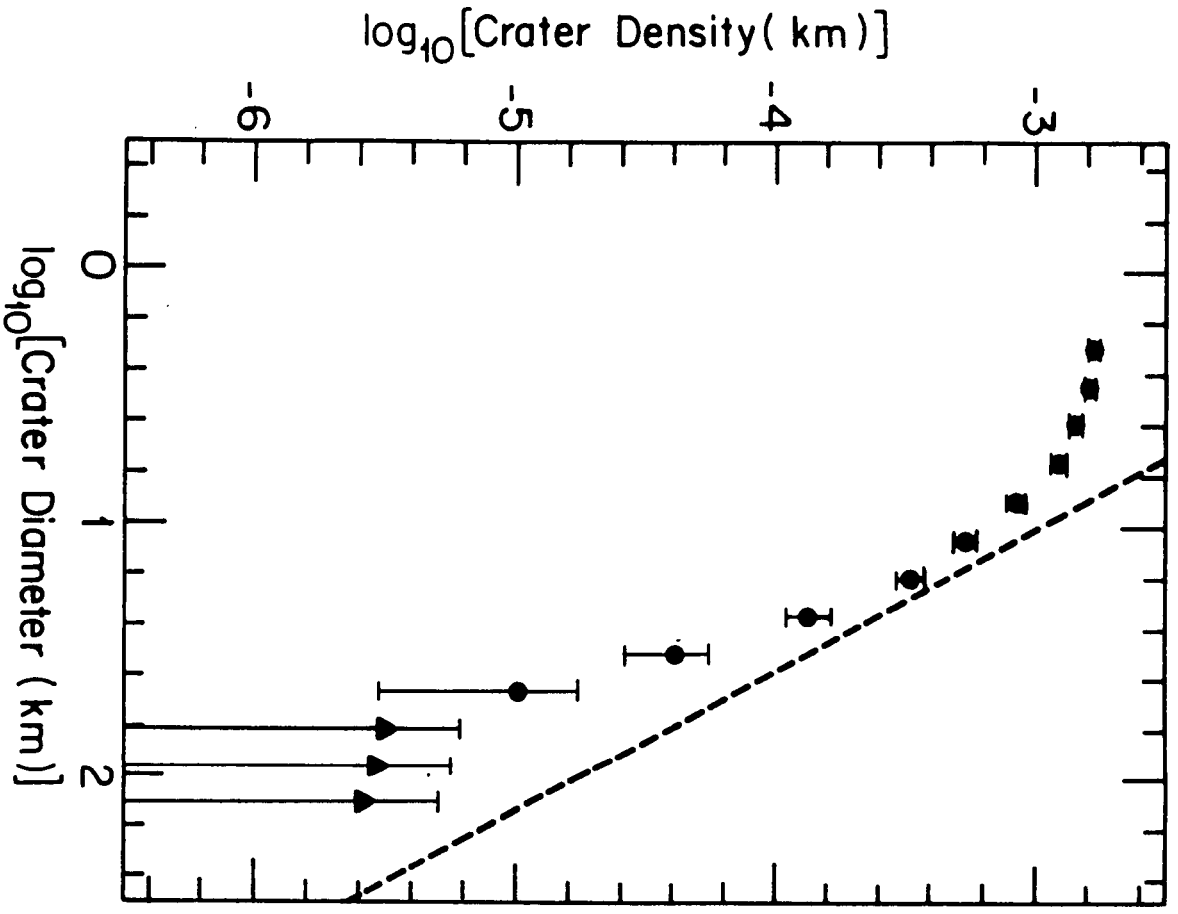
log10[Crater Density(km)]
-6
-5
-4
-3
log10[Crater Diameter (km)]
0
1
2

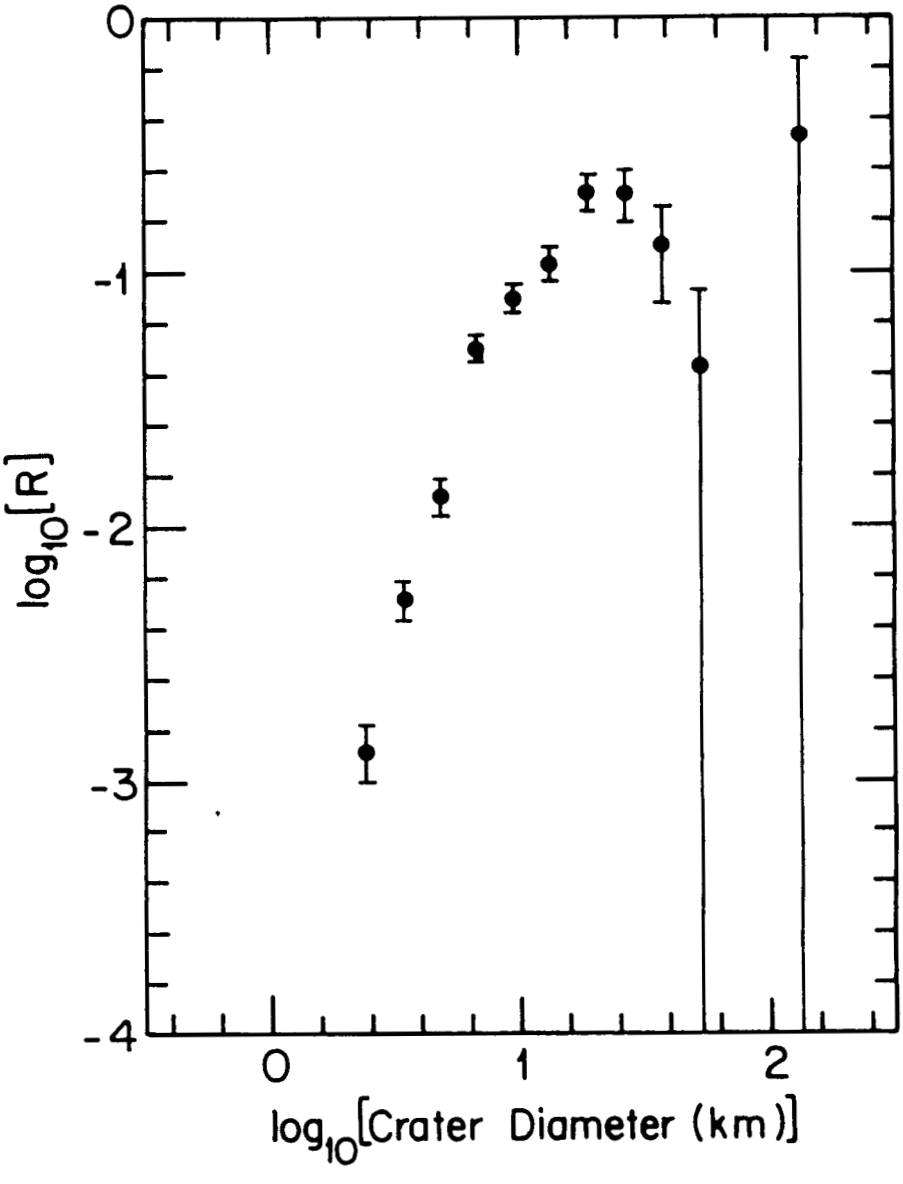
0
-1
-2
-3
-4
log10[R]
0
1
2
log10[Crater Diameter (km)]

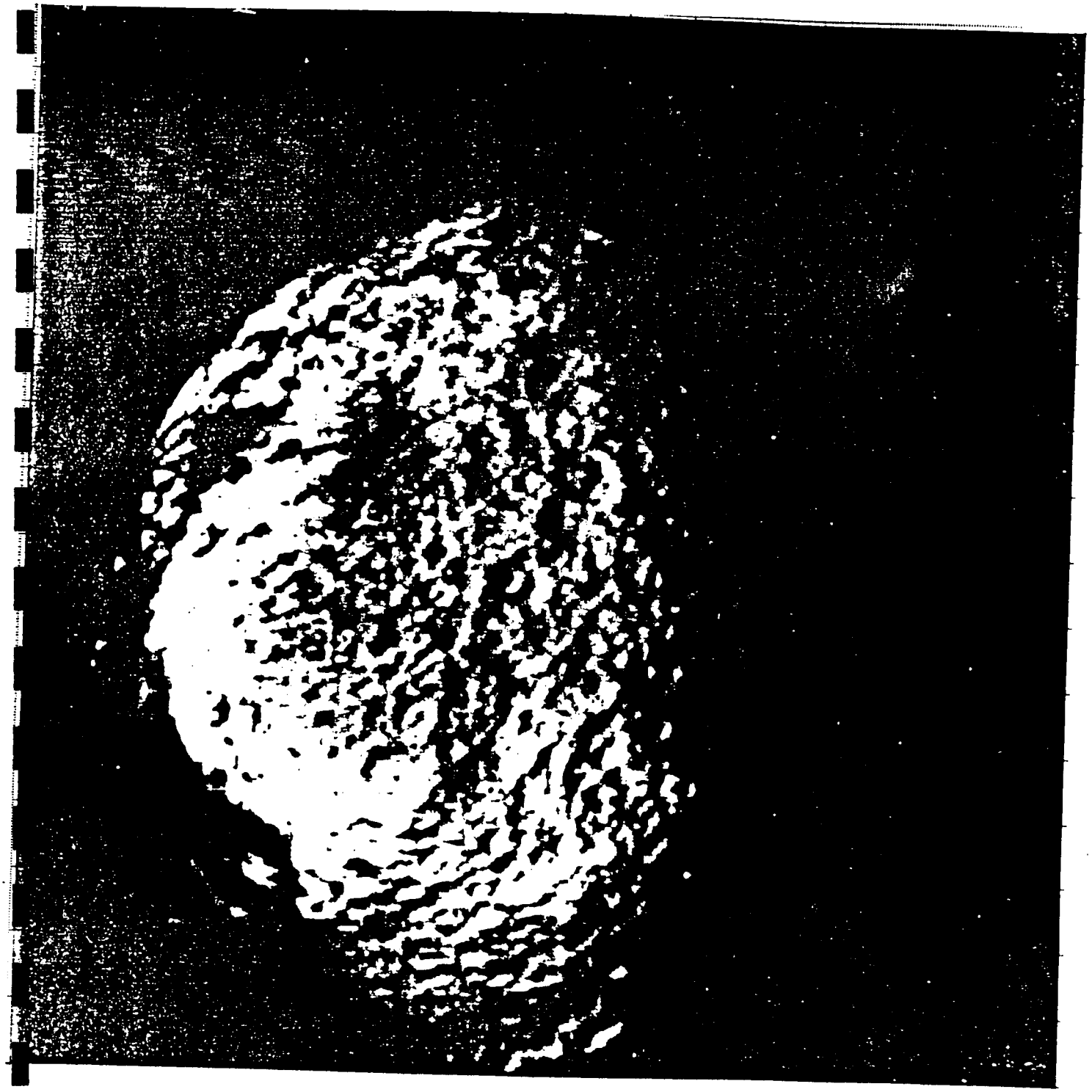

ORIGINAL PAGE
BLACK AND WHITE PHOTOGRAPH

Fig. 14a

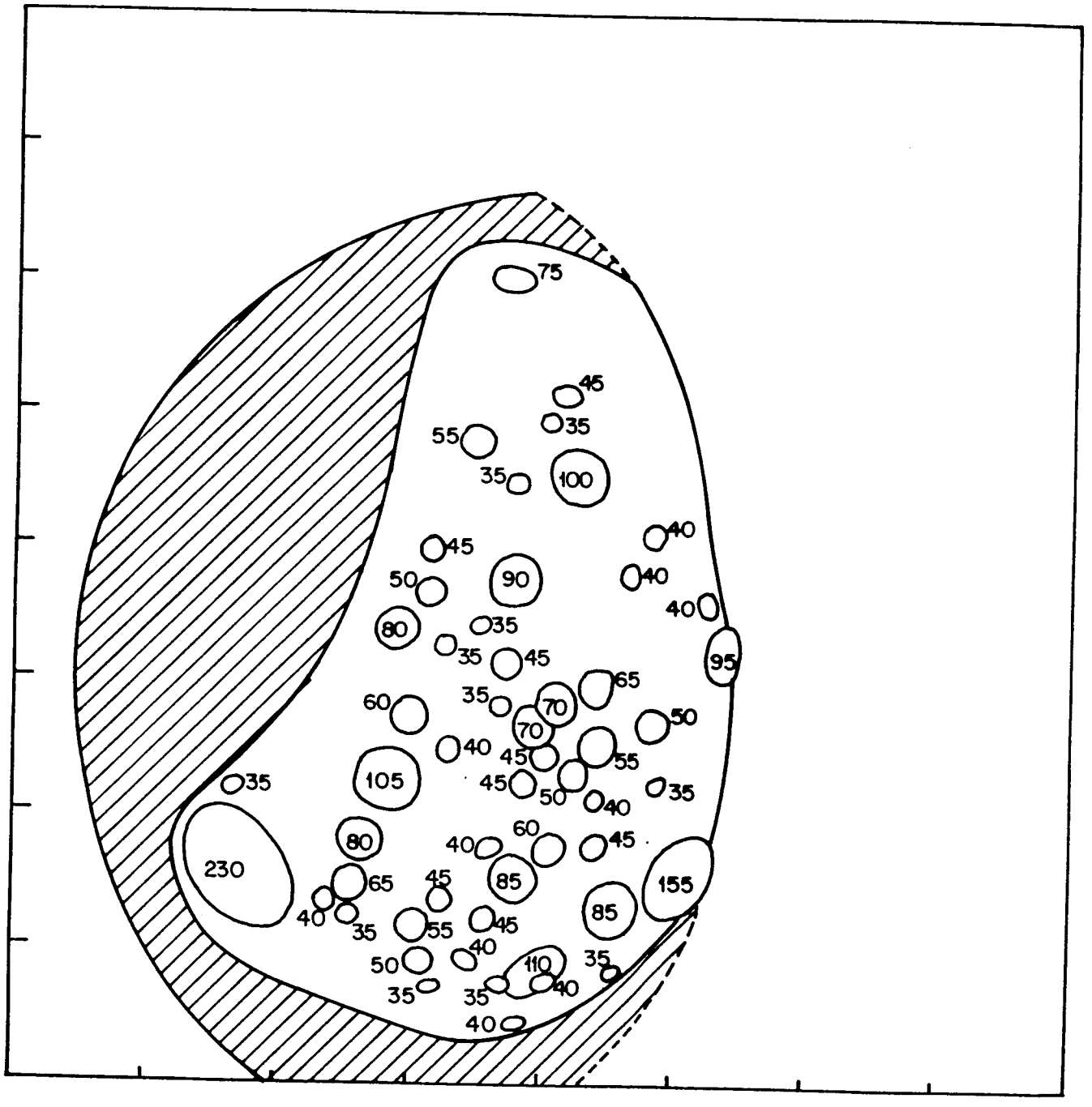
75
45
35
55
35
100
40
45
40
50
90
40
80
35
40
35
45
95
65
35
60
70
50
70
40
45
55
105
45
50
40
35
35
60
80
40
45
230
65
45
85
155
40
35
55
45
85
40
50
110
35
35
40
40

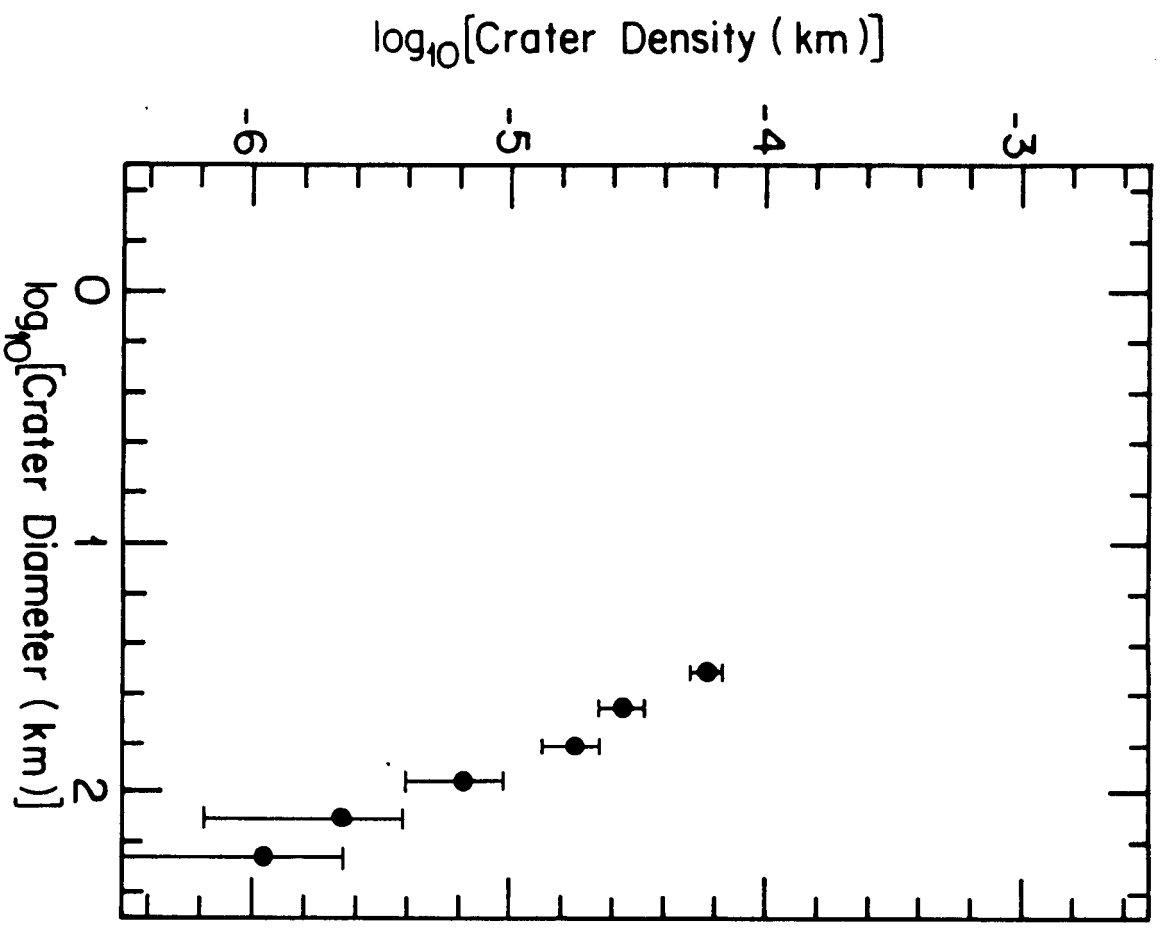
log10[Crater Density (km)]
-6
-5
-4
-3
log10[Crater Diameter (km)]
0
1
2

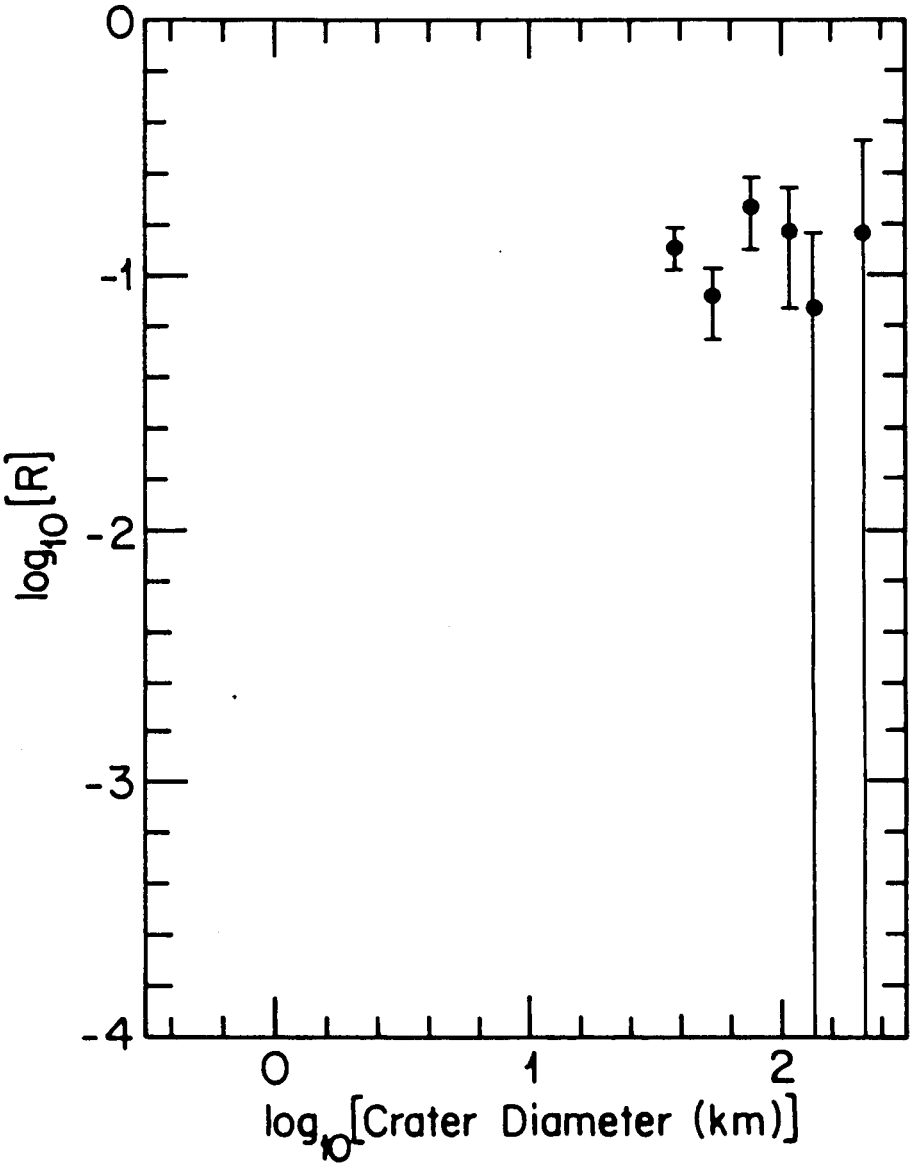
0
-1
-2
-3
-4
log10[R]
0
1
2
log10[Crater Diameter (km)]

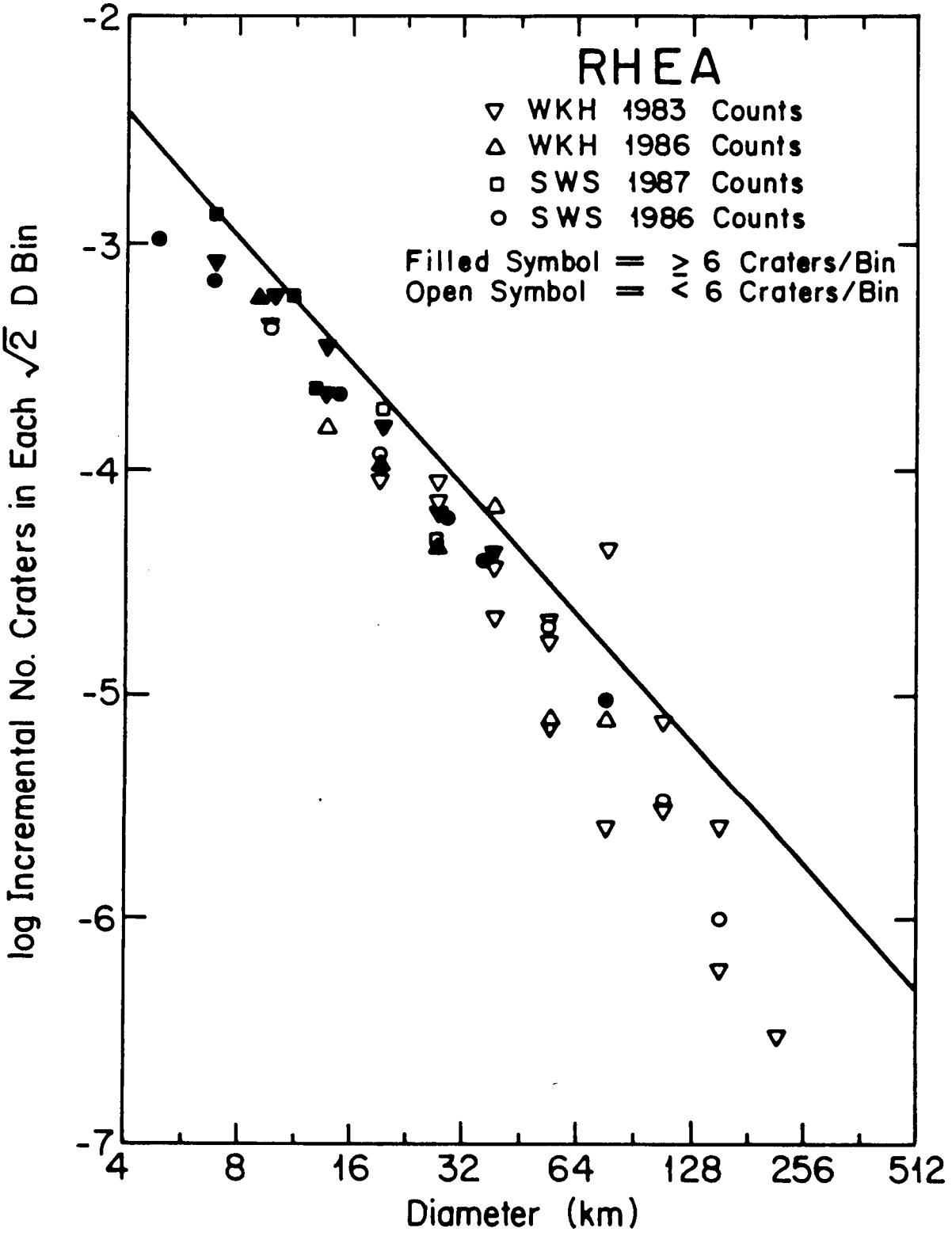
RHEA
WKH 1983 Counts
WKH 1986 Counts
SWS 1987 Counts
SWS 1986 Counts
Filled Symbol = ≥ 6 Craters/Bin
Open Symbol = < 6 Craters/Bin
log Incremental No. Craters in Each √2 D Bin
-2
-3
-4
-5
-6
-7
4
8
16
32
64
128
256
512
Diameter (km)

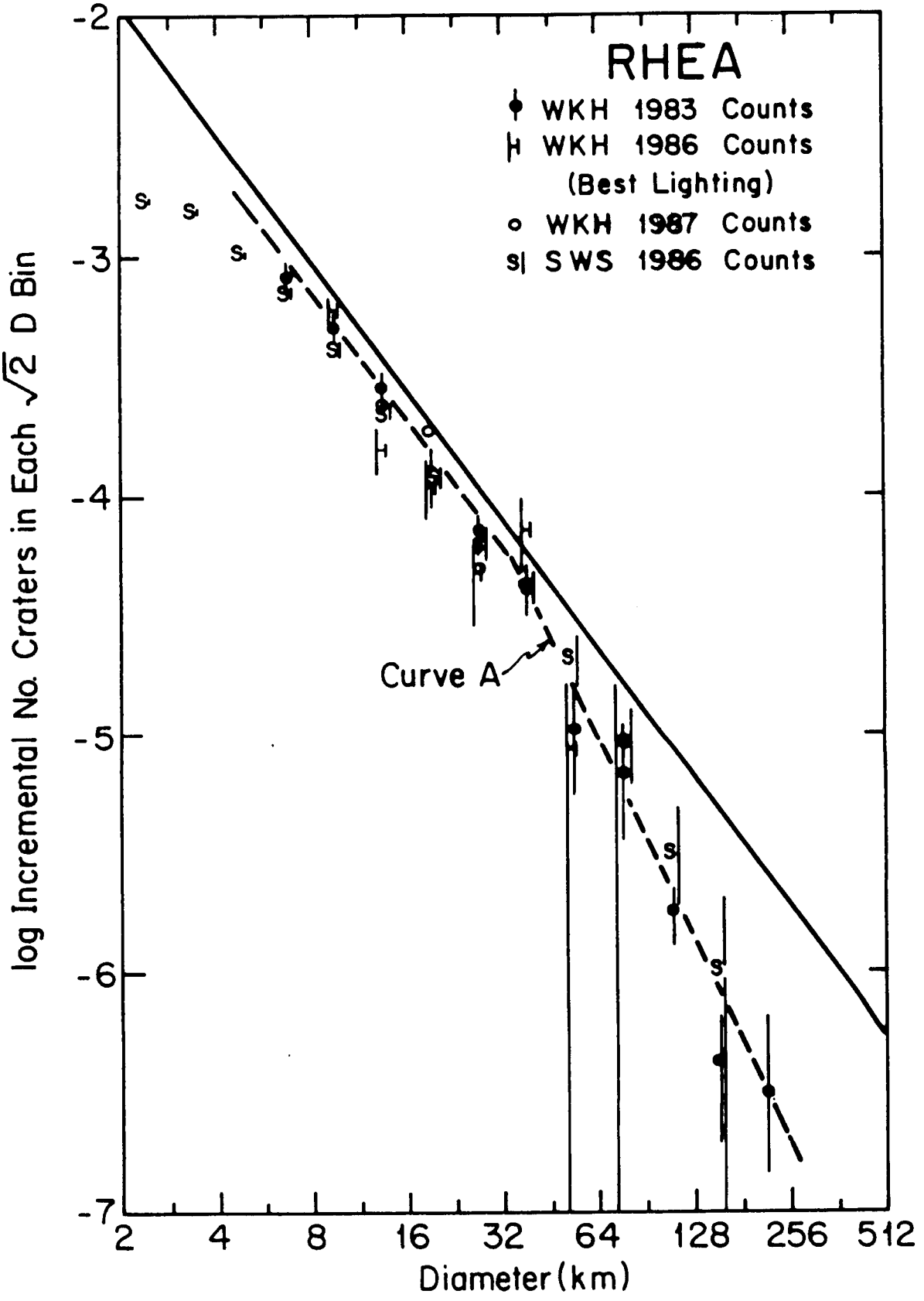
RHEA
WKH 1983 Counts
WKH 1986 Counts
(Best Lighting)
WKH 1987 Counts
SWS 1986 Counts
Curve A
log Incremental No. Craters in Each √2 D Bin
-2
-3
-4
-5
-6
-7
2
4
8
16
32
64
128
256
512
Diameter (km)

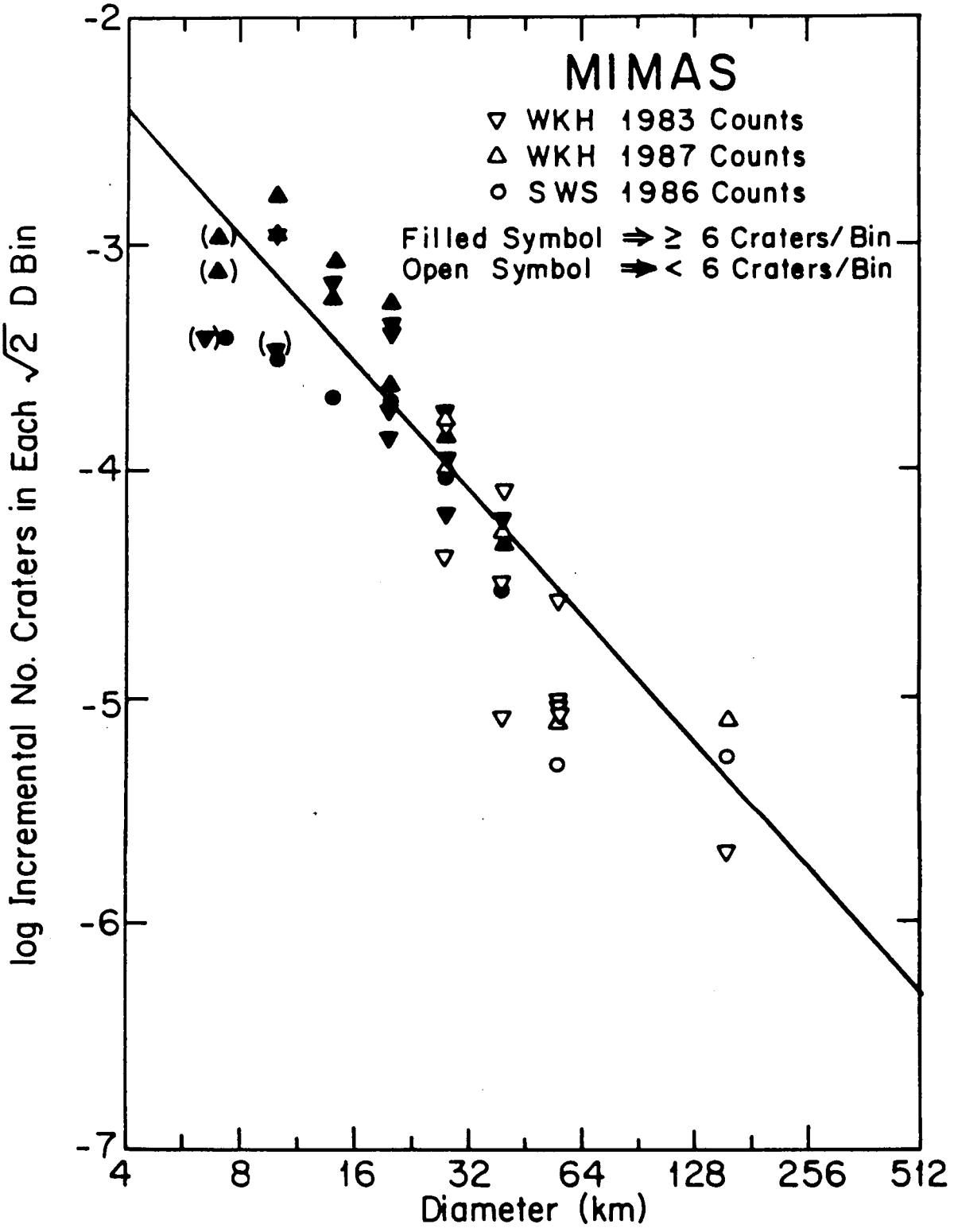
MIMAS
WKH 1983 Counts
WKH 1987 Counts
SWS 1986 Counts
Filled Symbol ⇒ ≥ 6 Craters/Bin
Open Symbol ⇒ < 6 Craters/Bin
log Incremental No. Craters in Each √2 D Bin
-2
-3
-4
-5
-6
-7
4
8
16
32
64
128
256
512
Diameter (km)

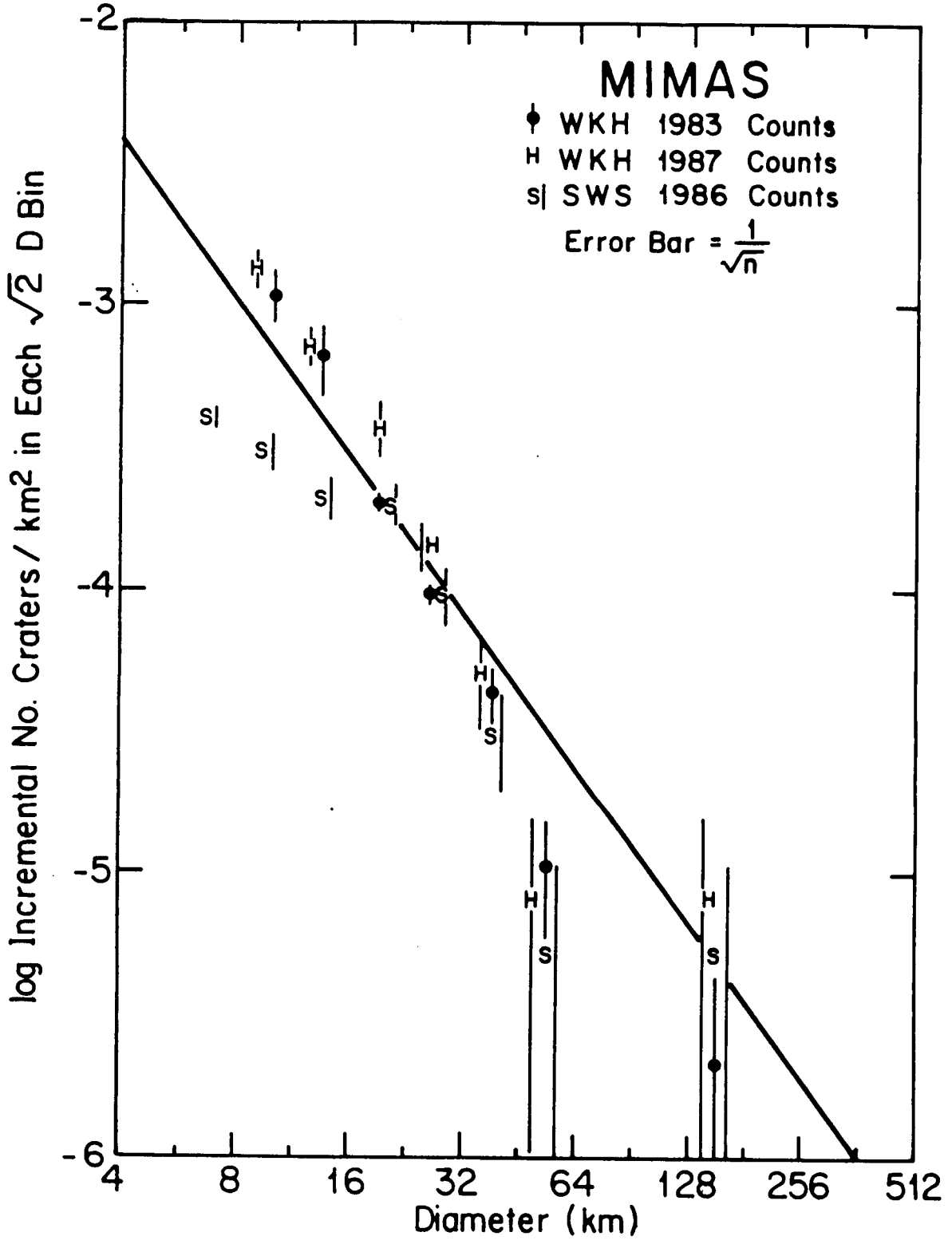
MIMAS
WKH 1983 Counts
H WKH 1987 Counts
S| SWS 1986 Counts
Error Bar = 1/√n
log Incremental No. Craters / km² in Each √2 D Bin
-2
-3
-4
-5
-6
4
8
16
32
64
128
256
512
Diameter (km)

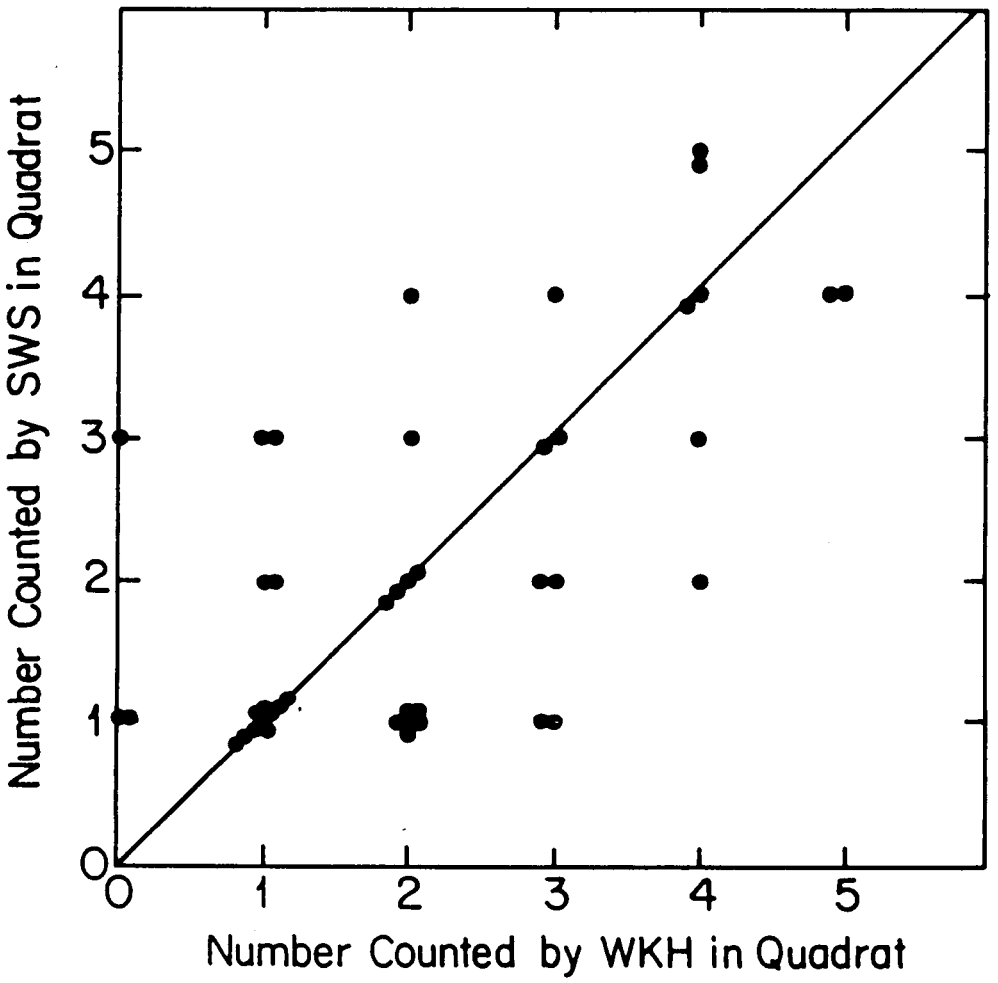
Number Counted by SWS in Quadrat
Number Counted by WKH in Quadrat
0
1
2
3
4
5

APPENDIX C

CRATER SATURATION EQUILIBRIUM IN THE SOLAR SYSTEM: NEW EVIDENCE

W. K. Hartmann, Planetary Science Institute, Tucson AZ 85719

At the 15th LPSC in 1984, (and Icarus, 60:56-74, 1984) the writer suggested that many planet and satellite surfaces in the solar system have reached a state of crater saturation equilibrium. At this crater density, further impacts make new craters, but old craters are obliterated, especially by giant basins and their ejecta blankets. Ejecta may drop the total crater density below the mean saturation level in parts of the area, at diameters corresponding to depths shallower than the new ejecta. Thus, once saturation equilibrium occurs in the absence of endogenic resurfacing, the crater diameter distribution evolves D-dependent structure, as well as oscillating around the mean saturation equilibrium value with time.

Attempts to model these effects by numerical simulation have led to controversies about the crater density level corresponding to saturation equilibrium curve in nature. The Voyager team, for example, in interpretations of outer solar system satellite surfaces, denies saturation equilibrium and assumes that all craters ever formed can be counted. Thus they translate structure in diameter distributions directly into structure in impactor populations. This conclusion appears internally inconsistent with their simultaneous conclusion that some of the same satellites have been hit so many times that they have been fragmented and reassembled. How can a satellite such as Mimas be fragmented and reassembled from impactors without attaining a crater-saturated surface, in the absence of any apparent endogenic resurfacing events?

The Icarus paper showed empirically that bodies such as Mimas, Rhea, Callisto, the moon, Phobos, and Deimos all have crater diameter distributions that reach maximum densities within a factor two or three of the curve

$$\log N_{HC} = -1.83 \log D_{km} - 1.33 \qquad (1)$$

where N_{HC} = incremental no. craters/km^2 in log $_2$ diameter bins and D = crater diameter (km). It was noted that crater counts on lunar maria permit a test of these ideas. They show three well-known segments, illustrated with data from Mare Cognitum in Figure 1. Segment A at $D \gtrsim 4$ km is attributed to primary impact. Segment B, 250 m $\lesssim D \lesssim$ 4 km, is more steeply sloped and is generally attributed to dominance of secondary ejecta. The important segment in this discussion is segment C, at $D \lesssim$ 250m, which rolls over to shallower slope. Segment D is the crater density in heavily cratered areas, i.e. equation (1). The important point is that segment C appears to flatten near the level of equation (1) consistent with the hypothesis that crater densities in nature do not exceed (1) because saturation sets in at that point. At the time of the 1984 work, I had mare crater counts only down to D ~ 62 m, not small enough to test whether the flattening really persisted to small D near equation (1). I proposed that a test of the saturation equilibrium

hypothesis would be to see if the flattening (segment C) persists to small sizes, and in particular to see if it falls near equation (1), the putative empirical saturation equilibrium level.

Although some other counts of small lunar craters have been published, it is important in these tests to use a homogeneous data set by one author, since different authors and different techniques (such as stereo viewing by some authors) may lead to different detection limits in heavily cratered terrain where rolling depressions may be seen as craters by some authors but not others (see Lissauer, Squyres, and Hartmann, these abstracts). For these reasons I have begun some new counts of small craters on lunar high resolution photos; these are added to my older counts obtained by the same methods during the last 22 years.

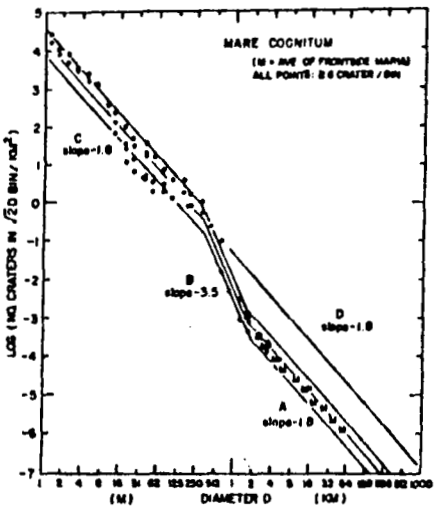

Fig. 1. Diameter distribution of craters in Mare Cognitum down to 1 m diameter.

The small craters relate to the question of saturation equilibrium through the pioneering work of Shoemaker (1966 Ranger VIII and IX reports, JPL Tech. Rep. 32-800; 1968 Surveyor Final Report, JPL Tech. Rep. 32-1265) and Gault (1970, Radio Science 5:273-291). They pointed out clearly that the formation of the mare regolith to depths of the order of tens of meters implied saturation cratering up to diameters sufficient to pulverize lavas to that depth. Indeed, Gault (Fig. 4) drew not only empirical but theoretical curves showing the rollover from segments B to C due to the saturation effect. In other words, they showed that segment C must fall along a saturation equilibrium line.

Figure 1 includes my new results on the position of segment C. Crater diameter distribtuions have been extended down to D = 1 m by combining lunar Orbiter photos with older Ranger impactor photos. Two important conclusions are drawn. (1) The craters at small D do not continue upward along the steep segment B slope, but flatten to a shallower slope along segment C. (2) Segment C falls roughly along the extension of segment D, i.e. near equation (1), which I previously identified as a hypothetical saturation equilibrium level. These results confirm Gault's. His results deserve further attention in the context of studies of heavily cratered surfaces, such as outer planet satellites.

I conclude that this supports the hypothesis that equation (1) lies close to an empirical saturation equilibrium level.

Further investigations of the behavior of curves in intensely cratered areas thus appear warranted, in view of their effect on Voyager and other interpretations, though present study has been retarded due to funding cutbacks. This work is supported through the NASA Planetary Geology and Geophysics Program.

APPENDIX D

CONF. ON GROWTH OF EARLY CONTINENTAL CRUST
OXFORD, JUL. 87

EARLY INTENSE CRATERING: EFFECTS ON GROWTH OF EARTH'S CRUST

William K. Hartmann, Planetary Science Institute, Tucson, AZ 85719

Observations of crater densities in lunar regions of various ages show that the cratering rate during the first 500 my of lunar history was $\geq 10^3$ x the present rate (1). Because of O isotope ratios and other evidence, we believe the moon formed close to Earth, and the same early intense cratering affected Earth, too. Probably it was a solar-system-wide phenomenon, resulting from sweep-up of the planetesimals at the end of planet formation.

In all probability, the cratering rate in the first 10-100 my averaged vastly higher. The mass flux needed to accumulate Earth and the moon within the permitted formation interval of 10-100 my is of the order $2(10^9)$ x the present rate (2). This is entirely understandable from accretion models, which indicate a very rapid accretion of planetesimals (3) and a longer, declining rate of sweep-up of the remaining planetesimals after the planets gained nearly their present mass (4).

This situation has two related effects on formation of crusts of Earth and other planets. First, as pointed out by Safronov (5) and Hartmann and Davis (6), the 2nd, 3rd, ... largest bodies accompanying the planets may have been large enough, relative to the planets themselves, to have dramatic effects, including disruption of large volumes of the planet, including mantle and crust if they had formed. Hartmann and Davis (6) attributed the moon's origin to such a giant, disruptive impact. Recent modelling (7,8) shows that large regions of any pre-existing crust and upper mantle could be vaporized and/or ejected as finely disseminated and heated dust, with consequent geochemical effects. Giant impacts would be stocastic events, dotted through the first 10^8 years or so, until the required large bodies collided with planets or were ejected from the solar system.

The second effect involves the more continual rain of impactors that were smaller (but large by present day standards). These would form a continuum with the "giant impacts." (The nature of the impactor size distribution was such that the smaller the body, the more of them.) Ringwood (9) discussed the possible production of a silicate atmospheres devolatized from the crust. Frey (10) proposed that large impacts punched holes in the early crust, piling up "continental" crustal ejected debris in other areas and exposing hot mantle areas where convection was enhanced; this could have abetted proto-continent formation. Hartmann noted that magma ocean evolution must be modelled in the presence of this process, which competes with crust formation by continually breaking up and redistributing the early, solid, anorthositic surface (11). Also, the impact rate at the close of planet forming period was high enough that impacts comparable to the proposed K-T boundary event happened on roughly a monthly-to-yearly basis (12).

Figure 1 (adapted from Fig. 12) illustrates some of these points. Curve "t=0" shows the approximate impact rate shortly after the close of

planet formation; curve "t=500 m.y." shows the rate 500 m.y. after planet formation. The curves are based on the above results. The actual impact rate declined approximately exponentially with time from the first to the second curve. As can be seen, during this interval there was opportunity for a few giant impacts, many impacts large enough to create basins comparable to the moon's Orientale and Imbrium basins (10^3-km-scale in diameter of disrupted zone), and thousands of smaller-scale craters.

Depending on the time-scale of crustal formation and evolution on Earth and other planets, models of proto-crustal evolution should take into account the possible competitive influence of repeated impact cratering, which would disrupt any hypothetically homogeneous proto-crustal layer, creating thick and thin spots, and affecting cooling timescales and global- or continental-scale topographic/structural/ tectonic features.

While the geographic expression of these effects may be long vanished on Earth because of tectonic and erosive effects, they may be still visible on Mars, where large impact basins may be detected, and where relatively young volcanics dominant one hemisphere, while a much older crustal surface dominates the other hemisphere. (13)

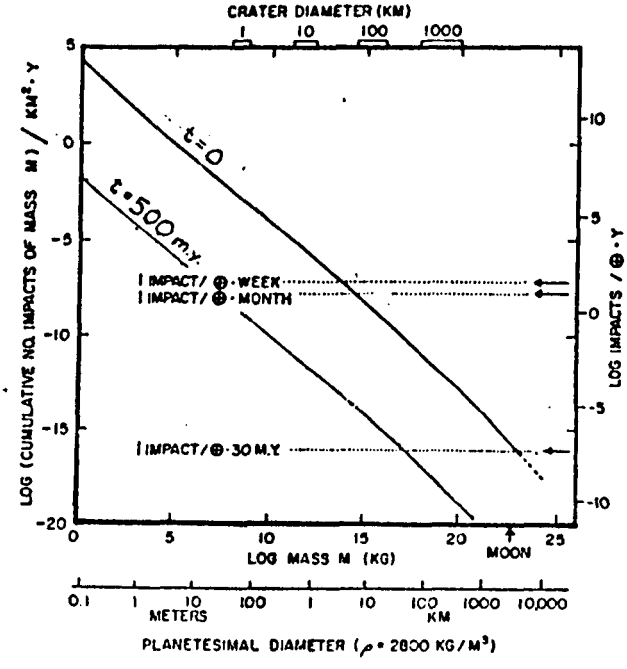

FIG. 1. Estimated impact cratering rate on early Earth at close of planet formation and 500 m.y. later. These rates are on the order of 10^9 and 10^3 times the present rate, respectively. (Adapted from ref. 12).

REFERENCES

1. Hartmann, W.K. (1972). Astrophys. Space Sci. 12, 48-64.
2. Hartmann, W.K. (1980). Icarus 44, 441-453
3. Greenberg, R., Wacker, J., Hartmann, W.K., and Chapman, C. (1978). Icarus 35, 1-26.
4. Wetherill, G.W. (1977). Proc. Lunar Sci. Conf. 8th, 1-16.
5. Safronov, V. (1966). Sov. Astron. AJ 9, 987.
6. Hartmann, W.K. and Davis, D.R. (1975). Icarus 24, 504-515.
7. Benz, W., Slattery, W., Cameron, A. (1986). In Origin of the Moon (Houston: Lunar & Planetary Inst.).
8. Melosh, H. and Sonett, C.P. (1986). In Origin of the Moon (Houston: Lunar & Planetary Inst.).
9. Ringwood, A.E. (1979). Origin of the Earth and Moon. (Springer-Verlag, New York), p. 295.
10. Frey, H. (1977). Icarus 32, 235.
11. Hartmann, W.K. (1980). In Proc. Conf. Lunar Highlands Crust (Houston: Lunar & Planetary Institute).
12. Hartmann, W.K. (1986). In Origin of the Moon (Houston: Lunar & Planetary Inst.).
13. Wilhelms, D.E. and Squyres, S.W. (1984). Nature 309, 138-140.